TECHNISCHE UNIVERSITÄT MÜNCHEN
Max-Planck Institut für Biochemie
Abteilung Strukturforschung
Biologische NMR-Arbeitsgruppe

Structural basis for the inhibition of cancer significant proteins Pin1 and Mdm2/Mdmx and high throughput approaches for screening for the inhibitors of these proteins

Weronika Agata Janczyk

Vollständiger Abdruck der von der Fakultät für Chemie der Technischen Universität München zur Erlangung des akademischen Grades eines

Doktors der Naturwissenschaften

genehmigten Dissertation

Vorsitzender: Univ.-Prof. Dr. M. Groll
Prüfer der Dissertation: 1. Univ-Prof. Dr. M Sattler
2. Prof. Dr. T.A. Holak, Jagiellonian Univ. /Polen

Die Dissertation wurde am 16.05.2012 bei der Technischen Universität München eingerichtet und durch die Fakultät für Chemie am 13.07.2012 angenommen.

To my Mother….

Aknowlegements

I would like to thank everyone who has contributed to this work.

First of all, I would like to acknowledge my supervisor, Prof. Tad A. Holak, for a possibility of working in his group, his encouragement and support.

I would like to thank all the colleagues: Kaja Kowalska, Anna Ducka, Linda Wolf, Anna Czarna, Michał Bišta, Tomasz Sitar, Marcelino Castro, Grzegorz Popowicz and Arkadiusz Sikora for creating a friendly atmosphere in the lab and the interesting scientific (but not only) discussions.

I am also very grateful to Prof. Dr. Michael Sattler, for being my thesis advisor.

I would like to thank Prof. Thorsten Berg and Dr. Martin Gräber for a fruitful cooperation in the Pin1 project

My thanks also go to Prof. Alexander Dömling and his coworkers for their encouragement in the development and synthesis of a dual MDM2/X inhibitor.

Last, but not least I would like to acknowledge all those who have contributed to this work in a non-scientific way, for their support.

Publications:

Parts of this thesis have been published or will be published due to course:

Bista M, Kowalska K, **Janczyk W**, Dömling A, Holak TA
Robust NMR screening for lead compounds using tryptophan-containing proteins.
J Am Chem Soc. 2009 Jun 10;131(22):7500-1.

Gräber M, **Janczyk W**, Sperl B, Elumalai N, Kozany C, Hausch F, Holak TA, Berg T.
Selective targeting of disease-relevant protein binding domains by
o-phosphorylated natural product derivatives
ACS Chem Biol. 2011 Oct 21;6(10):1008-14.

Janczyk W, Doemling A, Holak TA.
A sensitive NMR screening approach for developing small-molecule inhibitors of the MDM2/MDMX-p53 interaction
Manuscript under preparation

Contents

1 Introduction

1.1 Pin1

One of the most important and universal regulatory mechanisms in the cell is reversible phosphorylation of proteins (Hanes et al. 1989; Lu et al. 1999; Atchison et al. 2003). It represents a key switch for controlling the function of many signaling molecules in various cellular processes. In proteins, for all amino acids except proline, the *trans* conformation of the peptide bond is much more energetically favorable than the *cis*. For proline with a peptidyl-prolyl imide bond the free energy difference between the isomers is much smaller than in other amino acids. The *cis* conformation occurs with a frequency of 5-6% protein structures (Stewart et al. 1990; Pal and Chakrabarti 1999). Moreover, a large majority of observed *cis* peptide bonds occur in surface accessible bend coil or turn conformations (Pahlke et al. 2005a; Pahlke et al. 2005b). Thus, Xxx-Pro motifs in proteins have the potential to adopt two distinct conformations. They are typically exposed to solvent on the surface of the protein. The structural difference between these two isoforms constitutes fundamental molecular switch (Lu et al. 2007).

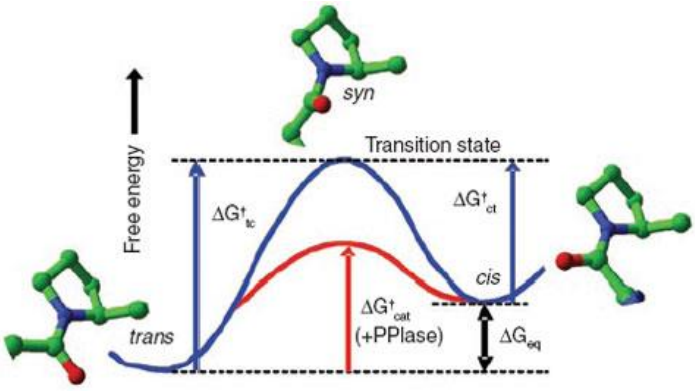

Figure 1.1.1 Energy diagram of prolyl cis-trans isomerization. Conformational exchange process through the twisted 90-syn high energy transition state in the intrinsic (blue curve) or PPIase-catalyzed (red curve) reactions (adapted from (Lu et al. 2007)).

Since a spontaneous isomerization between *cis* and *trans* forms of proline occurs slowly and phosphorylation of serine or threonine residues that proceed proline further slows down the process, conformational modifications of the Ser/Thr-Pro

phosphorylated proteins are catalyzed by the phosphorylation specific peptidyl-prolyl cis/trans isomerases (PPIases) (Yaffe et al. 1997; Lu et al. 2007; Lu and Zhou 2007) (Figure 1.1.1). The model of this process is shown in Figure 1.1.2.

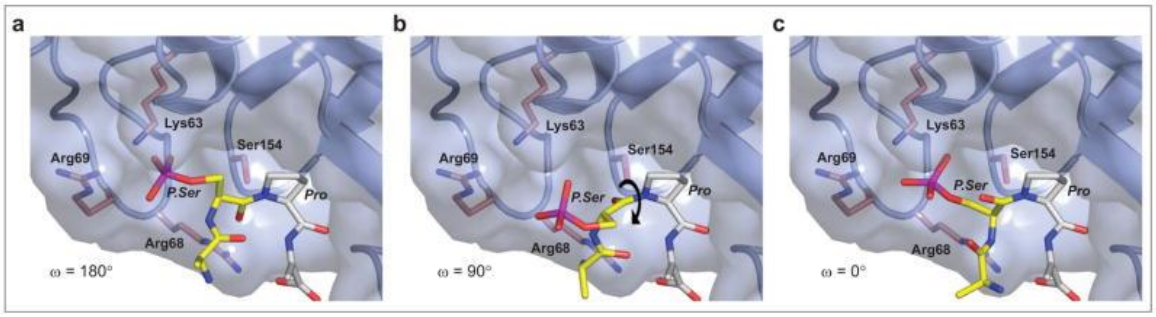

Figure 1.1.2 3D models depicting a possible isomerization trajectory of the P.Ser-Pro peptide bond. The P.Ser-Pro peptide bond depicted with an ω angle of 180° (trans) (A); the P.Ser Pro peptide bond depicted with an ω angle of 90° (B); the P.Ser-Pro peptide bond depicted with an ω angle of 0° (cis) (C). Adapted from (Zhang et al. 2007).

1.1.1 Pin1 - structure and function

Pin1 is a member of the evolutionary conserved peptidyl-propyl isomerases (PPIase) family of proteins. Prolyl isomerases comprise four structurally distinct subfamilies: cyclophylins, FK506-binding proteins (KBP), parviluns, and the protein Ser/Thr phosphatase 2A (PP2A) activator PTPA (Galat 2003; Magnusdottir et al. 2006). Pin1 is a parvulin and catalyzes the isomerization of proline amide bonds between *cis* and *trans* configurations - thereby altering the conformation of its substrate (Lu et al. 2006). Pin1 is unique from other parvulin family members, because it specifically recognizes phosphorylated Ser/Thr-Pro motifs and increases the rate of *cis/trans* isomer interconversion by as much as 1000-fold (Lu et al. 1996). Role of Pin1 in cell signaling is important because kinases and phosphatases specifically recognize the *cis* and *trans* conformations of the prolyl peptide bond of their substrate (Zhou et al. 2000; Werner-Allen et al. 2011).

Pin1 is an 18 kDa protein (Lu et al. 1996) and consists of two domains separated by a short linker region (Figure 1.1.3 A) (Lu et al. 1996; Ranganathan et al. 1997; Yaffe et al. 1997). The N-terminal WW domain (residues 1-39) is named after a pair of conserved tryptophan residues, located one near each terminus of the domain in the

primary sequence. It contains additionally a proline located near the C-terminus and a cluster of aromatic residues centrally in the primary sequence (Ranganathan et al. 1997). A highly compact modular domain adopts an antiparallel-3-stranded fold forming a binding groove for the substrate (Figure 1.1.3 B)(Lu et al. 1999).

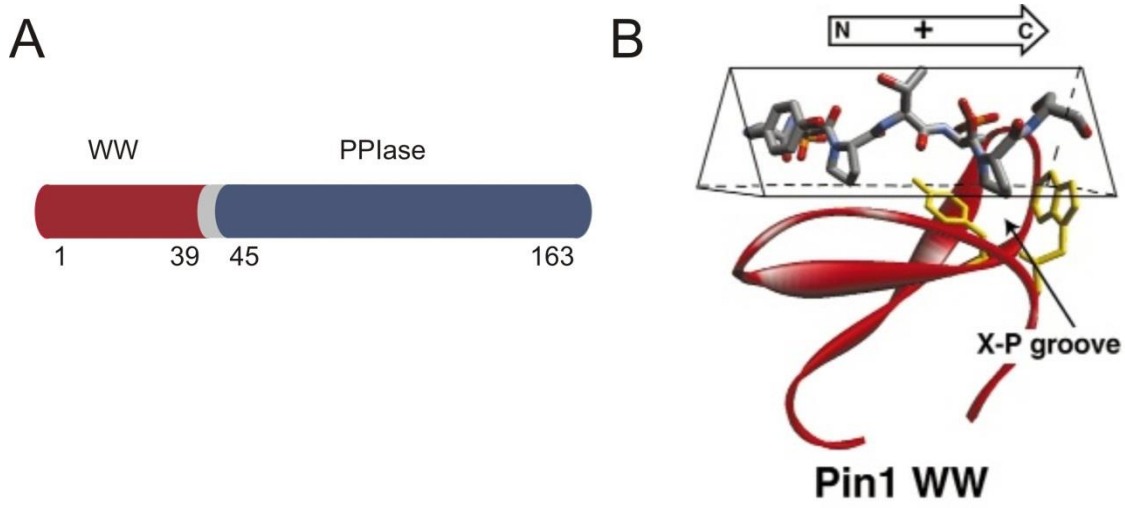

Figure 1.1.3 Domain organization of human Pin1 (A): the WW-domain (red); linker region (grey); PPIase domain (blue); Pin1 WW domain ligand binding pattern (B); Trp and Tyr residues responsible for ligand binding are presented as sticks; the graphic was adapted from (Zarrinpar and Lim 2000)**.**

The C-terminal catalytic PPIase domain (residues 45-163) consists of a four-stranded anti parallel β-sheets and in addition four α-helices surrounding the fatted half β-barrel (Figure 1.1.4). A set of absolutely conserved catalytic residues Leu122, Met130, Phe134 in the Pin1 class of PPIases projects outward from the barrel structure and defines the binding pocket for the proline and the bond peptide that undergoes *cis/trans* isomerization. Similarly, the side chains of residues Lys63, Arg68, Arg69 form a basic cluster that sequesters pSer/Thr of the substrate (Ranganathan et al. 1997). Out of these residues Lys63, involved in basic catalysis, is conserved both in Pin1 and other parvilun-type PPIases. In contrast, Arg68 and Arg69 are conserved only in the Pin1-type PPIases.

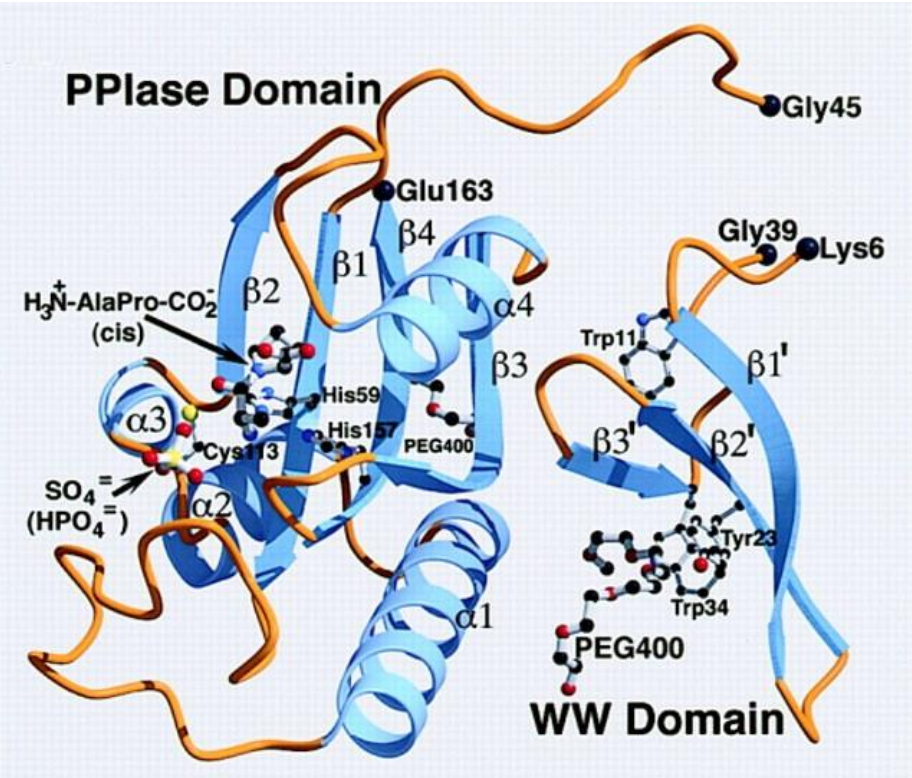

Figure 1.1.4 The overall fold of human Pin1 presents two domains: three-stranded WW domain (with the Trp and Tyr residues) and the PPIase domain with a boud cis Ala-Pro peptide. Residues His and Cys are also important for this interactin. Adapted from (Ranganathan et al. 1997).

Pin1 is tightly regulated by several mechanisms (Wulf et al. 2001; Lu et al. 2002; Ryo et al. 2002; You et al. 2002; Lee et al. 2009) and its deregulation can contribute to an increased number of diseases including aging, cancer, neurological disorders, and autoimmune and inflammatory diseases (Liou et al. 2002; Lu and Zhou 2007; Lee et al. 2011).

1.1.2 Regulation of Pin1

Pin1 expression is generally correlated with cell proliferative potential in normal human tissues, but it is unregulated in many human cancers (Atchison et al. 2003; Bao et al. 2004). Several studies have shown that Pin1 transcription, protein level, catalytic activity and function of its transcription are tightly regulated by many different mechanisms under physiological conditions (Lu et al. 2007; Lu and Zhou 2007).

Levels of Pin1 expression are regulated by transcription factor E2F, which specifically activates the PIN1 promoter via E2F binding sites. Pin1 protein levels are enhanced by oncogenic *Neu/Ras* signaling through the activation of E2F (Ryo et al. 2002). There was identified a single nucleotide polymorphism (aSNP) that reduces Pin1 expression (Lu et al. 2009). Another functional Pin1 promoter SNP (rSNP) completely abolishes the ability of transcription factor AP4 to bind to Pin1 promoter and suppress its expression leading to increased Pin1 expression (Lu 2004) (Figure 1.1.5). Additionally, a PIN1 gen is also most drastically suppressed by the tumor suppressor BRCA1 (MacLachlan et al. 2000).

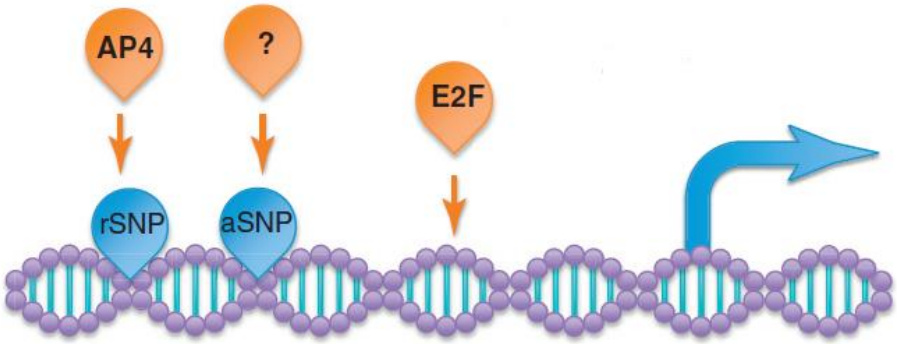

Figure 1.1.5 Molecular mechanism of transcriptional regulation of Pin1. Adapted from (Liou et al. 2011).

Pin1 is also regulated by the multiple post-translational modifications. Its phosphorylation is regulated in a cell-cycle dependent manner (Liou et al. 2011). The Polo-like kinase (Plk-1), a key regulator of mitosis, binds and phosphorylates Ser65 in the catalytic domain. This modification does not impair the enzymatic function of Pin1, but it stabilizes the protein, inhibits its ubiquitylation and later proteasome mediated degradation (Figure 1.1.6B) (Eckerdt et al. 2005). Phosphorylation of Ser16 by protein kinase A (PKA) can regulate the ability of Pin1 to interact with the substrate presumably by forming a hydrogen bond with a critical Arg17 residue (Figure 1.1.6A)(Lu et al. 2007; Lu and Zhou 2007). A similar effect has phosphorylation of Ser71 by death associated kinase-1 (DAPK1), a well-characterized tumor suppressor, which was identified to inhibit isomerase activity of Pin1 in the way that phosphorylated serine residue is forming hydrogen bond with the critical Arg69 residue (Figure 1.1.6C)(Lee et al. 2011).

Another type of the post-translational modifications of Pin1 leads to oxidative inactivation. This occurs in Alzheimers's Disease (Butterfield et al. 2006; Butterfield et al. 2006; Sultana et al. 2006).

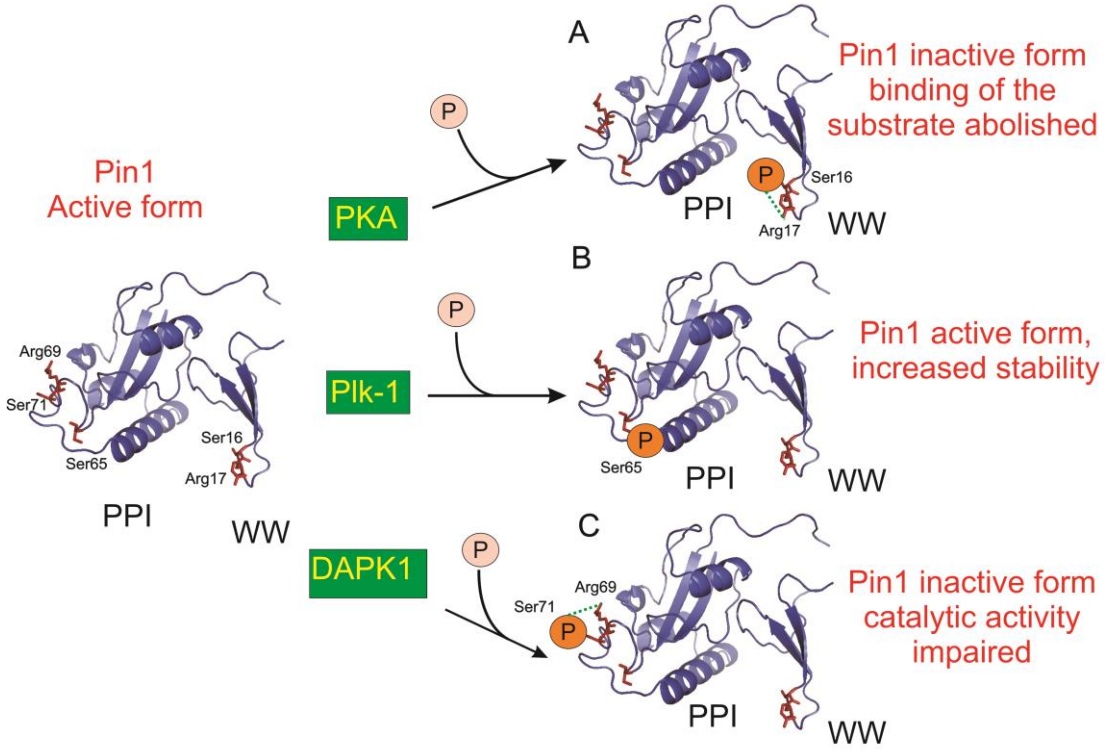

Figure 1.1.6 Molecular mechanism of posttranslational regulation of Pin1.

1.1.3 Pin1 in cell cycle

Pin1 was originally identified as one of three human proteins Pin1-Pin3 that physically interact with the *Aspergillus* mitotic kinase NIMA and functionally suppress its ability to induce mitotic catastrophe in yeast (Lu et al. 1996). Pin1 has a crucial role in mitotic regulation in yeast, mammalian cells and *Xenopus laevis*.

Progression through different phases of the cell cycle is driven by the timely activation and inactivation of different Pro-directed cyclin-dependent kinases (CDKs) (Nurse 2002). Pin1 has been shown to be a regulator of mitotic events by acting on numerous substrates such as CDC25C, Wee1, Emi1 and TopoIIα (Lu and Zhou 2007).

It catalyzes conformational changes in the mitosis-inducing phosphatase CDC25C to regulate its catalytic activity either directly, presumably by phosphorylation on different phosphorylation sites (Shen et al. 1998; Stukenberg and Kirschner 2001) or indirectly via promoting its dephosphorylation (Zhou et al. 2000). Pin1 is allowing normal mitosis progression by binding to Wee-box and inactivating mitosis inhibiting kinase Wee1 (Okamoto and Sagata 2007). In addition, Pin1 stabilizes Early mitotic inhibitor -1 (Emi1), which prevents the anaphase-promoting complex (APC) from acting on cyclin A and B during S and G2 phases. That in turn allows the coordination of S and M phases (Bernis et al. 2007). Finally, Pin1 interacts strongly and specifically with chromosomal DNA during G2/M phase (Figure 1.1.7). It also enhances phosphorylation of major structural protein on mitotic chromosomes: TopoIIα and facilitates its association with DNA (Xu and Manley 2007).

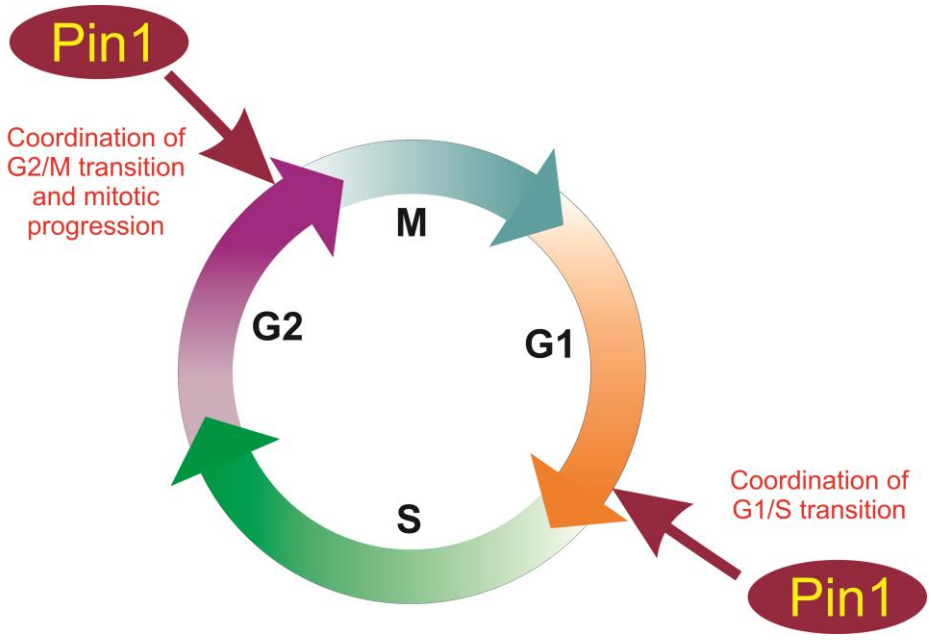

Figure 1.1.7 Schematic presentation of phases of cell cycle. The points under control of Pin1 are marked with red arrows.

Pin1 has also an important role in transition between G0/G1 and S phases, thus its substrates control this process. On one hand Pin1 increases transcription and stability of cyclin D1, a key regulator of G1-S phase progression (Ryo et al. 2001;

Wulf et al. 2001; Liou et al. 2002). On the other hand, Pin1 increases protein turnover of the transcription factor c-Myc and cyclin E, which are important for G1-S transition at different time points (van Drogen and Peter 2004; Yeh et al. 2004)(Figure1.1.7). Additionally, Pin1 has an important role in centrosome duplication and DNA synthesis. In S phase it specifically localizes to the centrosome and its ablation delays centrosome duplication and S phase synthesis. Pin1 overexpression induces centrosome amplification, chromosome aneuploidy and tumorigenesis (Suizu et al. 2006).

1.1.4 Pin1 in disease

Carcinogenesis

Pin1 is overexpressed in 60% of human cancers and this overexpression is correlated with poor clinical outcome (Wulf et al. 2001; Ayala et al. 2003; Bao et al. 2004; Fukuchi et al. 2006; Kuramochi et al. 2006; Leung et al. 2009; Wiegand et al. 2009; Tan et al. 2010). Pin1 activates a number of oncogenes and inactivates many tumor suppressors or growth inhibitors (Figure 1.1.8) (Liou et al. 2011).

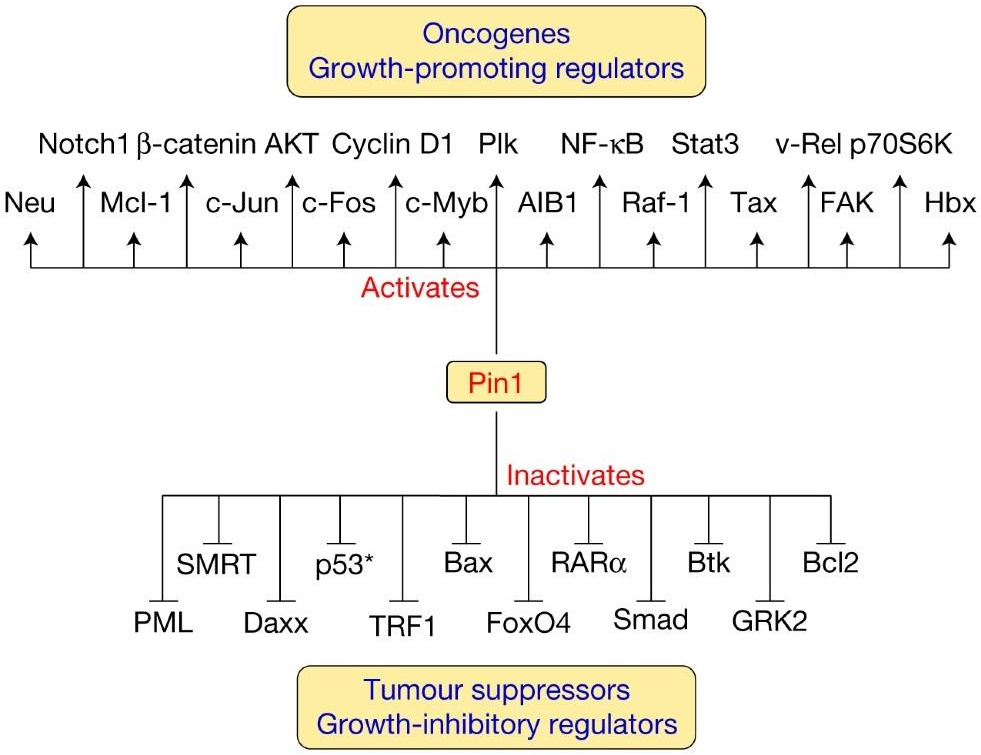

Figure 1.1.8 Pin1 promotes oncogenesis: by activating numerous oncogenes or growth enhancers, and by inactivating tumor suppressors or growth inhibitors (Lee et al. 2011).

Pin1 regulates the function of many transcription factors via many mechanisms including: modulation of transcriptional activity of c-Jun (Wulf et al. 2001) and c-fos (Monje et al. 2005), modulating protein stability of β-catenin (Ryo et al. 2001), NF-κB (Ryo et al. 2003) and c-Myc (Yeh et al. 2004), modulating of both in case of p53 (Wulf et al. 2002; Zacchi et al. 2002; Zheng et al. 2002; Mantovani et al. 2004). Overexpression of Pin1 is closely correlated with high levels of cyclin D1, a cell-cycle protein known to play a key role in the development of many cancers (Sherr CJ, 1996 Yo Q, 2001, Lamb J 2003). Pin1 regulates expression of cyclin D1 by multiple mechanisms including activation of the c-Jun/c-Fos, β-catenin/T-cell transcription factor (TCF) and nuclear factor (NF-κB)(Ryo et al. 2001; Wulf et al. 2001; Ryo et al. 2003). Pin1 can regulate cyclin D1 transcriptionally acting on the transcription factors, as well as post-transnationally by controlling stability of cyclin D1. The first mechanism of cyclin D1 regulation includes activation of MAPK kinase cascade upon growth stimulation of

growth factor receptor Neu which activates *Raf* and then *Ras*. MAP kinase phosphorylates c-Jun and c-fos thereby enhancing AP-1 transcriptional activity toward its downstream targets. MAP kinase also phosphorylates Raf to inactivate Raf in negative feedback loop (Figure 1.1.9 left panel) (Wulf et al. 2001). Pin1 can also regulate cyclin D1 expression on a transcription level by activating via Wnt and cytokine signaling pathways, where Pin1 acts on transcription factors β-catenin and NF-κB, respectively. Pin1 increases the stability of β- catenin by targeting pThr246Pro preventing its binding to adenomatous polyposis coli protein (APC) and thereby enhancing transcriptional activity of its target gens including cyclin D1 (Figure 1.1.9 middle panel)(Ryo et al. 2001). Pin1 can also target pThr254Pro motif in the p65/RelA subunit of NF-κB thereby preventing binding of its inhibitor IκB to p65 resulting in increased stability and transcriptional activity of NF-κB target gens like cyclin D1 and IκB (Figure 1.1.9 right panel)(Ryo et al. 2003). Increased stability of β-catenin and NF-κB prevents these proteins from being inhibited and exported to the cytoplasm for ubiquitin mediated degradation by their respective inhibitors APC and IκB. In addition, Pin1 is an E2F target gen, whose transcription is upregulated in response to activation of *Her/Neu* or *Ras*. Pin1 overexpression can enhance transformed phenotype by *Neu* or *Ras* induced cyclin D1. Furthermore, Pin1 can directly bind cyclin D1 pThr268-Pro, what stabilizes the protein by preventing its nuclear export and ubiquitin mediated degradation (Liou et al. 2002).

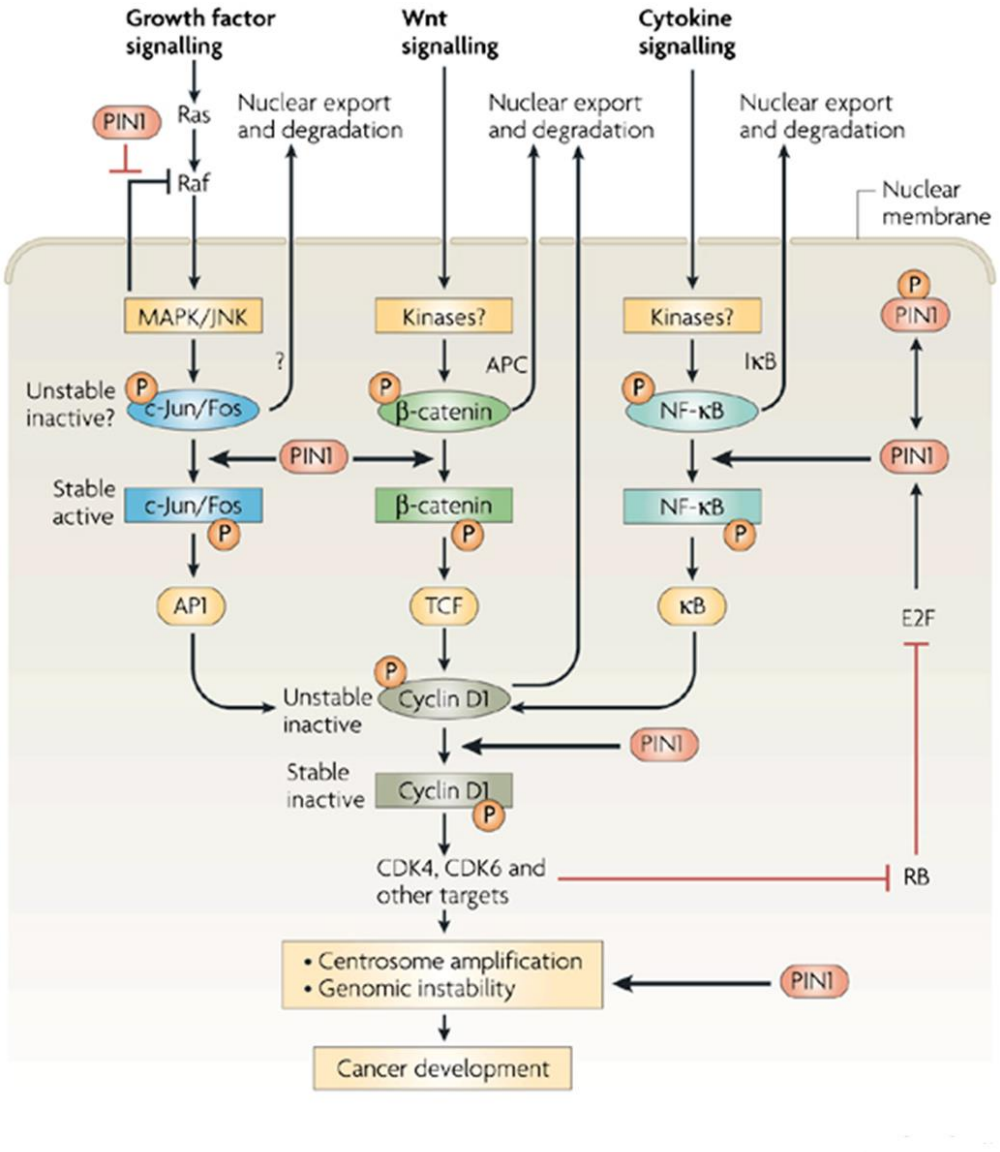

Figure 1.1.9 Pin1 promotes oncogenesis by regulating multiple oncogenic signaling pathways.

Under normal conditions, Pin1 regulates centrosome duplication, but its overexpression can lead to the deregulation, induce centrosome amplification, chromosome instability, and oncogenesis, additionally supporting the role of Pin1 in promoting cancer (Suizu et al. 2006).

Neurological diseases

Pin1 is mainly expressed in most neurons at high levels and its expression is induced during neuronal differentiation (Lu et al. 1996; Lu et al. 1999; Ryo et al. 2001; Wulf et al. 2001; Liou et al. 2003; Hamdane et al. 2006). Under normal conditions Pin1 regulates the biological function of neuronal substrates: tau and amyloid precursor protein (APP) (Liou et al. 2011). Deregulation of these substrates may lead to development of Alzheimer's disease (AD). Tau is a microtubule-binding protein that regulates the cytoskeleton structure by assembling microtubules. Hyperphosphotylation of tau may trigger multiple cellular responses like for example: cell cycle re-entry and deposition of neurofiblirarlly tanges (NFTs) (Balastik et al. 2007). As a result of hyperphosphorylation tau firstly detaches from microtubules leading to destabilization of cytoskeletal structure and cell death (Iqbal et al. 2009). Secondly, it precipitates into insoluble aggregates, forming paired helical filaments comprising later to larger NFTs (Andorfer et al. 2003). Pin1 binds to the pThr231-tau and, by inducing its *cis/trans* isomerization, restores its ability to bind microtubule and promote microtubule assembly (Lu et al. 1999)(Figure 1.1.10). Additionally, Pin1 facilitates tau dephosphorylation by PP2A (Zhou et al. 2000; Hamdane et al. 2006) .

The second mechanism responsible for AD is accumulation of aggressive β-amyloid peptides. APP can be processed by two alternative pathways: amyloidogenic or non-amyloidogenic (Nunan and Small 2002). The pathological, amylidogenic pathway, involves the cleavage of APP by β-secretase generating a soluble stub β-APP and intracellular fragment C99, which is than cleaved by γ-secretase leading to the 39-42 residue Aβ peptides and the APP intracellular domain (Thinakaran and Koo 2008). APP can also be processed through the nonamyloidogenic pathway in which cleavage by α-secretase produces α-APPs having neurotropic properties that prevents the production of Aβ (Mattson 1997). In case of APP, after the Thr668 phosphorylation, APP undergoes a conformational change to a new *cis* population, which exchanges very slowly with the *trans* isomer (Figure 1.1.10B). Pin1 greatly accelerates the pThr668 *cis-trans* isomerization and thereby can promote nonamyloloidogenic APP processing (Pastorino et al. 2006).

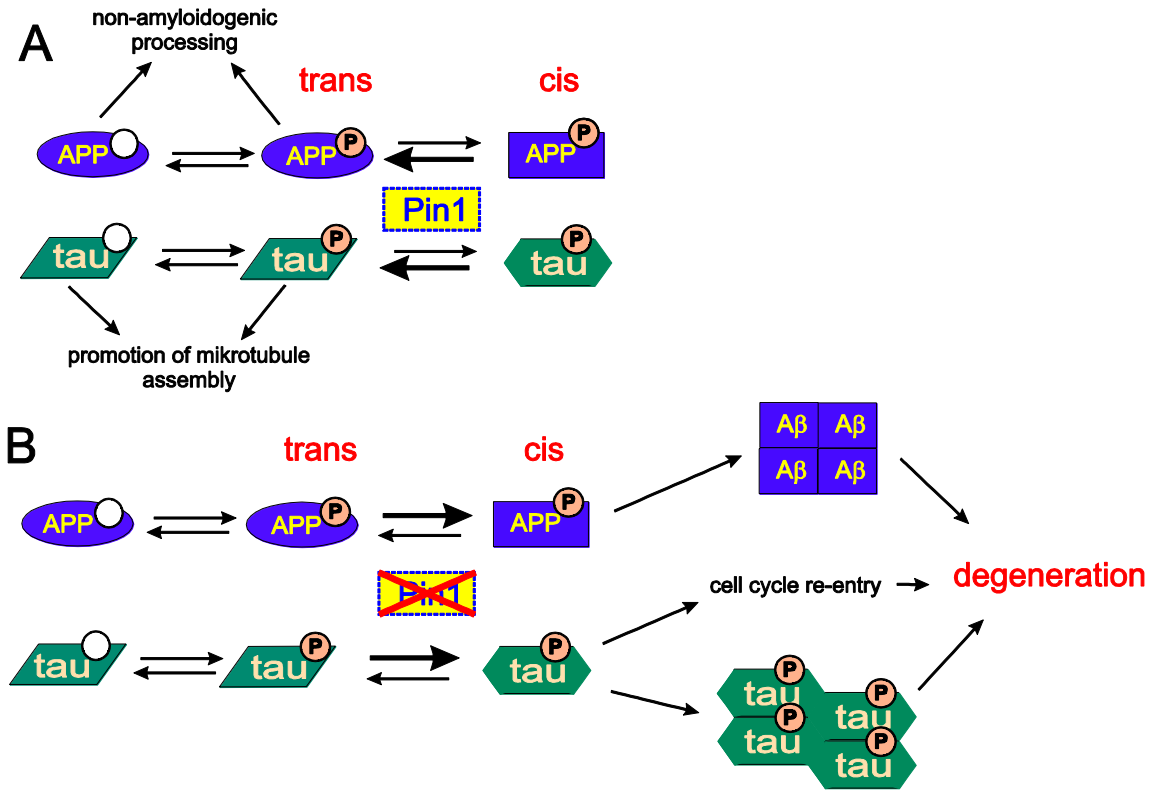

Figure 1.1.10 Schematic presentations of processes in: healthy (A); and Alzheimer's disease neurons (B).

Parkinson's disease is characterized by loss of dopaminergic neurons, formation of Lewi bodies and cytoplasmic inclusions which contain α-synuclein aggregates in surviving neurons (Lotharius and Brundin 2002). Pin1 accumulates in Lewy bodies and enhances the formation of α-synuclein inclusions by protecting α-synuclein from degradation. In this process Pin1 acts not directly, but binds synphylin-1 and the α-synuclein regulatory protein at pSer211Pro and pSer215Pro motifs to enhance its interaction with α-synuclein to facilitate the formation of the α-synuclein inclusions (Ryo et al. 2006).

In addition, Pin1 acts on the scaffolding protein gephrin and it is also crucial for a proper function of lycynergic synapses (Zita et al. 2007). Moreover, Pin1 has been shown to protect against spinal cord injury by preventing the JNK3-induced degradation of Mcl-1, cytochrome c release and apoptosis (Li et al. 2007).

1.1.5 Pin as a promising anticancer target

There are number of unique properties of Pin1 which make it a particularly attractive candidate for cancer diagnosis and treatment:

- Human Pin1 is an enzyme with an extraordinarily high substrate specificity and a well-defined active site (Ranganathan et al. 1997; Yaffe et al. 1997; Shen et al. 1998; Lu et al. 1999; Li et al. 2007).
- Pin1 uses its WW domain to target itself to the substrate, where its PPIase domain isomerises specific phosphorylated Ser/Thr-Pro motifs to regulate protein function (Lu and Zhou 2007). Since, the affinity of the PPIase domain towards substrates is weak; a potent catalytic inhibitor would effectively abolish Pin1 function.
- Pin1 is overexpressed in 60% of human cancers and this overexpression is correlated with poor clinical outcome (Wulf et al. 2001; Ayala et al. 2003; Bao et al. 2004; Fukuchi et al. 2006; Kuramochi et al. 2006; Leung et al. 2009; Wiegand et al. 2009; Tan et al. 2010). However, Pin1 polymorphisms, that reduce Pin1 expression, are associated with reduced cancer risk in humans (Ryo et al. 2001; Wulf et al. 2001; Ayala et al. 2003; Miyashita et al. 2003; Bao et al. 2004; Lu 2004; Pang et al. 2004; Lu et al. 2009; Han et al. 2010).
- Pin1 is required for activation or inactivation of numerous oncogenes or tumor suppressors, respectively (Eckerdt et al. 2005; Lu and Zhou 2007; Lam et al. 2008; Lee et al. 2009; Liao et al. 2009; Rustighi et al. 2009).
- Pin1 overexpression is able to confer transforming properties on normal cells and enhance transformed phenotype induced by other oncogenes such as *Neu* and *Ras* (Wulf et al. 2001; Ryo et al. 2002; You et al. 2002; Ryo et al. 2003). It can cause centrosome amplification, genomic instability, and tumorigenesis *in vitro* and *in vivo* (Suizu et al. 2006).
- Pin1 inhibition in cancer cells induces apoptosis or suppresses the transformed phenotype (Lu et al. 1996).

Although inhibitors of other PPIase families have been widely used clinically, they do not act on Pin1. Until now no clinically useful small-molecule inhibitors of Pin1 have

been developed (Liou et al. 2011). The known Pin1 inhibitors are: the natural product, Juglone (Hennig et al. 1998) and a small molecule PiB and its derivatives (Uchida et al. 2003). Juglone covalently inactivates a unique cysteine residue in the active site of Pin1 isomerases and has been used as a Pin1 inhibitor in several studies *in vitro*. However, given that Juglone potently inhibits many other proteins and enzymes (Chao et al. 2001; Ryo et al. 2003; Uchida et al. 2003), it is unlikely to be specific toward Pin1 in the cell. Similar to Juglone, PiB and its analogs also inhibit non-phosphorylation-specific prolyl isomerases such as Par14 (Hennig et al. 1998; Uchida et al. 2003). The remaining Pin1 inhibitors, identified by the PPIase binding-based screens, structure-based drug design or substrate-based drug design, either cannot enter cells or simply do not have enough potency (Wildemann et al. 2006; Zhang et al. 2007; Zhao and Etzkorn 2007; Guo et al. 2009; Xu and Etzkorn 2009; Dong et al. 2010; Potter et al. 2010) with the possible exception of the less-potent cyclic peptide inhibitor of Pin1 (Liu et al. 2010). Therefore, there is an urgent need for the development of highly specific and potent Pin1 inhibitor. The developed of such inhibitors might be highly effective anticancer drugs alone or in combination with established chemotherapeutic drugs or procedures (Lu et al. 2006).

1.2 MDM2/MDMX and p53

1.2.1 p53 a genome guardian

The protein p53 was identified in SV transformed cells where it is associated with Large T Antigen (Lane and Crawford 1979). p53, through its N-terminal domain, activates more than 300 different promoter elements (Zhao et al. 2000) thus modulating expression of several target gens. The protein is involved in a number of cellular processes such as: cell cycle arrest, senescence and apoptosis. This is why p53 is a powerful transcription factor and it has an essential function in protecting from an inappropriate cell proliferation and in maintaining genome integrity following genotoxic stress. In absence of an exogenous stress there is a balanced turnover of p53 and MDM2/MDMX. The protein has low expression levels and a short half-time because of a negative feedback loop mediated by MDM2 (Wu et al. 1993).

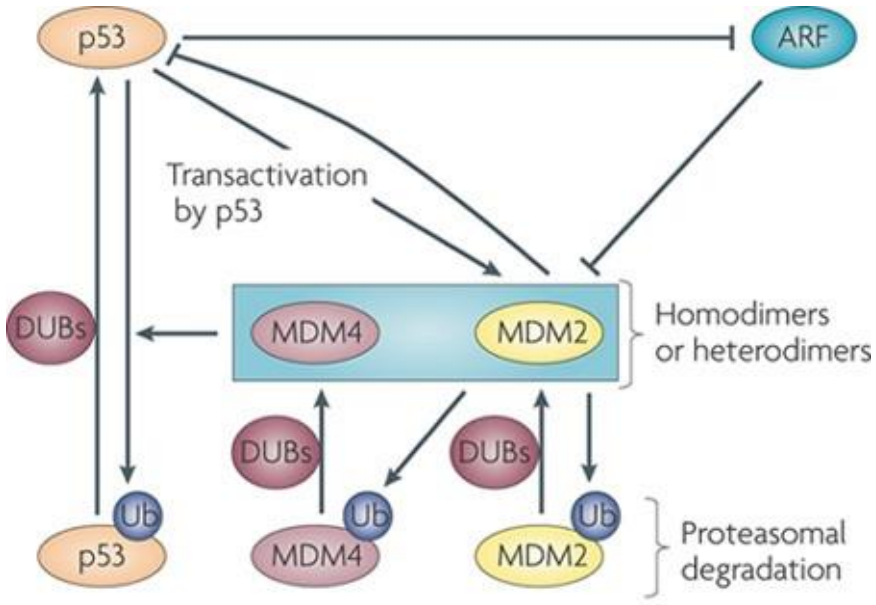

Figure 1.2.1 Negative feedback loop controls cellular levels of p53. Figure adapted from Brown et al. 2009.

The regulation of p53 and MDM2/MDMX is tightly connected (Figure 1.2.1). p53 increases transcription of MDM2 over the basal level and on the other hand MDM2 also inhibits p53 function by modulating its transcriptional activity by

preventing its interaction with the general transcription machinery (Momand et al. 1992). In addition to degrading p53, MDM2 also undergoes auto-degradation (Stommel and Wahl 2004) and targets MDMX for proteasome degradation (de Graaf et al. 2003; Kawai et al. 2003; Pan and Chen 2003). ARF (also known in humans as p14ARF) adds another level in control to the system by inhibiting MDM2 function (Zhang and Xiong 2001), the expression of which is in turn also repressed by p53 (Robertson and Jones 1998).

1.2.2 p53 structure

The human p53 protein contains 393 amino acids and has been divided structurally and functionally into four domains (Figure 1.2.2). The first 61 amino acids at the N-terminus are natively unfolded and constitute a transcriptional activation domain (TAD), divided into two subdomains TAD1(1-40) and TAD2 (40-61). It is a binding site for a multitude of interacting proteins like: components of the transcription machinery, the transcription co-activators p300/CBP (CREB-binding protein) or negative regulators MDM2/MDMX (Kussie et al. 1996; Schon et al. 2002; Marine and Jochemsen 2005). The Proline Rich Region (PRR), which links TAD and the DNA-binding domain in human p53 was identified to contain five PXXP motifs, but their exact role until now is poorly understood.

Figure 1.2.2 Domain organization of full-length p53; TAD1 and TAD2 – N-terminal transactivation domain (TAD), proline rich region (PRR), DNA-binding domain, tetramerization domain (TET), C terminus (CT).

The sequence specific DNA-binding domain is localized between amino acids 94 and 292 in a primary sequence. It is protease resistant and independently folded domain containing Zn^{2+} ion which is required for its sequence specific DNA-binding activity. The domain folds into a four-standed and five-standed anti parallel β-sheets that provide a

basic scaffold for the DNA-binding surface. This surface can be divided into two structural motifs that bind the minor and major groove. Loop L1, β-stands S2 and S2', parts of β-stands S10 and the C-terminal helix and in the major groove: two large loops L2 and L3 stabilized by a Zn ion (Figure 1.2.3)(Joerger and Fersht 2008).

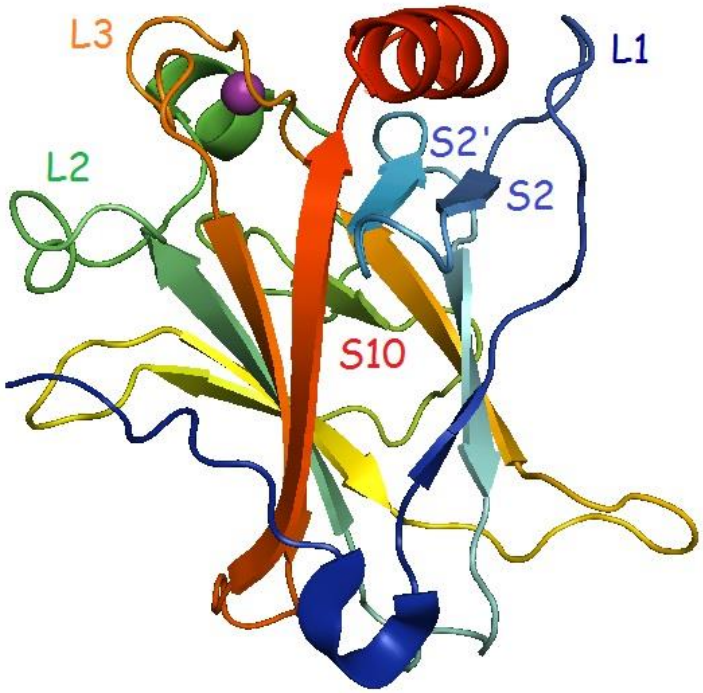

Figure 1.2.3 Structure of DNA binding domain shown in rainbow color gradient blue to red (PDB entry: 2OCJ).

The native p53 is a tetramer in solution and amino acids residues 325-356 of tetramerization domain are required for the oligomerization of the protein. The structure of this domain contains a dimer of primary dimers with two short β- sheets and two α- helices linked by a sharp turn. Two dimers are held together by a large hydrophobic surface of each helix pair, which than forms a four helix bundle (Figure1.2.4) (Jeffrey et al. 1995).

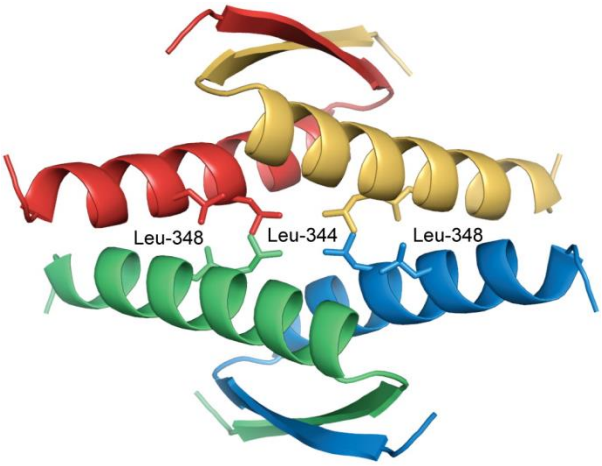

Figure 1.2.4 Assembly of the p53 tetramerization domain as a dimer of dimers (PDB entry: 1C26) adapted from Joerger and Fersht 2008.

The tetramerization domain (TET) is linked to the sequence–specific DNA binding domain by a flexible linker of 37 residues (287-323) (Jeffrey et al. 1995). The 26 amino acids on the C-terminal (CT) are intrinsically disordered, but may undergo local disorder-to-order transitions upon binding to other proteins or nonspecific DNA (Lee et al. 1994; Joerger and Fersht 2008).

1.2.3 The MDM2 and MDMX structures

The human MDM2 is a phosphoprotein and interacts through its N-terminal domain with p53. It is a E3 ligase that ubiquitinates p53 (Kussie et al. 1996; Haupt et al. 1997) for proteasome degradation (Haupt et al. 1997; Kubbutat et al. 1997) and modulates its nuclear export (Geyer et al. 2000). MDMX is not an E3 ligase (Shvarts et al. 1996; Finch et al. 2002), but it cooperates with MDM2 biochemically by forming MDM2-MDMX heterooligomers, which are much more effective in targeting p53 for ubiquitynation and degradation than MDM2 homooligomers. MDMX is being degraded by the ubiquitin ligase activity of MDM2 (Migliorini et al. 2002).

Human MDM2 and MDMX are structurally related proteins of 490 and 491 amino acids, respectively. The greatest similarity of more than 50% between them is at the N-terminus, a region comprising p53-binding domain. The residues required for the interaction with p53 are strictly conserved in MDM2 and MDMX (Shvarts et al. 1996) and

on the other hand within p53 the same residues are required for interaction with both MDM2 as well as with MDMX. Two signaling sequences: NES-nuclear export sequence and NLS- nuclear localization sequence are present in MDM2. The central region of MDM2 and MDMX show no significant similarity. However, both proteins are rich in acidic residues and have a Zn-finger.

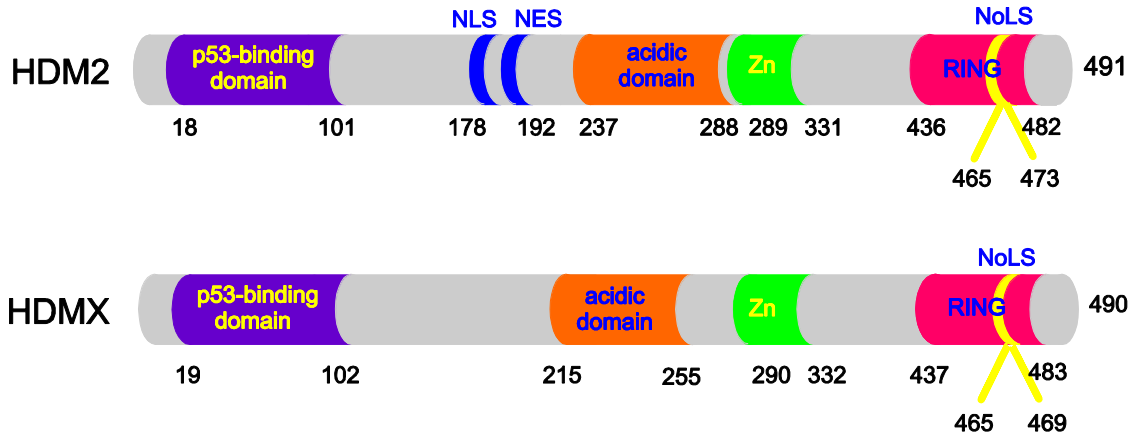

Figure 1.2.5 Domain organization of the full-length human MDM2 and MDMX; the p53-binding domain, the nuclear localization sequence (NLS), the nuclear export sequence (NES), an acidic domain, the zinc finger (Zn), the ring domain (RING),the nucleoar localization sequence (NoLS).

The C-terminal segments are another well-conserved region of MDM2 and MDMX. They contain a RING (really interesting new gene) domain of the rare type C2H2C4 type (Kostic et al. 2006). This nomenclature refers to the cysteine and histidine residues required to form a Zn^{2+} chelating structure important for the ring function (Brooks and Gu 2006). Within the RING domain in both proteins there are signaling sequences responsible for the MDM2/X nucleoar localization (NoLS).

1.2.4 Interaction of p53 with MDM2/X

Traditional understanding of the protein structure and function relationship relies on protein function being critically dependent on a well-defined three dimensional protein structure. However, recent studies have revealed that the true functional state for many proteins and protein domains is intrinsically unstructured (Mohan et al. 2006). An example of such a domain is a transactivation domain of p53, TAD1. Its fragment

comprising residues 15-29, adopts α-helical conformation upon binding to a hydrophobic cleft in the N-terminal domain of MDM2 and MDMX.

MDM2 and MDMX are structural analogs; they both have same folding mode composed of two approximately 40 residue long repetitions β1α1β2α2β3 and β1'α1'β2'α2'β3' (Figure1.2.6).

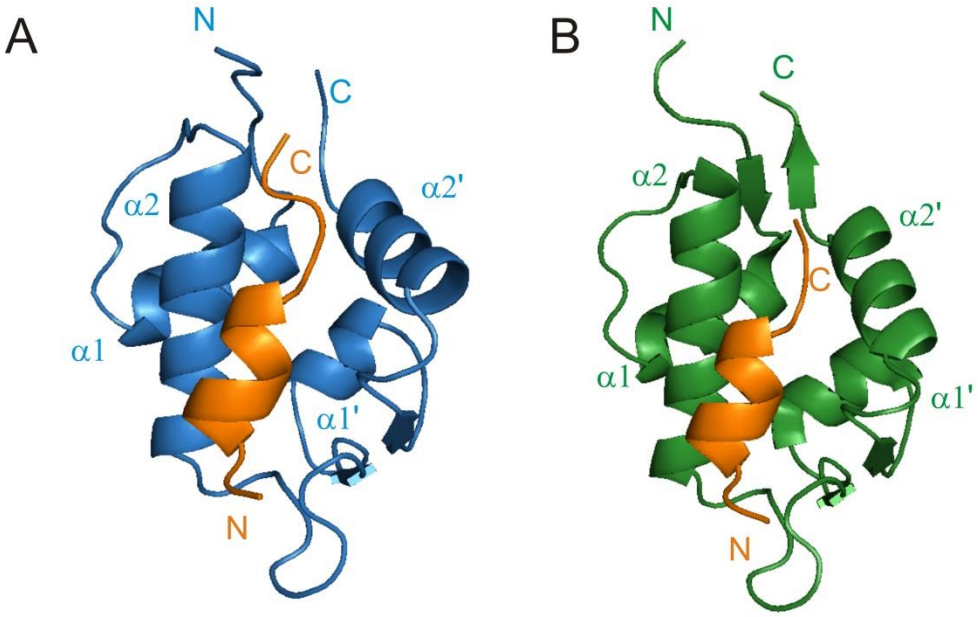

Figure 1.2.6 The overall fold of a complex of the human p53 peptide (15-29) and a human MDM2 (A); MDMX (B).

The long helices (α2 and α2') form the sides of the cleft and short helices (α1 and α1') constitute its bottom, β strands formed by two β-sheets at the opposite ends of the cleft, cap its end. Despite the fact that both proteins contain the repeats of the secondary structure their binding cleft is not symmetric. Helix α2 is about one turn longer than the corresponding helix α2' and a middle β-sheet is larger than the terminal. As a result the cleft is wide and deep within the part responsible for the primary hydrophobic contacts with the p53 helix. The remaining part is narrower and shallower and its character is only little hydrophobic (Kussie et al. 1996).

The nature of the interaction between MDM2/X and p53 is mostly hydrophobic. The exact analysis of the residues responsible for binding of p53 shows that the critical residues are: Phe19, Leu22, Trp23 and Leu26, which stabilize hydrophobic interactions

within the binding pocket. The two residues Phe19 and Trp23 of p53 form hydrogen bonds with Gln72 and Leu54, Leu53 of MDMX (Kussie et al. 1996) (Figure 1.2.7).

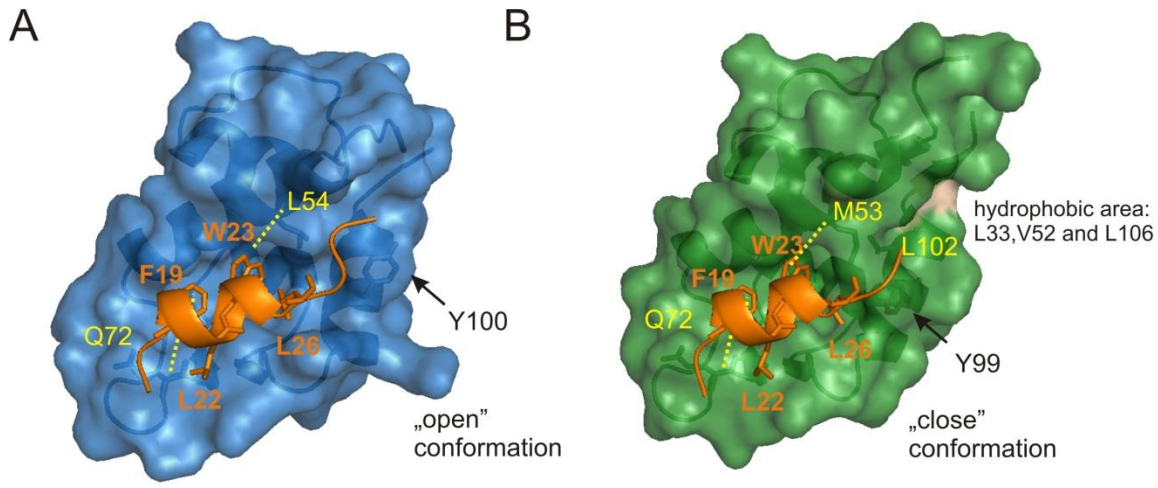

Figure 1.2.7. Binding mode of p53 peptide (15-29) with the human: MDM2 (A); MDMX (B).

Despite the fact that MDM2 and MDMX are structural analogs and they show significant structural similarity, the binding cleft is not identical. The specific feature of the binding cleft of MDMX is that it is smaller than in MDM2 because Met53 and Tyr99 (Figure 1.2.7 B) protrude into the binding pocket thus blocking the part of the cleft (Popowicz et al. 2007; Popowicz et al. 2008). Additionally, the Met50 side-chain is bigger than the analogous Leu46 of MDM2. Significant differences are also observed in Leu26-binding pocket. In MDMX Met53 side-chain is located there and it is bigger than Leu53 in MDM2. Another important difference is the presence of the secondary hydrophobic area in proximity of Leu26 formed by Leu33, Val52 and Leu106 separated from the Leu26 binding site by the side chains of Met53 and Leu102 (Figure 1.2.7 B). Moreover, the region Pro95-Tyr99 of MDMX has different shape. Tyr99 shows the "close conformation", different to Tyr100, where we can observe that this residue is flipped away from the binding pocket in the "open conformation" (Figure 1.2.7.A) (Popowicz et al. 2008).

1.2.5 p53 in cancer

p53 is a key protein responsible for cell's defense against cancer. p53 can arrest the cell cycle in potentially cancerous cell and induce apoptosis (Vogelstein 2000, Vousden 2002).

In approximately 50% of all human cancers function of p53 is inactivated directly by mutations (Hollstein et al. 1994). The mutations are mostly localized within the DNA-binding domain (Olivier et al. 2002) and can be divided into two groups: contact and structural mutations, depending on weather they directly contact DNA or play a role in the structural integrity of the DNA-binding surface. It has been also shown that mutations not only impair tumor suppressive properties of p53, but also significantly destabilize already unstable core domain (Bullock and Fersht 2001). There are known approaches, like peptides (Friedler et al. 2002), antibodies (Foster et al. 1999; Mayer et al. 1999), and small molecules (Boeckler et al. 2008), which rescue many diverse mutants mostly leading to their thermal stabilization.

In tumors having wild-type p53, in a significant percentage, inactivation of p53 occurs through overexpression and/or amplification of MDM2/X (Momand et al. 1998). In this case the therapy would be focused on dissociating the MDM2/X complex in order to recover the p53 function.

1.2.6 Targeting MDM2/X and p53 interaction

The development of a new drug to treat cancer has undergone a renaissance in the past decade, spearheaded by the development of both small-molecule and biological agents that have shown remarkable clinical activity, without the toxicity associated with the conventional cytotoxic therapy. However, the new agents are highly selective and effective only in minority of cancers, which are identified by specific lesions or alterations (Brown et al. 2009). Inhibiting p53 may deliver a possibility for universal and non-invasive cancer therapy.

The early studies on the MDM2/X inhibitors have led to the discovery of the peptides (Picksley et al. 1994). As a result of numerous experiments, based on different approaches like: mutation or applications of p53 peptides containing non-natural amino

acid variants of p53 with the nanomolar potency towards MDM2/X have been developed (Czarna et al. 2009; Pazgier et al. 2009). However, application of peptides as inhibitory agents has a number of drawbacks. Despite the high potency peptides displayed only modest effect in cellular context, mostly because of a poor membrane permeability and protease digestion. One possibility to improve a therapeutic potential of peptides is to minimize their proteolysis. This approach resulted in a design of the proteolysis resistant D-peptides (Liu et al. 2010). Another possibility is converting linear peptides into cyclic forms by the means of chemical crosslinking using modified amino acids. Such process, called stapling, converts linear peptides into drug-like molecules. The staple makes peptides resistant to proteolytic digestion and also, by altering their character distribution and biophysical properties, it makes them more effective biologically (Moellering et al. 2009).

The sites of protein-protein interactions are usually large and shallow. The high affinity is achieved through the summation of many week interactions. Surfaces of several protein-protein interactions are not featureless an do not rely on wide distribution of weak interactions, but they are mediated by a set of key interactions that contribute to a large component of the binding affinity. A small molecule must efficiently mimic these interactions while maintaining good drug-like properties (Clackson and Wells 1995). An example of such an interaction is interaction of MDM2/X with p53, what makes it a promising drug target.

The first potent small-molecule MDM2 antagonist, Nutlin, belongs to a class of *cis*-imidazoline compounds. It was identified by the means of combined methods of high-throughput screening and structure-based drug design (Vassilev 2004). After several steps of optimization Nutlin-3 has gained the inhibitory potency of 90 nM.

Analysis of the crystallographic structure has demonstrated that nutlin-2 (Figure 1.2.8 A) binds to the p53 pocket of MDM2 in the way that is remarkably mimicks the interaction of the three key amino acids of p53 (Figure 1.2.8 B and C). One bromophenyl moiety sits deeply in the Trp23 binding pocket, the other occupies Leu26 binding site and the ethyl ether side chain is directed towards the Phe19 pocket. The hydroxyl group forms the hydrogen bond with the side-chain of Gln72. Conformation of Tyr100 in the complex with Nutlin-2 is pointing into the pocket, different from the one

observed in the complex with the p53 peptide, for which the “induced fit” is observed upon binding. Nutlin-3 inhibits MDM2-p53 interaction leading to activation of p53 pathway also in cell-based tests (Vassilev et al. 2004).

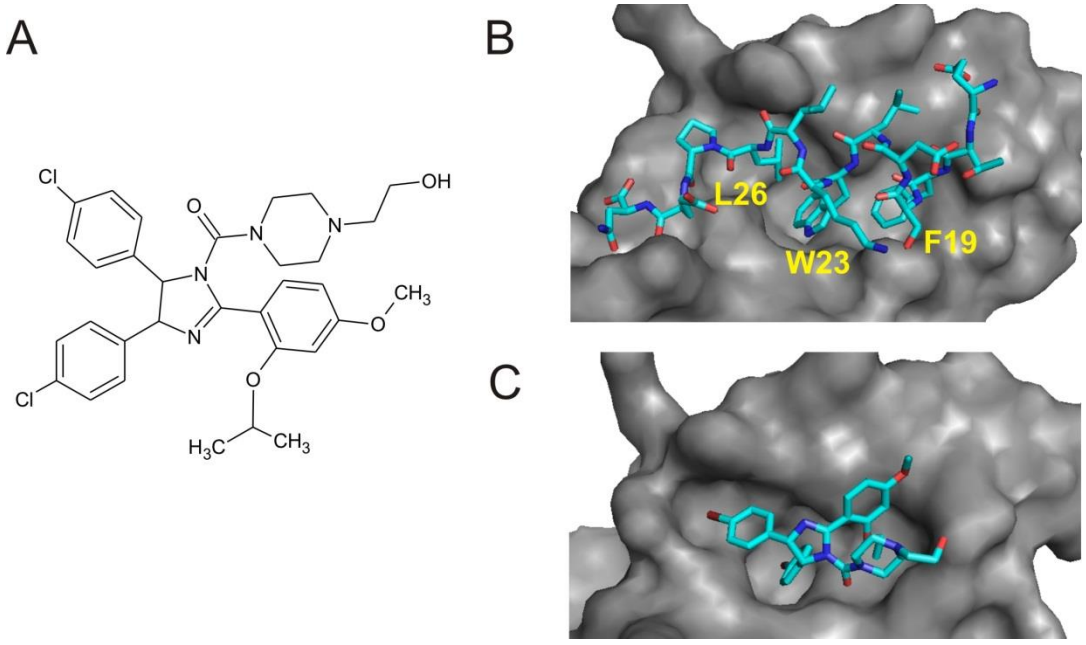

Figure 1.2.8 Structure of Nutlin-2 (A); Structure of human MDM2: with a p53 peptide (residues: 15-29) (PDB entry: 1YCR)(B); with Nutlin-2 (PDB entry: 1RV1)(C).

Further investigations have led to discovery of the compound from the family of benzodiazepines, named TDP222669, which after several steps of optimization, improving its bioavailability, gained Ki of 80nM in vitro. (Grasberger et al. 2005). The binding pattern of the compound is similar to Nutlin-2 (Figure 1.2.9 A). The two para-chlorophenyl rings occupy the Trp23 and Leu26 binding pockets, and the iodo-phenyl group is located in Phe19 pocket. Here also can be observed the induced fit, similar to the one which takes place upon binding of Nutlin-2.

The two other compounds MI-63 and MI-219 are spiro-oxoindole derivatives (Gomez-Monterrey et al. 2010), which have inhibitory potential towards MDM2: 5 and 3 nM, respectively (Ding et al. 2006). One of the analogs of MI-63 has been crystalized (Figure 1.2.9 B). The structure has shown, that oxindole closely matches the interaction made by Trp23, the spirooxo-pyrrolidine ring in these molecule provides a rigid scaffold that can mimic the interactions of the side chains of Phe19 and Leu26. Tyr100 of MDM2

is in this case in an “open” conformation thus allowing enough space for the halogen atom (Popowicz et al. 2010).

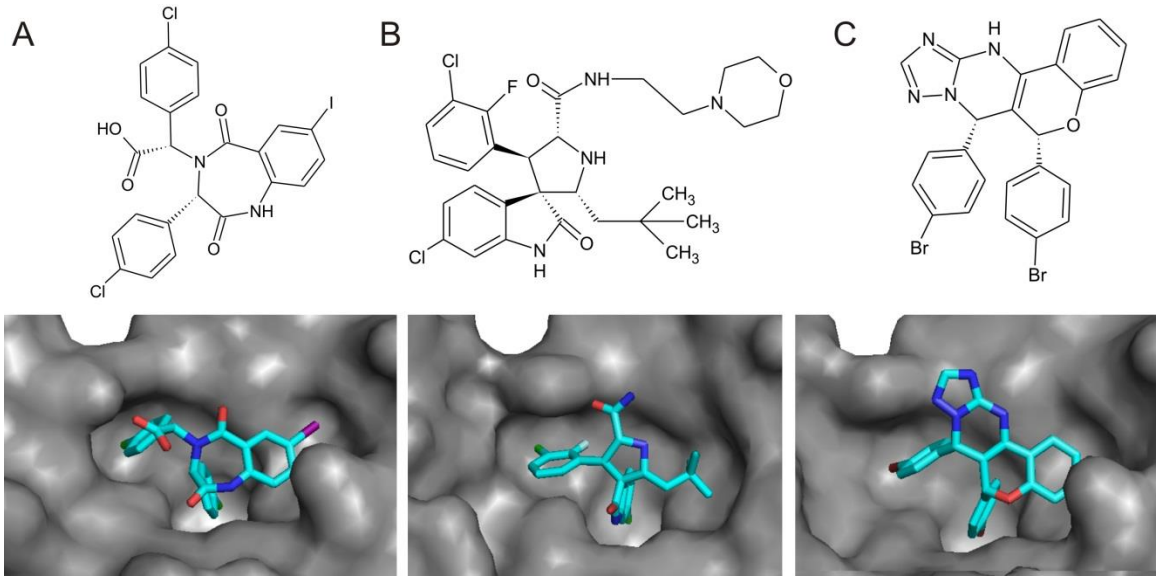

Figure 1.2.9 Structure of human MDM2 with inhibitors:TDP222669: PDB entry: 1T4E(A); MI-63 analog: PDB entry: 3LBL (B); chromenotriazolopyrimidine1: PDB entry: 3JZK (C).

One of the most recent findings in the inhibitors of p53-MDM2/X interactions was a representative of chromenotriazolopyrimidines. The fairly rigid chromenotriazolo-pyrimidine core was shown to be an efficient scaffold from which two substituents can projet into the key p53 binding pockets of the MDM2 protein. The binding occurs in the similar fashion as that in the binding of Nutlin-2 (Figure 1.2.9 C). The two bromophenyl rings occupy the Trp23 and Leu26 pockets of MDM2 and benzene ring is located in Phe19 binding site (Allen et al. 2009).

All of the mentioned compounds show up to nano molar activity towards MDM2, but their binding to MDMX was in the middle micro molar range. It was concluded that small difference in the structure between MDM2 and MDMX lead to significant differences in their affinities towards small binding molecules (Popowicz et al. 2008; Czarna et al. 2009). All known small molecule inhibitors were optimized towards MDM2., Due to the missing crystallographic structure of MDMX it was not possible to optimize the compounds in the way which would improve their affinity to MDMX. Lately, two groups simultaneously have developed a compound from imidazo-indole core family

named WW298 or Novartis-101, a candidate for being a MDM2/X dual inhibitor (Figure 1.2.10).

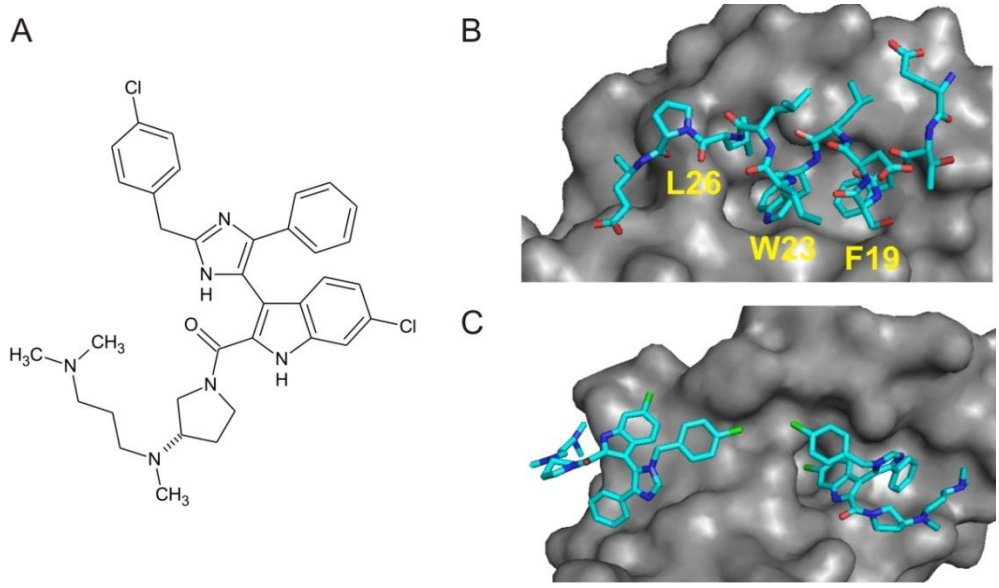

Figure 1.2.10 Structure of WW298/Novartis-101(A); Structure of human MDMX: with a p53 peptide (residues: 15-29) (PDB entry: 3DAB) (B); with WW298/Novartis-101 (PDB entry: 1LBJ) (C).

Despite the moderate affinity to MDMX, the compound was the first small-molecule inhibitor whose structure was solved in a co-crystal with MDMX. The WK298 binds to MDMX in the way mimicking the interaction of the native peptide; the Trp23 pocket is filed with the 6-chloroindole group, which builds a hydrogen bond with Met53, the 4-chlorobenzyl ring penetrates the Leu26 pocket and the phenyl ring fills the Phe19 pocket. Upon binding of the ligand the general fold of the MDMX remains unchanged when compared to the complex with p53 peptide. However, the binding pocket undergoes substantial induced fit: the effect is visible in the whole Trp23 pocket and propagates into Leu26 pocket, the position of Tyr99 is altered, but remains in a close orientation.

The ideal case would be to compare this structure with the structure of the same compound with MDM2. Unfortunately such crystals were not obtained, but only the crystals and the structure of the compound from the same family, WK23 (Figure 1.2.11).

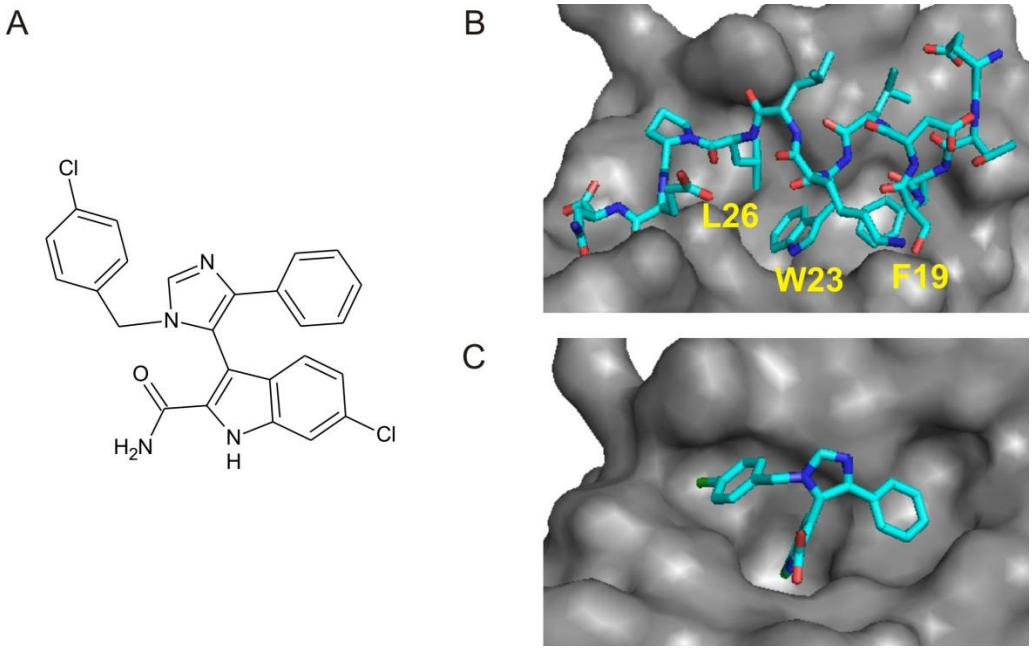

Figure 1.2.11 Structure of WK23 (A); Structure of human MDM2: with a p53 peptide (residues: 15-29) (PDB entry: 1YCR) (B); with WK23 (PDB entry: 1LBJ) (C).

The compound efficiently fills the whole p53 binding pocket of MDM2. Despite the differences between the binding pockets of MDM2 and MDMX the 4-chlorobenzyl fills the Leu26 subpocket and 6-chloroindole ring substitutes the native tryptophan. These two groups seem to be suitable for both proteins. The major challenge for developing the dual inhibitor is Leu26 pocket. The chlorophenyl group present in all known MDM2 inhibitors is not optimal for MDMX. While the position of Tyr100 is varying among the structures with MDM2 inhibitors the equivalent Tyr99 remains in the closed conformation and this feature must be taken into account when optimizing the inhibitors towards MDMX (Popowicz et al. 2010; Popowicz et al. 2011).

1.3 NMR for drug discovery

Currently, the drug discovery process within the pharmaceutical industry employs high-throughput screening, identifying lead compounds, optimizing the “hits” and validating therapeutic targets. There are several features of NMR which make it an effective tool at multiple steps in the drug discovery pathway. Firstly, NMR directly detects interaction between the ligand and the protein. Secondly, the measurement can be performed under native conditions. Additionally, information on the binding site and affinity are obtained readily (Stark and Powers 2012).

NMR screening methods are based on the difference of magnetic properties between the free protein or ligand and a protein-ligand complex. They can be divided into two groups: ligand-based in which changes in the spectrum of a ligand (Ludwig and Guenther 2009) or a target-based in which changes within the spectrum of a protein upon binding of a ligand are being observed.

The differences in a spectrum between the ligand and ligand-protein complex in the ligand-based methods are the result of a significant difference of molecular weight between the small-molecule ligand and usually much bigger target protein (Stark and Powers 2012). As a result of binding several events can be observed in the ligand spectrum; ligand adopts the properties of the larger molecular-weight protein: increasing typically low for small molecules relaxation rate R2, producing positive NOE cross-peaks and decreasing translational diffusion coefficient (Lepre et al. 2004). The ligand-based method is fast (up to 10 min.), it is mostly performed as a 1D ^{1}H-NMR experiment, allows checking a mixture of the compounds simultaneously and does not require isotopic labeling of the protein, as well as it is possible to examine the compounds not only qualitatively but also quantitatively (Pellecchia et al. 2002). However, the method does not provide structural information about the protein ligand-complex.

The target-based screening focuses on the changes of the protein spectrum upon binding of the small molecule ligand. Since the 1D spectrum in this case is too complex, 2D heteronuclear experiments, 2D ^{1}H,^{13}C/^{15}N NOESY/TOCSY, are used (Muhandiram et al. 1997). These experiments require protein labeling and much longer acquisitions. However, they provide information about a ligand binding site on the protein. Based on the analysis of the chemical shift perturbation upon titration with a

ligand, it is also possible to estimate K_D in this approach. Recent advances like: SOFAST-HMQC experiment (Schanda and Brutscher 2005; Schanda et al. 2005) and the Fast HSQC (Mori et al. 1995; Mercier et al. 2006) experiment have decreased the time and amount of the protein necessary for the measurement

1.3.1 AIDA

We have recently described an NMR-based assay for studying the effect of antagonists on protein−protein interactions (D'Silva et al. 2005; Rothweiler et al. 2008). The method, named AIDA-NMR (for the Antagonist Induced Dissociation Assay-NMR), belongs to the target protein-detected NMR screening methods (Pellecchia et al. 2008) and provides unambiguous information on whether an antagonist of a protein−protein interaction is strong enough to dissociate the complex and whether its action is through denaturation, precipitation, or release of a protein in its functional folded state.

The experiment is based on binding of two proteins of a different molecular weight, the small one (less than 20kDa) is either ^{15}N or ^{13}C labeled and the second one bigger (larger than 30kDa) is not labeled. Upon titration the lines of the $^{15}N/^{13}C$-HSQC spectrum of the smaller protein gets broaden, what can finally lead to a complete disappearance of the NMR resonances.

Addition of a potent inhibitor causes dissociation of the complex as a result of binding to one of the proteins. The release of the labeled protein leads to recovery of the NMR spectrum (Figure 1.3.1). This approach can be applied for all proteins which fulfill the mentioned criteria. The method requires labeling and relatively high amounts of the protein.

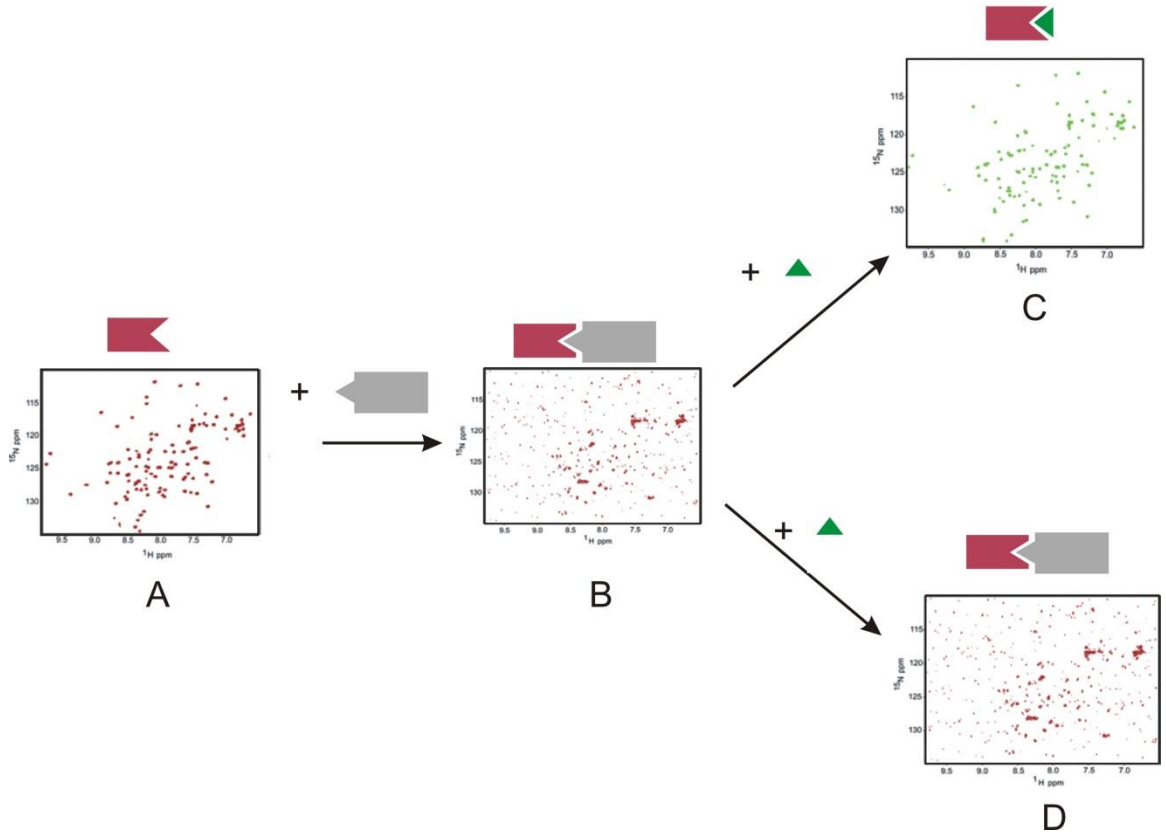

Figure 1.3.1 Schematic presentation of 2D AIDA-NMR; the ^{1}H-^{15}N/^{13}C spectrum of: a labeled protein (A); the protein from (A) upon addition of a binding partner (B); spectrum of protein from (A) after addition of a potent inhibitor (C); protein from (A) after addition of a not binding inhibitor (D).

For 1D proton NMR variant of AIDA on unlabeled proteins (Figure 1.3.2), one must have or introduce an amino acid "reporter" that has at least one non overlapped NMR signal sensitive to the binding of a ligand to the investigated protein. Since signal overlap in proton 1D spectra of proteins may present a problem. That is why we have chosen to use tryptophan, because it is the only amino acid whose $^{N}H^{\epsilon}$ indole side chain gives an NMR signal at ~10 ppm at physiological pH. The signal is well separated from the bulk of amide protons and can be easily monitored. In order to be used in our NMR assay, the Trp residue must be positioned near a potential antagonist binding site and, importantly, its indole side-chain must be flexible so that its high motion gets restricted upon binding of the Trp-reporter protein to its proteinous target.

By using tryptophan-bearing proteins, we showed that a 1D proton NMR version of AIDA-NMR is faster than the 2D version and can be used universally in competition

experiments for monitoring ligand/protein−protein complexes (D'Silva et al. 2005; Krajewski et al. 2007; Rothweiler et al. 2008). In addition, such tryptophan-containing proteins can be used for studying binary interactions between ligands and target proteins with 1D NMR.

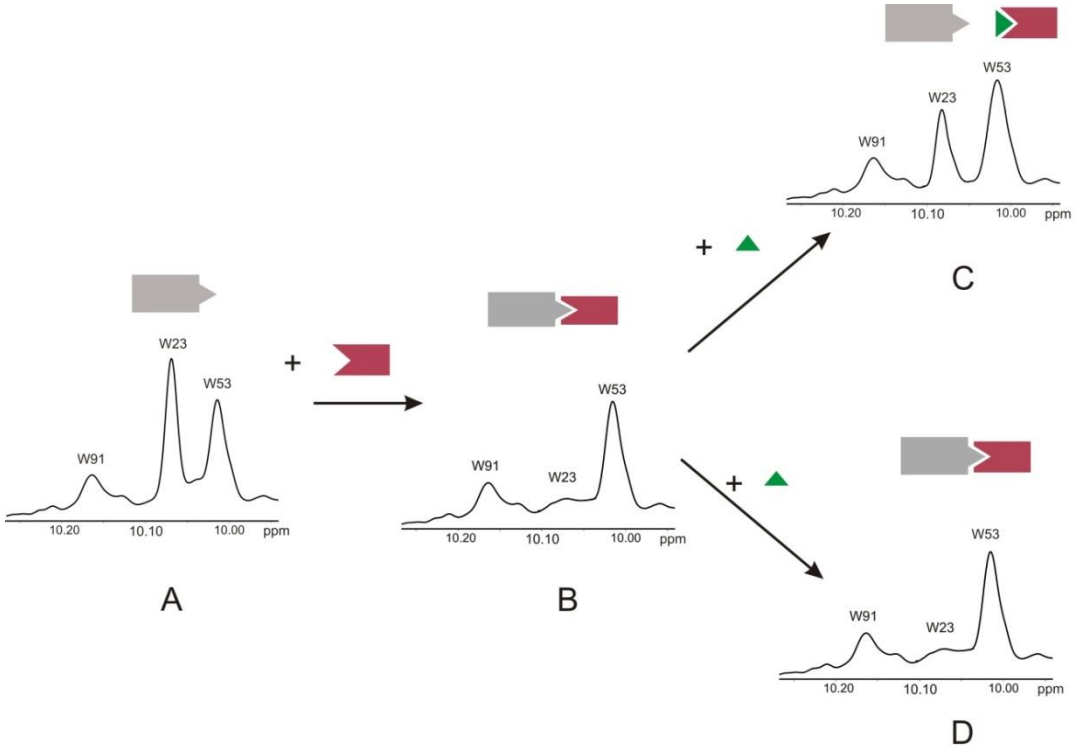

Figure 1.3.2 Schematic presentation of 1D AIDA-NMR; (A) 1D ^{1}H spectrum of protein with well-dissolved tryptophan resonances in this case p53 (residues 1-321); (B) the protein from (A) upon addition of a binding partner MDM2 or MDMX; (C) spectrum of protein from (A) after addition of a potent inhibitor; (D); spectrum of the protein from (A) after addition of a not binding inhibitor.

In case of the interaction of MDM2/X with p53 the two-dimensional assay can be simplified to 1D proton experiment without introducing additional reporter tryptophan residue. p53 itself contains tree tryptophan residues Trp23, Trp53, Trp91 which have well-separated NH indole side chain NH^{ε} signals at around 10 ppm in physiological pH so are perfectly suitable to be used in the 1D AIDA-NMR experiment.

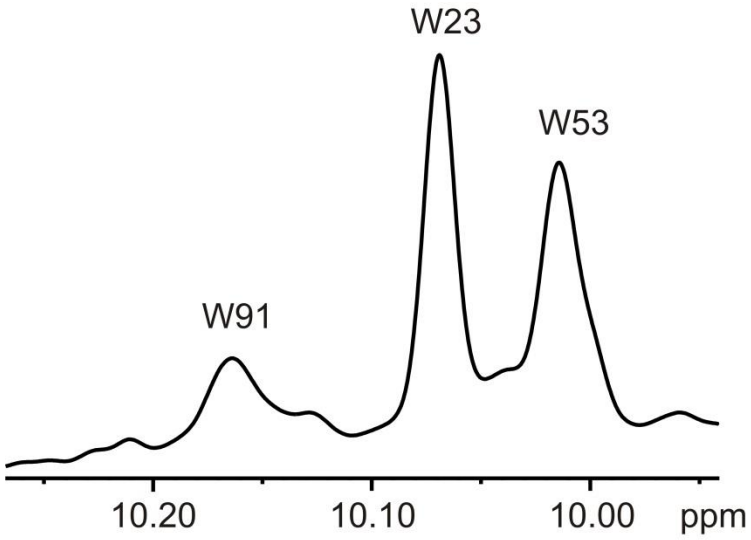

Figure 1.3.3 Magnification of the Trp region of 1D 1H spectrum of p53.

One of the tryptophan residues, Trp23, is located within the binding pocket of MDM2/X. Upon binding with MDM2/X the signal corresponding to its indol proton disappears proportionally to the amount of the added protein (Figure 1.3.2). This property is the result of a tight binding of both MDM2/X to p53. Addition of the inhibitor causes complex dissociation and recovery of the Trp23 resonance. Since the signal is proportional to the amount of the added compound it is possible to estimate its K_D.

1.3.2 SEI-AIDA

SEI-AIDA is a method that combines the 1D Trp screening technique with a selective NMR pulse sequence (SEI, for Selective Excitation-Inversion). The pulse sequence (Figure 1.3.4) incorporates a Gaussian-shaped pulse of angle α ≥90°, followed by a modified WATERGATE sequence for residual water signal suppression. The rSnob profile (Kupce et al. 1995) is used for selective refocusing of downfield shifted protein resonances in the spin−echo part of the experiment. The Gaussian pulse has the duration of 1 ms and α of 103°. Selective pulses are applied at 10 ppm. Gradient strengths are 22% and 20% for G1 and G2, respectively; δ was set to 100 μs, the gradient recovery delay to 100 μs, and the acquisition time t_1 to 300 ms, giving the total scan time T_{scan} 300 ms.

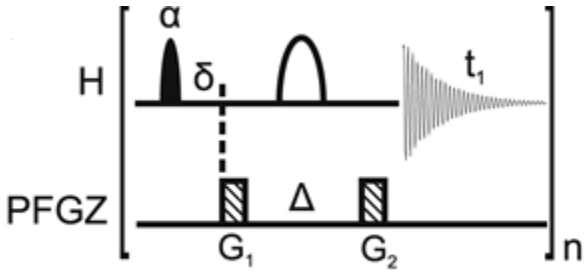

Figure 1.3.4 Experimental scheme of the SEI experiment.

Spin relaxation is the main factor limiting the sensitivity of NMR experiments (Ernst 1987). Fast transverse relaxation rates cause spectral line broadening, whereas slow longitudinal relaxation requires introduction of long magnetization recovery delays in NMR experimental schemes. Since biomolecular NMR experiments are performed in aqueous solutions, the repetition rate in a 1D ^{1}H NMR experiment is determined by longitudinal relaxation of water, and thus the highest sensitivity per time unit is achieved when the sum of acquisition and relaxation periods included in the experiment is ca. 3 s (Ernst 1987).

The SEI pulse sequence employs selective pulses only on well-separated NMR signals (e.g., Trp HN$^{\varepsilon}$ signals). Application of this pulse sequence has several advantages over a corresponding 1D ^{1}H sequence with a 90° hard pulse. First, it is possible to adjust selective pulses' lengths and offsets so that the water magnetization is not moved from the +Z axis and excellent water suppression is achieved in a single scan. Moreover, since the slowly relaxing water magnetization is not saturated, no long recycle delays are necessary and the Ernst angle excitation is possible (Ernst 1987). Considering that only a small fraction of spins of a macromolecule is in a non-equilibrium state, the dipole interactions between the excited spins and other spins in the protein and in bulk water significantly speed up the longitudinal relaxation. (Pervushin et al. 2002; Schanda and Brutscher 2006). Thus for the SEI sequence, the duration of a single scan can be decreased down to 300 ms without significant reduction in the signal-to-noise ratio per scan. With faster acquisition, the experimental time can be reduced by an order of magnitude or protein concentration may be decreased by ca. 70% compared

our 1D proton “Trp” version of AIDA described previously. (Krajewski et al. 2007; Rothweiler et al. 2008).

Thus increasing the sensitivity of a 1D ^{1}H NMR experiment ca. 3 times and reducing the experimental time by an order of magnitude compared to AIDA experiment performed with a hard pulse 90º followed by a Watergate -W3 sequence (Figure1.3.5).

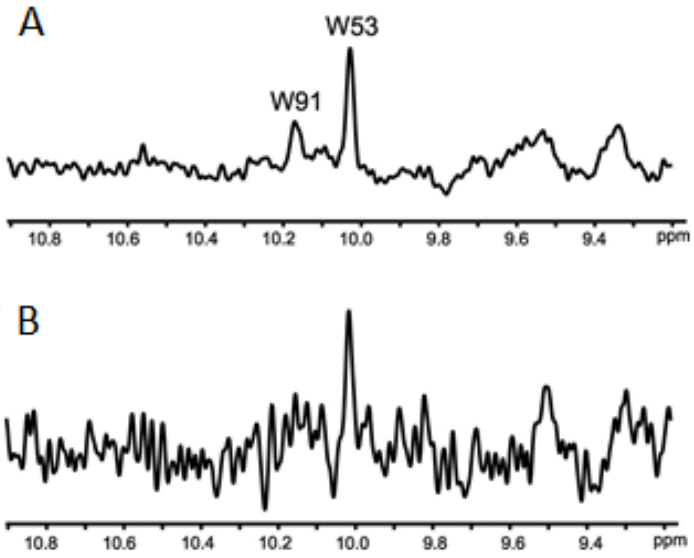

Figure 1.3.5. 1D ^{1}H NMR spectra of the 35 μM Mdm2−p53 complex; two NHε signals of Trp of p53 are visible. Both spectra were acquired in 2.5 min using: the SEI pulse sequence (A); 90° hard pulse followed by the WATERGATE-W3 sequence (B).

2 Materials and methods

2.1 Materials

2.1.1 Chemicals

All chemicals were of the analytical grade obtained from Merck (Germany) or Sigma Laboratories (USA) or Roth (Germany), unless otherwise mentioned.

2.1.2 Enzymes

Phussion DNA polymerase	Finzymmes (Finland)
DpnI	New England Biolabs (USA)
Thrombin	Sigma (USA)

2.1.3 Kits

QIAquick PCR Purification Kit	Qiagen (Germany)
QIAquick Gel Extraction Kit	Qiagen (Germany)
QIAprep Spin Miniprep Kit	Qiagen (Germany)

2.1.4 Oligonucleotides

All the nucleotides have been obtained from Metabion (Germany).

2.1.5 Bacterial stains

Cloning One Shot TOP10	Novagen (Canada)
Expression BL21 Star (DE3) RIL	Invitrogen (Holland)

2.1.6 Vectors

pET 28a(+)	Novagen (Canada)
pET 20b(+)	Novagen (Canada)
pET 41 Ek/LIC	Novagen (Canada)
pET 46 Ek/LIC	Novagen (Canada)

2.1.7 Protein and nucleic acid markers

Prestained protein ladder	Fermentas (Lithuania)
1Kb DNA marker	New England BioLabs (USA)

2.1.8 Stock solutions

- Stock solutions for preparation of minimal media:

Thiamine: 1% (w/v) dissolved in deionized water, sterilized by filtration

$MgSO_4$: 1 M dissolved in deionized water, sterilized by filtration

Glucose: 20% dissolved in deionized water, autoclaved

Zn-EDTA solution: 5 mg/ml EDTA

8.4 mg/ml $Zn(Ac)_2$

dissolved separately, sterilized by filtration, combined together

Trace elements solution: 2.5g/l H_3BO_3

2g/l $CoCl_2 \cdot 6H_2O$

1.13g/l $CuCl_2 \cdot 2\ H_2O$

9.8g/l $MnCl_2 \cdot\ H_2O$

2g/l $Na_2MoO_4 \cdot 2\ H_2O$

pH lowered by citric acid or HCl

- Stock solutions of antibiotics:

Ampicilin: 100 mg/ml dissolved in deionized water, sterilized by filtration, stored in aliquots at -20˚C until used; working concentration 150 μg/ml

Kanamycin: 100 mg/ml dissolved in deionized water, sterilized by filtration, stored in aliquots at -20˚C until used; working concentration 100 μg/ml

Chloramphenicol: 34 mg/ml dissolved in ethanol, stored in aliquots at -20˚C until used; working concentration 34 μg/ml

- Stock solution of IPTG

1M IPTG dissolved in deionized water, sterilized by filtration, stored in aliquots at -20˚C until used.

- Solutions for making competent cells:

Buffer A	100 mM $MgCl_2 \cdot 6H_2O$
Buffer B	100 mM $CaCl_2$
	15 % (v/v) glycerol

2.1.9 Buffers

- 50X TAE buffer (for 1 l):

	40 mM Tris-acetate 242 g of Tris base
	1 mM EDTA 100 ml of 0.5 M EDTA (pH 8.0)
	Glacial acetic acid 57.1 ml

- Buffers for purification under native conditions using immobilized metal-chelate chromatography (IMAC).

With phosphate:

Lysis buffer:	50 mM Na_2HPO_4
	300 mM NaCl
	10 mM imidazol
	pH 8.0
Wash buffer:	50 mM Na_2HPO_4
	300 mM NaCl
	50 mM imidazol
	pH 8.0
Elution buffer:	50 mM Na_2HPO_4
	300 mM NaCl
	200 mM imidazol
	pH 8.0

With Tris:

Lysis buffer: 5 mM Tris
500 mM NaCl
10 mM imidazol
1 mM β-mercaptoethanol
1% (v/v) Tween 20
pH 7.5

Wash buffer: 25 mM Tris
500 mM NaCl
10 mM imidazol
1 mM β-mercaptoethanol
pH 7.5

Elution buffer: 5 mM Tris
500 mM NaCl
250 mM imidazol
1 mM β-marcaptoethanol
pH 7.5

- PBS : 40 mM NaCl
2.7 mM KCl
10 mM Na_2HPO4
1.8 mM KH_2PO_4
0.05% NaN_3
pH 7.3

- Buffers for purification of a protein from inclusion bodies

Lysis buffer: PBS

Wash buffer: PBS

0.05% Triton X-100 (v/v)

Solubilization buffer: 6 M Guanidin hydrochloride
100 mM Tris-HCl
1 mM EDTA
10 mM β-merkaptoethanol
pH 8.0

Dialysis buffer: 4 M guanidine hydrochloride
10 mM β-merkaptoethanol
pH 3.5

Refolding buffer: 10 mM Tris-HCl
1mM EDTA
pH 7.0

Buthyl Sepharose elution buffer: 100 mM Tris-HCl
10 mM β-merkaptoethanol
pH 7.2

- Phosphate buffer for gel filtration: 50 mM KH_2PO_4
50 mM Na_2HPO_4
150 mM NaCl
5 mM β-mercaptoethanol
pH 7.4

- Tris-buffer for crystallization: 5 mM Tris-HCl
50 mM NaCl
10 mM β-mercaptoethanol
pH 8.0

- HEPES-buffer for crystallization: 10 mM HEPES
  100 mM NaCl
  1mM β-mercaptoethanol
  pH 7.5

- Buffers for ion-exchange chromatography:
  Starting buffer-buffer 0 20 mM Tris-HCl
  10 mM β-mercaptoethanol
  pH 7.0

  Final buffer-buffer 100 20 mM Tris-HCl
  1M NaCl
  10 mM β-mercaptoethanol
  pH 7.0

- Thrombin storage buffer: 50 mM sodium citrate
  200 mM NaCl
  0.1% PEG-8000
  50% glycerol
  pH 6.5

- Thrombin cleavage buffer: 20 mM Tris-HCl
  150 mM NaCl
  2.5 mM CaCl
  pH 8.4

2.1.10 Media for bacteria growth

Luria-Bertani-Medium (LB) (for 1l)**:** 10 g bacto tryptone
5 g bacto yeast extract
10 g NaCl

pH was adjusted to 7.0. For the preparation of agar plates, the medium was supplemented with 15 g agar. The mixture was autoclaved.

Minimal media (MM): for uniform enrichment with ^{15}N (for 1 l):

0.5 g NaCl
1.3 ml trace elements solution
1 g citric acid monohydrate
36 mg ferrous citrate
4.02 g KH_2PO_4
7.82 g $K_2HPO_4 \cdot 3H_2O$
1 ml Zn-EDTA solution
1 g $^{15}NH_4Cl$

pH was adjusted to 7.0 with NaOH, the mixture was autoclaved, upon cooling, separately sterilized solutions were added: 25 ml glucose, 560 µl thiamin stock, antibiotics, 2 ml of the $MgSO_4$ stock.

2.1.11 Reagents and buffers for the SDS-PAGE

- Anode buffer (+): 200 mM Tris pH 8.9

- Cathode buffer (-): 100 mM Tris
  100 mM tricine
  0.1% SDS
  pH 8.25

- Separation buffer: 1 M Tris
  0.3% SDS
  pH 8.8

- Stacking buffer: 1 M Tris
  0.3% SDS
  pH 6.8

- Separation acrylamide: 48% acrylamide
  1.5% bis-acrylamide

- Stacking acrylamide: 30% acrylamide
  0.8% bis-acrylamide

Pouring polyacrylamide gels:

Separation gel: 1.675 ml H_2O
2.5 ml separation buffer
2.5 ml separation acrylamide
0.8 ml glycerol
25 µl APS
2.5 µl TEMED

Intermediate gel: 1.725 ml H_2O
1.25 ml separation buffer
0.75 ml separation acrylamide
12.5 µl APS
1.25 µl TEMED

Stacking gel: 2.575 ml H_2O
0.475 ml stacking buffer
0.625 ml stacking acrylamide
12.5 µl 0.5 M EDTA, pH 8.0
37.5 µl APS
1.9 µl TEMED

2.1.12 Protein visualization

Coomassie-blue solution:	45% ethanol
	10% acetic acid
Destaining solution:	5% ethanol
	10% acetic acid

2.1.13 Chromatography equipment, columns and media

ÄKTA explorer 10	Amersham Pharmacia (Sweden)
Peristaltic pump P-1	Amersham Pharmacia (Sweden)
Fraction collector RediFrac	Amersham Pharmacia (Sweden)
Recorder REC-1	Amersham Pharmacia (Sweden)
UV flow through detector UV-1	Amersham Pharmacia (Sweden)
BioloLogic LP System	Biorad (USA)
HiLoad 26/60 Superdex S75pg	Amersham Pharmacia (Sweden)
HiLoad 16/60 Superdex S75pg	Amersham Pharmacia (Sweden)
HiLoad 16/60 Superdex S200pg	Amersham Pharmacia (Sweden)
HiLoad 10/30 Superdex S75pg	Amersham Pharmacia (Sweden)
HiLoad 10/30 Superdex S200pg	Amersham Pharmacia (Sweden)
HiTrap SP FF	GeHealthcare (Germany)
Ni-NTA-agarose	Qiagen (Germany)

2.2 Methods

2.2.1 DNA techniques

2.2.1.1 Isolation of plasmid DNA

The preparation of plasmid DNA from *E. coli* was carried out using dedicated plasmid purification kits from Qiagen. The kits employ a standard alkalic lysis of the precipitated bacteria in the presence of RNAse and a strong ionic detergent, SDS, followed by neutralization/DNA renaturation with acetate. For purification, a crude cell lysate is loaded onto a silica gel column, washed with an ethanol-containing buffer, and eluted in a small volume, yielding up to 20 µg of the plasmid DNA.

2.2.1.2 Electrophoresis of DNA

The purity and quality of isolated plasmid DNA was checked by the agarose gel electrophoresis. For this purpose 1% of agarose in the TAE buffer was repaired. The mixture was supplemented with the Sybr®safe. The DNA samples were mixed with the 6x concentrated loading buffer prior to application on a gel. The samples were run along with the 1 kb DNA ladder (NEB) at 100-120 V DC. Results were visualized using UV illumination.

2.2.1.3 Mutagenesis

Site directed mutagenesis of p53 and hPin1 were performed using PCR. The mutagenic primers were designed according to the guidelines to the QuickChange Site-directed mutagenesis kit (Stratagen). The desired mutation was in the middle of the primer of ~ 15-42 bp of a corrected sequence on both sides (Table 2.2.1). Vectors pET 46 Ek/LIC and pET 28a, containing copies of human p53 and Pin1 gene, were used as DNA templates. In case of the p53 double mutants L22IL26V and L22VL26V as a template were used previously obtained plasmids containing the p53 gene with single mutations p53-L22I and p53-L22V, respectively. High concentration of the template

combined with the low number of PCR cycles as well as high accuracy of the Phussion DNA Polymerase minimizes the occurrence of unwanted mutations.

The mutagenic PCR reaction mixture contained:

5× HF reaction buffer	10 µl
dNTP mix (2mM)	5 µl
plasmid (5 ng/µl)	0.5 µl (10 ng)
oligonucleotide primer forward	0.5 µl (125 ng)
oligonucleotide primer rewerse	0.5 µl (125 ng)
Phussion DNA polymerase (2.5 U/µl)	1 µl
Milli-Q to a final volume of 50 µl	37.5 µl

PCR cycling parameters:

denaturation:	98°C, 1’30’’
denaturation:	98°C, 30’’
annealing:	64-74°C, 30’’
synthesis (1 min for 1000 bp):	64-72°C, 6’
final extension	64-72°C 10’

Following the temperature cycling the product was treated with DpnI (10U, 37°C, for 4 h). DpnI endonuclease recognizes methylated and hemimethylated DNA sequences (5´-Gm^{6}ATC-3´) and is used to digest the parental DNA template and select for mutation containing the (not methylated) synthesized DNA. 1-5 µl of the mixture was used to transform Top10 chemically competent cells. Plasmid DNA was isolated using the QIAprep Spin Miniprep Kit (Qiagen) and was subjected to verification by automated sequencing.

Table 2.2.1 Primers for mutagenesis

Primers for p53	
F19A	forward: 5’-CTGAGTCAGGAAACAGCTTCAGACCTATGG-3’
	reverse: 5’-CCATAGGTCTGAAGCTGTTTCCTGACTCAG-3’
F19Y	forward: 5’-CTGAGTCAGGAAACATATTCAGACCTATGG-3’
	reverse: 5’-CCATAGGTCTGAATATGTTTCCTGACTCAG-3’
L22A	forward: 5’-GAAACATTTTCAGACGCATGGAAACTACTTCCT-3’
	reverse: 5’-AGGAAGTAGTTTCCATGCGTCTGAAAATGTTTC-3’
L22I	forward: 5’-GAAACATTTTCAGACATATGGAAACTACTTCCT-3’
	reverse: 5’-AGGAAGTAGTTTCCATATGTCTGAAAATGTTTC-3’
L22V	forward:5’-AAACATTTTCAGACGTATGGAAACTACTTCCT-’
	reverse: 5’-AGGAAGTAGTTTCCATACGTCTGAAAATGTTTC-3’
L26I	forward: 5’-GACCTATGGAAACTAATACCTGAAAACAAC-3’
	reverse: 5’- GTTGTTTTCAGGTATTAGTTTCCATAGGTC-3’
L26V	forward: 5’-GACCTATGGAAACTAGTTCCTGAAAACAAC-3’
	reverse: 5’-GTTGTTTTCAGGAACTAGTTTCCATAGGTC-3’
L22IL26V	forward: 5’-GACATATGGAAACTAGTTCTTGAAAACAAC-3’
	reverse: 5’-GTTGTTTTCAAGAACTAGTTTCCATATGTC-3’
L22VL26V	forward: 5’-GACGTATGGAAACTAGTTCCTGAAAACAAC
	reverse: 5’-GTTGTTTTCAGGAACTAGTTTCCATACGTC-3’
Primers for Pin1	
R14A	forward: 5’-CCCGGCTGGGAGAAGGCCATGAGCCGC-3’
	reverse: 5’-GCGGCTCATGGCCTTCTCCCAGCCGGG-3’

2.2.2 Preparation of chemically competent bacteria

A single colony of an overnight grown bacteria from a LB agar plate was inoculated into 100 ml of the LB media in a 500 ml flask. Culture was incubated at 37°C with vigorous agitation, monitoring the growth of cells. Cells were grown till the OD_{600} reached ~ 0.6. The bacterial culture was transferred to sterile, disposable, ice-cold 50 ml polypropylene tubes and cooled down to 4ºC on ice for 10 min. Cells were recovered by

centrifugation at 3000 g for 10 min at 4ºC. Supernatant media was decanted and tubes were kept in an inverted position on a pad of a paper towel for 1 min to allow the last traces of media to drain away. Pellets were resuspended by gentle vortexing in 50 ml of the ice-cold $MgCl_2$ solution. Again, cells were recovered by centrifugation at 3000 g for 10 min at 4ºC. The supernatant solution was decanted and tubes were kept in an inverted position on a pad of a paper towel for 1 min to allow the last traces of solution to drain away. Pellet of the cells was recovered by gentle vortexing in 2 ml of ice-cold 0.1 M $CaCl_2$ containing 15% glycerol, for each 50 ml of original culture. After this cells were dispensed into aliquots of 50 µl, flash frozen in liquid nitrogen and stored at -80ºC.

2.2.3 Transformation

Approximately 50 µg of plasmid DNA or 1-5 µl of cleaved product of PCR reaction was added to 50 µl of chemically competent cells. The mixture was incubated on ice for 30 min followed by a heat shock of 45 s at 42ºC, 2 min cooling on ice, and the addition of 300µl LB medium. After 1 h of incubation at 37ºC, 20-50 µl of the mixture was spread out on LB agar plates (supplemented with a selective antibiotic) and incubated overnight at 37ºC. A number of factors have been elucidated to increase transformation efficiency. Such factors include: prolonged incubation of bacteria with $CaCl_2$, addition of multiple cations, such as Mg^{2+}or Cs^{2+}, into the transformation mixture and treatment of bacteria with dimethyl sulfoxide (DMSO), polyethylene glycol, hexaminecobalt, and dithiothreitol in the presence of both monovalent and divalent cations (Chung et al. 1989). After incubation with DNA, in order to make the cells retain the plasmid and to be certain that they survive, the cells were heat-shocked for several seconds to induce heat shock genes, which aid in survival and recovery. The cells were then incubated at 37ºC without selective pressure; sufficient time was given for expression of antibiotic resistance genes. Plating on selective media enabled recovery of those cells that actually received the DNA.

2.2.4 Protein expression

2.2.4.1 E. coli expression in LB medium

A fresh single bacterial colony was inoculated into 30 ml of the LB with an antibiotic and incubated overnight at 37ºC with vigorous shaking (170 rpm) in a 50 ml falcon tube. These overnight cultures were used as an inoculum for a 1 l of the LB medium, also supplemented with an appropriate antibiotic. Cultures were incubated at 37ºC with vigorous shaking (170 rpm) until the OD600 reached 0.7 - 0.8. For proteins expressed in the native fraction, cells were induced by addition of 0.5 mM IPTG (final concentration) and grown at 18-20ºC for further 16 h. For proteins obtained from the inclusion bodies, IPTG was added to final concentration 1 mM. Upon induction the cells were grown at 37ºC for 3-5 h. Cells were harvested by centrifugation at 4000 g for 20 min at 4ºC. The cell pellet after the expression was used directly for protein purification or stored at -20ºC until used.

2.2.4.2 E. coli expression in MM

5 ml of LB medium was inoculated with a single colony and incubated at 37°C with vigorous shaking (170 rpm) in a 15 ml falcon tube for 8-10 h. Then 100 µl of this culture was used to inoculate a 100 ml of MM. The bacteria were grown overnight at 37ºC with vigorous shaking (170 rpm) in a 250 ml flask. 10-15 ml of the overnight culture was inoculated into 1 l of MM. Further steps were identical to expression in the LB medium.

2.2.5 Sonication

Pulsed mode of operation was applied (output control 8, 60% duty cycle) and sonication was carried out on ice, in 5 steps of 2 min each, with 5 min intervals between steps, to avoid overheating of the sample.

2.2.6 Protein purification

Obtaining high amount of a pure protein is always the aim of any purification process. Usually, the procedure requires several steps (Figure 2.2.1). Each of them separates protein based on different properties like: size, charge, hydrophobicity or biorecognition. A step of gel filtration chromatography, which was always performed in this work at the end of purification process, additionally has allowed for removing protein aggregates.

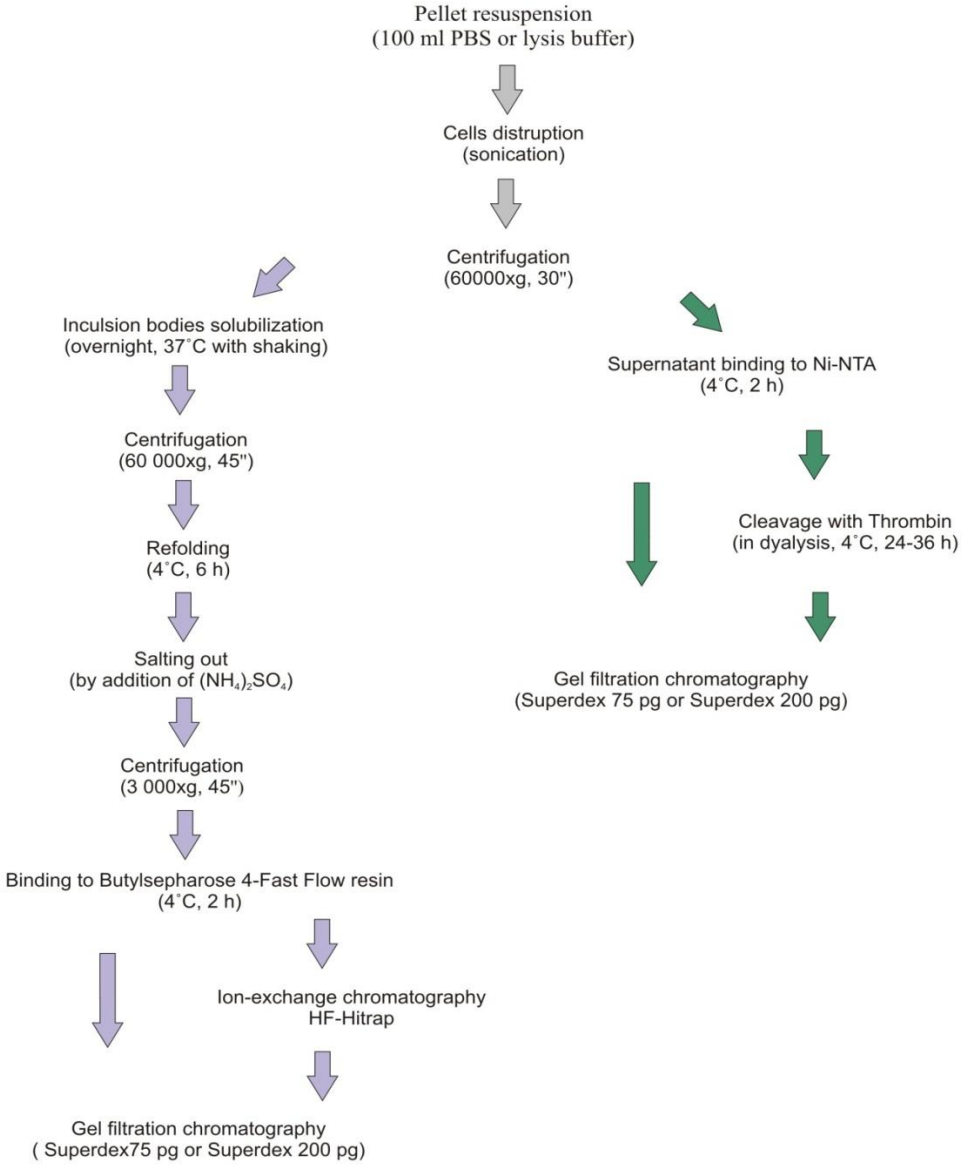

Figure 2.2.1 Schematic presentation of protein purification steps for a native fraction and inclusion bodies

2.2.6.1 Purification form inclusion bodies

Purification of MDM2

For expression of MDM2 were used two systems; for crystallization purposes residues 18-125 were cloned into pET20 (Novagen) and for application in NMR spectroscopy and FP assays residues 1-125 were cloned into pET-11a. In both cases the protein was expressed in inclusion bodies. A Cell pellet of bacteria was resuspended in PBS and sonicated 5 times for 2 min using a macrotip (output control 8, 80%). Lysate was centrifuged at 60 000 x g for 30 min at 4ºC. The supernatant was poured out. Inclusion bodies were washed twice with PBS supplied with 0.05% TritonX-100 followed each time by low speed centrifugation at 12 000 x g for 25 min After that inclusion bodies were solubilized overnight in 6 M guanidinium hydrochloride, 100 mM Tris-HCl, pH 8.0, including 1 mM EDTA and 10 mM β-mercaptoethanol at 37ºC with vigorous shaking. Next, the solubilized inclusion bodies were centrifuged at 60 000 x g for 45 min at 4ºC in order to remove not solubilized poteins. The supernatant was transferred to the dialysis membrane and dyalised against 4 M guanidinium hydrochloride, pH 3.5, 10 mM β-mercaptoethanol for approximatelly 6 h. Refolding was performed in 10 mM Tris-HCl, pH 7.0, including 1 mM EDTA, 10 mM β-mercaptoethanol by adding protein in several pulses. Refolding was performed overnight at 4ºC. Next, $(NH_4)_2SO_4$ up to 1.5 M, was added. 2 h after salting out the refolding buffer was centrifuged at 3000 x g for 35 min at 4ºC. The supernatant was poured down and supplied with 10 ml of the bed volume of the Butylsepharose 6 Fast Flow and incubated for 1.5 h with stiring at 4ºC. The protein was eluted with 100 mM Tris-HCl, pH 7.2, 10 mM β-mercaptoethanol. The fractions containing the protein of interest were pooled, concentrated and purified by gel filtration in 50 mM KH_2PO_4, 50 mM Na_2HPO_4, pH 7.4, 150 mM NaCl, 5 mM β-merkaptoethanol.

Purification of MDMX for crystallization

MDMX crystallization construct, without tag, comprising residues 23-111 was cloned into pET-46Ek/LIC (Novagen) and was expressed in inclusion bodies. The protein has pI 8.0. It is positively charged and can bind to a cation exchangers in a buffer of a lower pH. The purification of MDMX was performed the same way as purification of MDM2 until the protein was eluted from the Butylsepharose 6 Fast Flow. After elution, the fractions containing the protein of interest were pooled and dialyzed against 20 mM Tris-HCl, 10 mM β-mercaptoethanol pH 7.0. Protein was applied on the HiTrap SP FF column, washed with the starting buffer and eluted with the linear gradient of concentration of NaCl. The fractions containing the protein of interest were pooled, concentrated and purified by gel filtration Superdex 75 in crystallization buffer: 5 mM Tris-HCl, pH 8.0, 50 mM NaCl, 10mM β-mercaptoethanol.

2.2.6.2 Purification from native fraction

Purification of p53, MDMX and hPin1

The residues 1-321 of p53 were cloned into pET23 (Novagen); in case of MDMX the construct comprised residues 18-111 cloned into pET46Ek/LIC (Novagen) and in case of Pin1 the full-length protein was cloned into plasmid pET28a (Novagen). The cell pellet was resuspended in a lysis buffer, 50 mM Na_2HPO_4, 300 mM NaCl, 10 mM imidazole pH 8.0 and sonicated 5 times for 2 min using a macrotip (output control 8, 80%). The lysate was centrifuged at 60 000 x g for 30 min at 4˚C. The supernatant was added to the Ni-NTA resin and incubated with (rotation) for 2 h at 4ºC. The non-specifically bound protein was washed out with 5 bed volumes of the wash buffer: 50 mM Na_2HPO_4, 300 mM NaCl, 10 mM imidazole pH 8.0. The protein was eluted with elution buffer: 50 mM $NaHPO_4$, 300 mM NaCl, 10 mM imidazole, pH 8.0. The fractions containing the protein of interest were pooled, concentrated and purified by gel filtration in PBS.

Purification of hPin1 for crystallization

Purification of hPin1-R14A was performed similarly to the purification of other, already mentioned proteins expressed in native fraction. The cell pellet was resuspended in a lysis buffer: 5 mM Tris, 500 mM NaCl, 10 mM imidazol, 1 mM β-marcaptoethanol, 1% (v/v) Tween 20, pH 7.5 supplied with the protease inhibitors and sonicated 5 times for 2 min using a macrotip (output control 8, 80%). The lysate was centrifuged at 60 000 x g for 30 min at 4˚C. The supernatant was added to the Ni-NTA resin and incubated with (rotation) for 2 h at 4ºC. The non-specifically bound protein was washed out with 5 bed volumes of the wash buffer 25 mM Tris, 500 mM NaCl, 10 mM imidazole, 1 mM β-marcapto- ethanol, pH 7.5. The protein was eluted with the elution buffer: 5 mM Tris, 500 mM NaCl, 250 mM imidazole, 1 mM β-marcaptoethanol pH 7.5. After elution, the His-tag was removed by digestion with thrombin (Sigma) during dialysis against 50 mM Tris-HCl (pH 8.0), 150 mM NaCl, 5 mM $MgCl_2$, 2.5 mM $CaCl_2$, 1mM β-mercaptoethanol, 10% (v/v) glycerol for 24 h at 4ºC. The residual His-tagged protein was removed by binding to Ni-NTA; protein without tag was isolated from the flow-through. The protein was fractionated by gel filtration on a Superdex 200 column (Pharmacia) equilibrated in 10 mM HEPES pH 7.5, 100 mM NaCl, and 1 mM β-mercaptoethanol. The hPin1-R14A containing fractions were collected and concentrated up to 18 mg/ml.

2.2.7 Determination of protein concentration

Determination of protein concentration was performed spectrophotometrically. Absorption at 280 nm was measured and converted to a protein concentration on the basis of theoretical extinction coefficients. It has been shown that it is possible to estimate the molar extinction coefficient E_{λ}(Prot) of a protein from knowledge of its amino acid composition (Gill and von Hippel 1989). From the molar extinction coefficient of tyrosine, tryptophan and cystine (cysteine residues do not absorb appreciably at

wavelenghts >260 nm, while cystine does) at a given wavelength λ the extinction coefficient of a protein can be computed using the equation:

$$E_{\lambda}(Prot) = Numb(Y)xExt_{\lambda}(Y) + Numb(W)xExt_{\lambda}(W) + Numb(C)xExt_{\lambda}(C)$$

Protein concentration (C_p) can be calculated using the following formula:

$$A_{\lambda}(Prot) = E_{\lambda}(Prot) \times C_p(Prot) \times (path\ length\ in\ cm)$$

2.2.8 Protein analysis

SDS-PAGE electrophoresis

The SDS polyacrylamide gel electrophoresis was carried out at various stages of purification to check the purity and identity of the eluted proteins. For all of the expressed proteins, tricine gels were applied (Schagger and von Jagow 1987). The protein samples were prepared by mixing 20 µl of the protein solution with 5 µl of the sample buffer (SB) followed by 5 min incubation at 100ºC.

Visualization of separated proteins

For visualization of protein bands, the gels were stained in a Coomassie-blue solution. The background was cleared by incubation of the gel in a destaining solution. Both processes were greatly accelerated by brief heating with microwaves of the gel submerged in an appropriate solution.

2.2.9 NMR measurements

All NMR spectra were acquired on a Bruker DRX 600 MHz spectrometer equipped with a cryoprobe at 300 K. NMR samples contained up to 0.3 mM of protein. NMR data were processed using Topspin 1.3.

Standard 1D ^{1}H NMR spectra were recorded using a 90° hard pulse followed by the WATERGATE 5 sequence for water suppression. SEI-AIDA NMR spectra were recorded using the pulse sequence, which incorporates a Gaussian-shaped pulse of

angle α > 90° for selective excitation of well-separated signals (in this case these were Trp residues around 10 ppm), followed by a modified WATERGATE sequence for the residual water signal suppression. All spectra were recorded with a sweep-width of 10 000 Hz and a time domain of 32 K complex points.

For the $^{1}H,^{15}N$-HSQC spectrum (Mori et al. 1995) a total of 4096 complex points in *t*2 and 128 *t*1 increments were acquired. Water suppression was carried out using the WATERGATE-5 sequence. Titration experiments were performed using a series of ^{1}H, ^{15}N-HSQC of the ^{15}N-labeled protein. The compounds were dissolved in water or in d6-DMSO. The protein sample containing 10% (v/v) D_2O or d_6-DMSO was titrated to yield the following stoichiometry of protein to compound: 1:0.5, 1:1, 1:1.5, and 1:2 depending on the experiment. Quantitative analysis of induced chemical shifts was performed on the basis of spectra obtained at saturating conditions. Analysis of ligand-induced shifts was performed by applying the equation of Pythagoras to weighted chemical shifts:

$$\Delta\delta\ (^{1}H,\ ^{15}N) = \ [\Delta\delta(^{1}H)]^{2} + [0.2 * \Delta\delta\ (^{15}N)]^{2}\ \}^{0.5}$$

2.2.10 ITC measurements

ITC has been used extensively to study the binding of small molecules to proteins, but it can also be a valuable tool when looking at protein–protein interactions. The method allows for quantitative estimation of molecular interactions. ITC measures the equilibrium directly by determining the heat evolved on association of a ligand with its binding partner. In a single experiment, the values of the binding constant (K_a), the stoichiometry (*n*), and the enthalpy (ΔH) and enthropy (ΔS) of binding are determined. All ITC experiments were carried out on a Microcal iTC200 calorimeter according to references provided by the manufacturer. Heat generated by protein dilution was determined in separate experiments by injecting a protein solution into the sample chamber filled with a proper buffer. All data were corrected for the heat of protein dilution. Data were fitted using χ^2 minimization for a model assuming a single set of sites to calculate the binding affinity K_D. All steps of the data analysis were performed using ORIGIN 7.0 software provided by the manufacturer.

Titrations of Pin1

For measurements of Pin1 with dexamethasone-21-phosphate (DP) and betamethasone-21-phosphate (BP), titrations settings were: 20 injections, 22ºC cell temperature, 10 µcal/s reference power, 60 s initial delay, 0.147 mM Pin1 cell concentration, 2 mM dexamethasone-21-phosphate and the 5 mM betamethasone-21-phosphate syringe concentration, respectively, and a stirring speed of 1 000 rpm. The 1st injection was 0.1 µl with an injection time of 0.2 s, while all further injections were 2 µl (4 s injection times). Gaps between injections were 150 s and data points were recorded every 2 s. All experiments were performed in triplicate.

Titrations of p53-wt and p53 mutants

For measurements of p53-wt and mutants of p53 with MDM2 and MDMX titrations settings were: 20 injections, 25ºC cell temperature, 10 µcal/s reference power, 600 s initial delay, 0.012-0.030 mM p53 cell concentration, 0.1-0.3 mM of titrant (MDM2 or MDMX) syringe concentration, and a stirring speed of 800 rpm. The 1st injection was 0.4 µl with an injection time of 0.2 s, while all further injections were 2 µl (4 s injection times). Gaps between injections were 150 s and data points were recorded every 5 s. All experiments were performed in duplicate.

2.2.11 Fluorescence polarization assay

Fluorescence polarization experiments were read on an Ultra evolution or Infinite F500 384-well plate reader (Tecan) with 485 nm excitation and 535 nm emission filters. The fluorescence intensities parallel (Int_parallel) and perpendicular (Int_perpendicular) to the plane of excitation were measured in 384-well NBS assay plates (Corning) at room temperature (~20˚C). The background fluorescence intensities of a blank sample containing the reference buffer were subtracted and steady-state fluorescence polarization was calculated using the equation:

$$P = \frac{Int_{parallel} - Int_{perpendicular}}{Int_{parallel} + Int_{perpendicular}}$$

A correction factor G (G = 0.998 determined empirically) was introduced to eliminate differences in transmission of vertically and horizontally polarized light. All fluorescence polarization values were expressed in milipolarization units. The binding affinities of fluorescent peptides P5: 5-carboxyfluorescein-CPPLSQETFS DLWKLLSENN) and P6: 5-carboxyfluorescein- ETFEHWWSQLLS) towards MDM2 and MDMX, respectively were determined in the buffer: 10 mM Tris, pH 7.3, 1 mM EDTA, 50 mM NaCl.

Peptide sequences were: Pin1: 5-carboxyfluorescein-GWFYpSPRLKK-OH. Final concentrations: 10 nM; Pin1: 2000 nM. Peptide and protein stocks were diluted in 10 mM Tris (pH 8.0), 50 mM NaCl, 1 mM EDTA, 0.1 % Nonidet P-40, and 10 % DMSO. Inhibition was calculated based on curve fits using SigmaPlot (SPSS Science Software) or Origin 8.5G.

2.2.12 X-ray crystallography

Crystals of human Pin1-R14A (Zhang et al. 2007), MDM2 and MDMX were obtained using the sitting-drop vapor-diffusion method. The proteins, either pure in case of Pin1, or with a three-fold access of an inhibitor in case of MDM2/MDMX, were concentrated up to 18 mg/ml and 10 mg/ml, respectively. Then the protein was mixed between1:0.5-2 (v/v) with mother liquor. Crystals appeared at 4ºC within two days in case of Pin1 and within two weeks in case of MDM2/MDMX. Crystals of the ligand-bound complexes of Pin1 with DP were prepared by adding 0.2 µl of a 10 mM dexamethasone-21-phosphate (DP) solution (in water) to crystals in mother liquor for a period of 24 h before harvesting. Prior to data collection, all crystals were transferred to a cryosolvent containing 30% glycerol in the mother liquor. The crystals were frozen in liquid nitrogen. Data sets were collected on the SLS beamline PXII at the Paul Scherrer Institute, Villigen, Switzerland. The collected data were integrated, scaled and merged by XDS and XSCALE (Kabsch 2010). The structures were determined by molecular

replacement using Molrep (Vagin and Teplyakov 2010) from the CCP4 Collaborative Computational Project, (1994). Models were refined by Refmac5 (Murshudov et al. 2011) and rebuilt by MiFit (McRee 2004) and by a subsequent Refmac5 refinement. The refinement was carried out for the resolution range from 19.7-1.4 Å. Signals outside this range did not carry sufficient information to improve the model. Water molecules were added by Arp/Warp (Perrakis et al. 1997). The final models were evaluated using Procheck (Morris et al. 1992).

2.2.13 Pin1 isomerase assay

The *cis*/*trans* peptidyl-prolyl isomerase activity of Pin1 was determined as described (Lu et al. 1999; Kozany et al. 2009). Suc-AEPF-*p*NA (Bachem) was used as the peptide substrate (Behrsin et al. 2007). The peptide substrate was dissolved at 4 mM in dry trifluoroethanol containing 470 mM LiCl. Isomerization assays were measured in the buffer containing 50 mM HEPES, pH 7.5, 100 mM NaCl, and 5 mM NaN_3. Solutions and buffers used were pre-cooled to 4ºC. The *cis*/*trans* peptidyl-prolyl isomerase (PPIase) activity of Pin1 was determined by mixing of 25 µl of the 40x concentrated protein solution (dilution series ranging from 500 to 7.8125 nM) with 850 µl of the assay buffer. To this end, 100 µl 60 mg/ml chymotrypsin in the assay buffer were added and the reaction was started by addition of 25 µl peptide substrate. Increasing absorption was monitored at 390 nm at 4ºC in a Beckman Coulter DU500 photometer. Inhibition of the *cis*/*trans* peptidyl-prolyl isomerase activity of Pin1 was analyzed by addition of 5 µl 200x concentrated inhibitor (1:2 dilution series) to the reaction. Pin1 was incubated with the inhibitors for 10 min before the mixtures were transferred to cuvettes and the reactions were started by adding chymotrypsin and Suc-AEPF-*p*NA. The amount of released *para*-nitroanilide (*p*NA) is directly proportional to the *trans* isomer of the peptide substrate starting from a *cis*/*trans* mixture. The molecular extinction coefficient of *p*NA at 390 nM is 13 300 cm^{-1} M^{-1}. With the molar extinction coefficient the measured absorption can be correlated to the amount of released *p*NA. Curves were analyzed using a three parameter fit (single) for an exponential rise to the maximum in SigmaPlot (SPSS Science Software). Experiments were performed in triplicate.

3 Goals of the study

The study comprises application of the structural biology methods for identification of new small-molecule inhibitors for the proteins that are significant in cancer development. The whole study can be divided into three subprojects.

The goal of the first project was the identification of a binding mode and determination of a crystallographic structure of dexamethasone 21-phosphate a selective inhibitor of peptidyl-prolyl isomerase (Pin1).

The second topic was focused on the development of new NMR screening approaches for identification of the MDM2/MDMX inhibitors.

The third aim of the study was to discover the scaffold and eventually develop a dual inhibitor for p53 and MDM2/MDMX interactions as well as examine the structural aspects of the binding of this inhibitor to its target proteins.

4 Results and discussion

4.1 Pin1

The aim of the study was to explore the database of small-molecule compounds, mostly natural products or natural products derivatives in order to identify new possible non-reactive non-peptic ligands of the phosphorylation dependent protein binding domains. Since protein kinases and protein phosphatases belong to the group of the proteins deregulated in human diseases, it makes the phosphorylation dependent proteins highly desirable targets for drug discovery. The study led to the identification of two O-phosphorylated natural product derivatives: Fosfosal O-phosphorylated derivative of the natural product salicylic acid and dexamethasone 21-phosphate as selective inhibitors of two protein domains considered to be antitumor targets: the SH2 domain of the transcription factor STAT5 and the substrate binding domain of peptidyl-prolyl *cis/trans* isomerase Pin 1, respectively.

4.1.1 Purification of Pin1

Purification of Pin1-wt and Pin1-R14A for crystallization was performed as described in the chapter 2.2.6.2 After elution from the Ni-NTA resin, the protein was either directly applied on a gel filtration Superdex 200 pg or for crystallization purposes the tag was depleted using thrombin. In order to check the cleavage of the tag after 24 h, gel electrophoresis was performed.

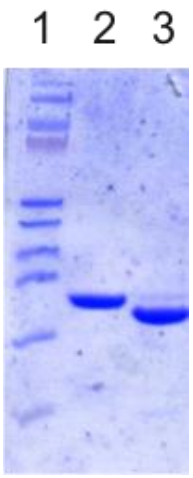

Figure 4.1.1 SDS-PAGE analysis of Pin1 before- (line 2) and after the 24 h cleavage with thrombin (line-3), line 1: marker.

The result indicates that the approximately 2 kDa His –Tag was mostly depleted (Figure 4.1.1). The band in line 3 corresponding to the uncleaved form, is hardly visible. In order to separate the cleaved protein from the leftovers of the protein with the Tag (what could impair the crystallization), the protein solution was supplemented with 10 mM imidazole and applied on the Ni-NTA column. The cleaved protein was isolated from the flow-through and applied on a gel filtration Superdex 200 pg.

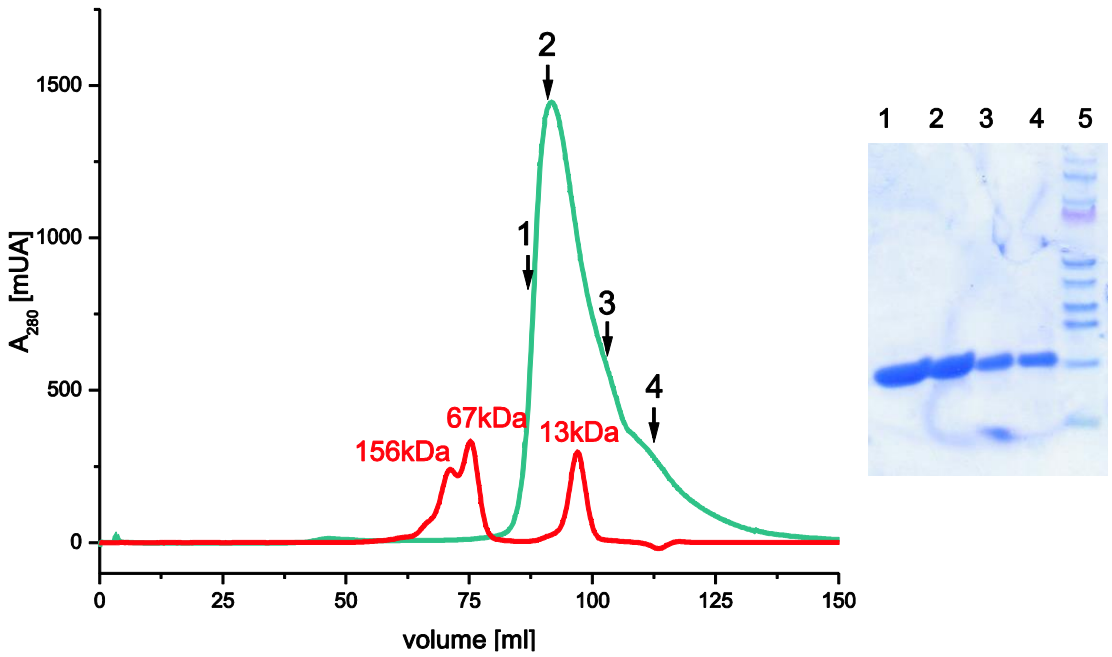

Figure 4.1.2 Chromatogram and the SDS-PAGE analysis of the cleaved Pin1 after gel filtration.SDS-PAGE (lines 1-4: fractions marked on the chromatogram with arrows, respectively, marker: line 5)

Gel electrophoresis has indicated that obtained 18 kDa Pin1- R14A was pure and did not contain the fractions with the His-Tag (Figure 4.1.2). All the fractions containing the protein were pooled concentrated and used for crystallization.

4.1.2 Fluorescence polarization measurements

The screening of the described above database of the natural products and their derivatives identified dexa-methasone-21-phosphate (DP) to be a selective ligand for Pin1 (Figure 4.1.3 A). Crucial for this interaction is phosphate group, since both dexamethasone and dexamethasone-21-acetate were almost inactive in fluorescence polarization assay (data not shown).

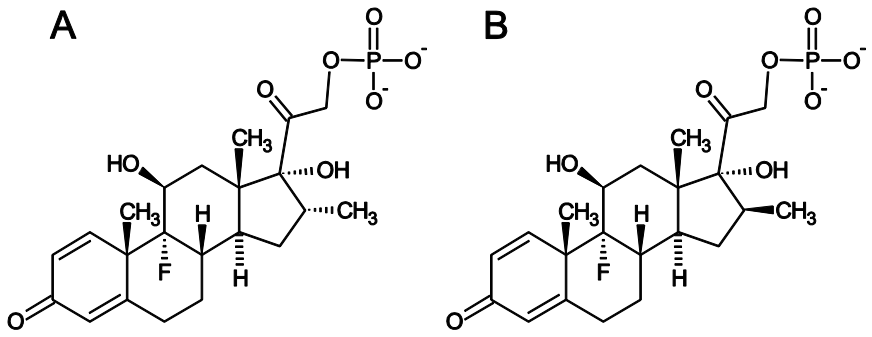

Figure 4.1.3 Structures of dexamethasone 21-phosphate (A) and its C-16 epimer beta-methasone-21-phosphate (B).

Important is also the conformation of the methyl group in the C-16 position, which leads to approximately 35-fold weaker interaction of betadexamethasone-21-phosphat (BP) (Figure 4.1.3B) with Pin1.

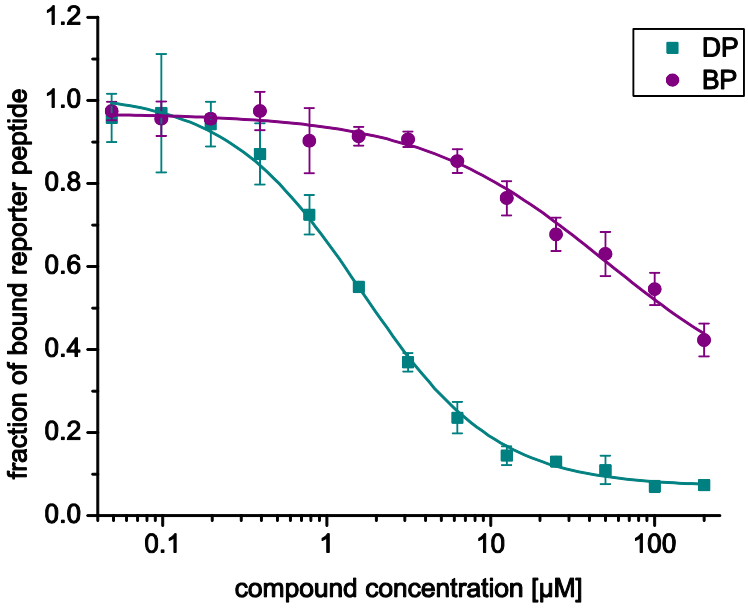

Figure 4.1.4 Activities of dexamethasone-21- phosphate (DP) (magenta line) and betadexamethasone-21-phosphate (purple line) against Pin1 in the fluorescence polarization assay.

4.1.3 ITC measurements

IC_{50} values calculated from the fluorescence polarization data in Figure 4.1.5 were converted to the Ki values as described in (Nikolovska-Coleska et al. 2004). The estimated Ki values were 2.2 ± 0.1 µM and 76.8 ± 15.9 µM for dexa-methasone-21-phosphat (DP) and betadexamethasone-21-phosphat (BP), respectively. A significantly lower affinity of BP to Pin1 has been also confirmed by its higher dissociation constant determined by isothermal titration calorimetry (ITC) (Figure 4.1.5), the K_D values in this case were 6.8 ± 0.2 µM for DP and 542± 81 µM for BP.

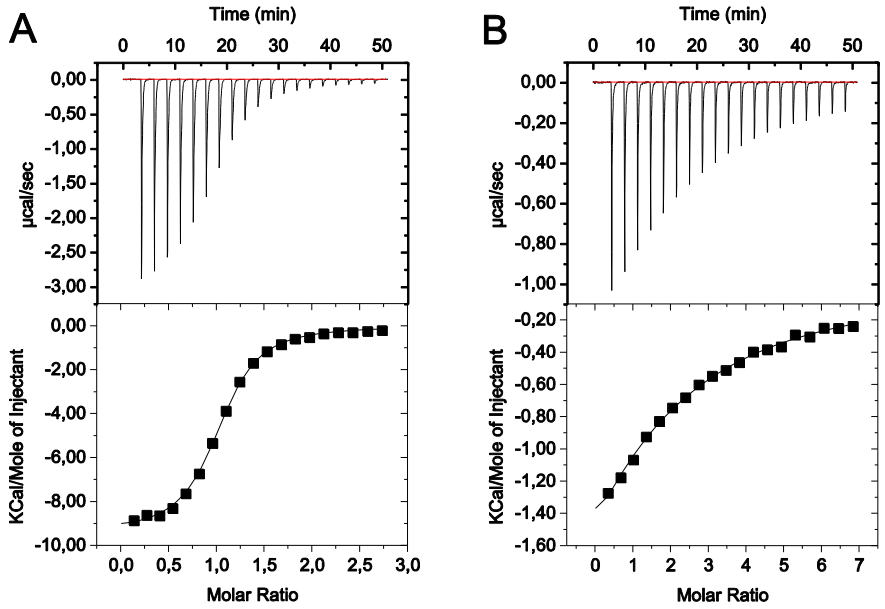

Figure 4.1.5 Results of isothermal titration calorimetry (ITC) of binding of dexamethasone-21-phosphate (A) and betadexamethasone-21-phosphate (B) to Pin1-wt.

4.1.4 Enzymatic measurements

The enzymatic assay also indicates that DP is potent in inhibiting isomerization of the Pin1 substrate Suc-AEPF-pNA. Similarly to previous experiments, the potency of BP was much lower (Figure 4.1.6). This further proofs that DP is able to efficiently block function of Pin1.

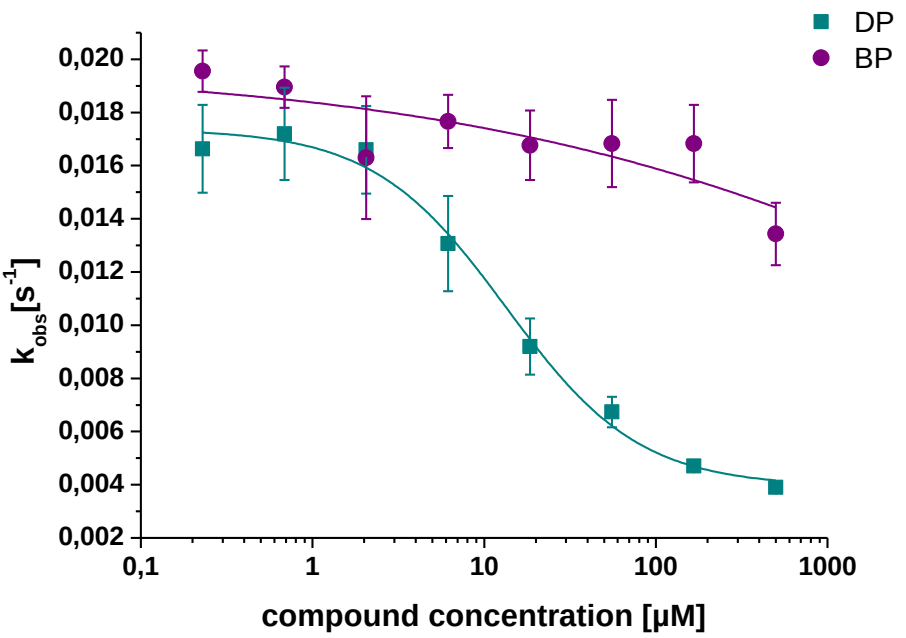

Figure 4.1.6 Inhibition of cis/trans isomerization of the Pin1 substrate Suc-AEPF-pNA by DP dexamethasone-21-phosphate (megenta line) and BP betadexamethasone-21-phosphate (purple line).

4.1.5 NMR measurements

In order to map the binding site of the ligands on Pin1 the ^{1}H-^{15}N HSQC titrations with DP and BP were carried out. Buffer conditions used in these experiments were as follows: 50 mM Na_3PO_4, 50 mM Na_2SO_4, 1mM β-mercaptoethanol, 5 mM EDTA, pH 6.6.

Titration of Pin1 with DP has caused numerous perturbations in the chemical shifts of signals of Pin1 (Figure 4.1.7).

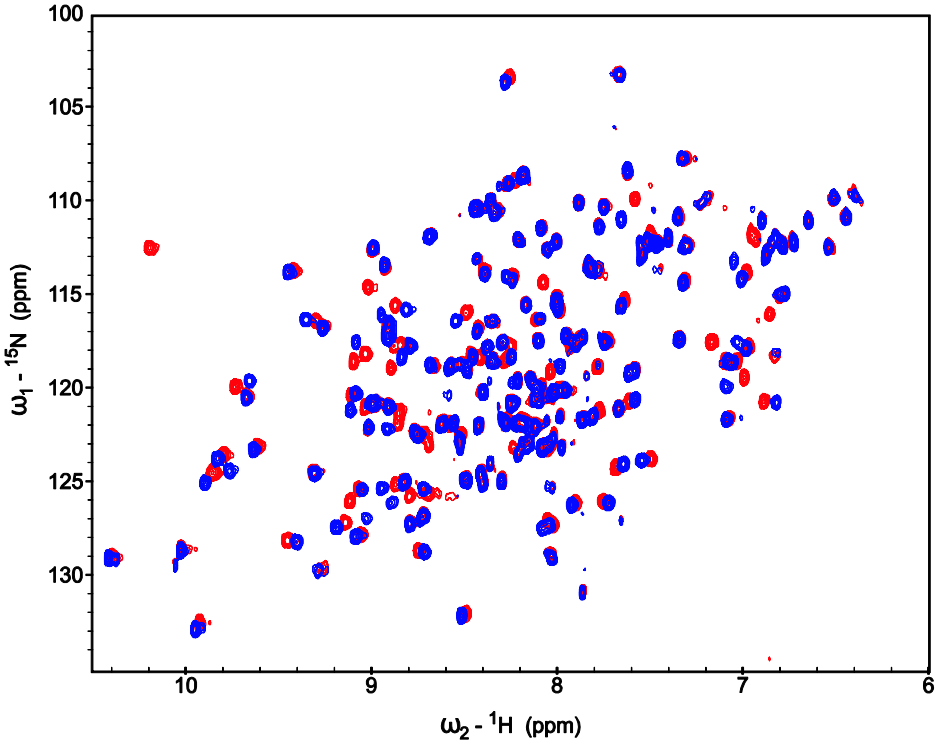

Figure 4.1.7 ^{1}H-^{15}N HSQC spectrum of Pin1-wt with an access of dexamethasone-21-phosphate; Pin1 (300 µM) red- reference spectrum; Pin1 (300 µM) with the 600 µM compound – blue.

Amino acids with strong and the DP dose-dependent shifts of their amide resonances include Ser154 and His59, which interact with the carbonyl oxygen of the peptide bond to be isomerized by the enzyme (Figure 4.1.8)(Zhang et al. 2007). Similarly, Phe134 at the bottom of the hydrophobic proline binding pocket also displayed strong shifts in the presence of DP. All of the strong shifts were localized within the substrate binding domain (Figure 4.1.9). In contrast, fewer and only weak shifts of the backbone amide resonances were observed in the WW domain upon addition of DP.

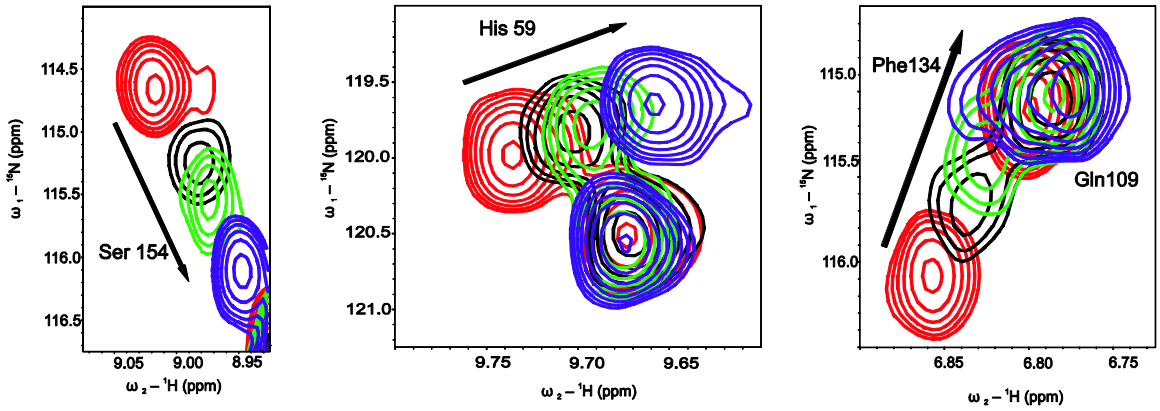

Figure 4.1.8 The amide resonances of Ser154, His59, and Phe134 of the ^{15}N-labeled Pin1 (300 μM) in the absence of DP (red) show strong and dose-dependent chemical shifts upon addition of DP (150 μM, green; 300 μM, dotted black; 600 μM, blue).

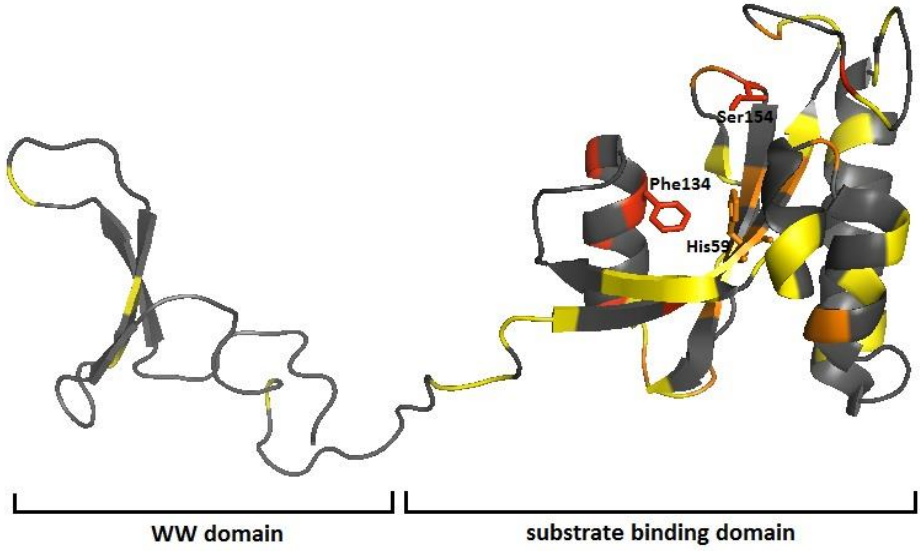

Figure 4.1.9 Graphic representation of the chemical shifts in the ^{1}H,^{15}N-HSQC-NMR of the full-length Pin1 (300 μM) observed after addition of DP (600 μM). The shifts are superimposed onto the solution structure of Pin1 (PBD code: 1NMV)(Bayer et al. 2003). Color code: red, very strong shift (Δδ ≥ 0.125 ppm); orange, strong shift (0.075 ppm ≤ Δδ < 0.125 ppm); yellow, medium shift (0.025 ≤ Δδ < 0.075 ppm); light blue, weak shift (Δδ < 0.025 ppm).

Consistent with its weaker affinity for Pin1, the epimer betamethasone-21-phosphate (BP) showed less and weaker shifts in the ^{1}H,^{15}N-HSQC NMR spectrum (Figure 4.1.10).

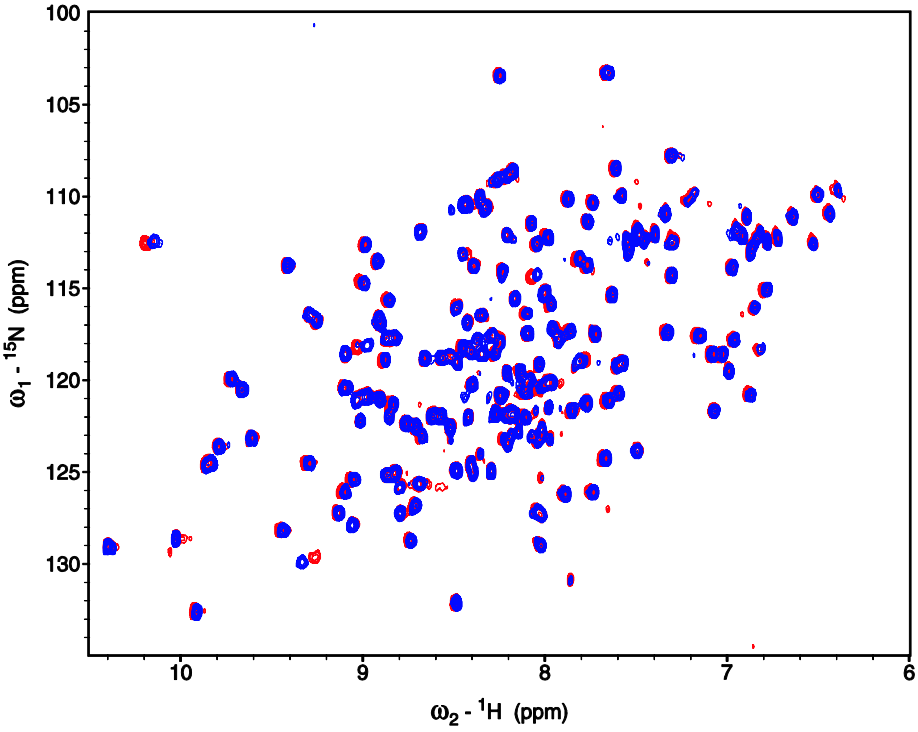

Figure 4.1.10 $^{1}H,^{15}N$ –HSQC spectra of Pin1-wt with an access of dexamethasone-21-phosphate (A) and betadexamethasone-21-pospahate (B); Pin1 (300 µM) red: the reference spectrum, Pin1 with the 600 µM compound, blue.

The presence of phosphate and sulfate ions has a stabilizing effect on the protein structure, what can be clearly seen from the good-quality ^{1}H, ^{15}N-HSQC spectrum in these conditions. In the crystallographic structure of the Pin1-wt apoprotein the sulpahte residue is located within the positively charged pocket comprising residues: Lys63, Arg68, Arg69 and Ser154 (Figure 4.1.11A). Exactly these residues are building close contacts with the phosphate from a threonine of the D-peptide, substrate of the Pin1 isomerization reaction (Figure 4.1.11B).

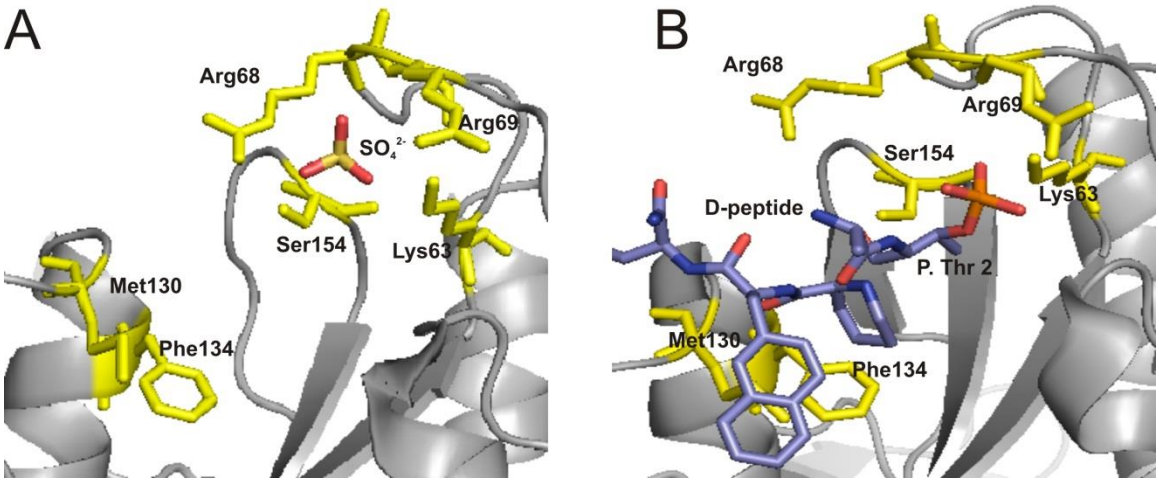

Figure 4.1.11 Comparison of the position of the sulfate residue in a crystallographic structure of apo Pin 1-wt (A) and position of phosphate group of the threonine from the D-peptide bound to Pin1 (B); adapted from pdb the files: 1PIN and 1FKB, respectively.

Since DP contains a phosphate residue it is possible that it also occupies the positively charged pocket of Pin1 and in the buffer containing sulfate and phosphate ions its binding can be weaken, because of the competing effect. The measurements have indicated 0.4 and 2 mM K_D calculated for the titration of the Pin1 PPIase domain with sulfate and phosphate, respectively (Bayer et al. 2003). In order to investigate the influence of sulfate and phosphate ions on binding of DP to Pin1, the titration with the compound was performed in 50 mM Tris, 1mM β-mercaptoethanol, pH 6.6 (Figure 4.1.12).

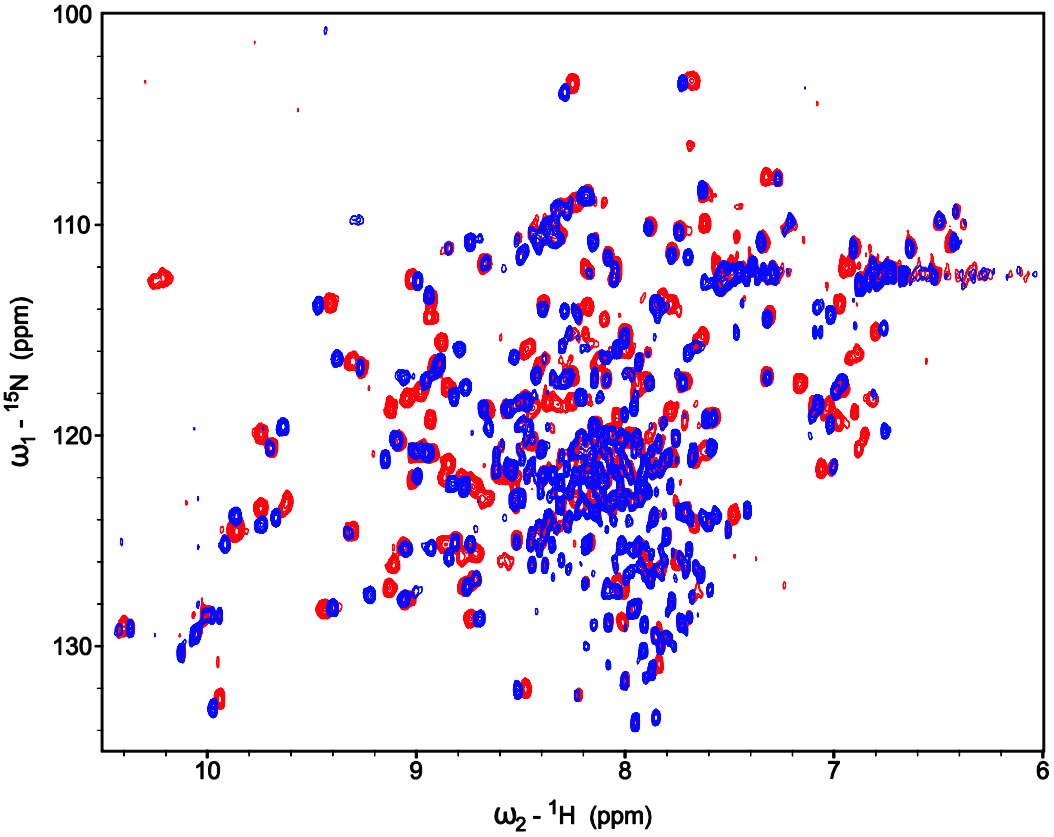

Figure 4.1.12 $^{1}H,^{15}N$-HSQC spectra of Pin1-wt with an access of dexamethasone-21-phosphate; Pin1 (300 µM) red: the reference spectrum, Pin1 with the 600 µM compound, blue. The measurement was performed in 50 mM Tris, 1mM β-mercaptoethanol, pH 6.6.

Titration of Pin1 with DP in the Tris buffer showed lower protein stability. The reference spectrum shows much stronger shifts upon addition of DP (Figure 4.1.13). The result is consistent with the results of the previous experiments, which have shown the occupancy of the positive patch with the phosphate or sulfate residue. In presence of phosphate and sulfate the DP is an antagonist of binding to the protein, because the part of its binding pocket is already occupied with one of the ions.

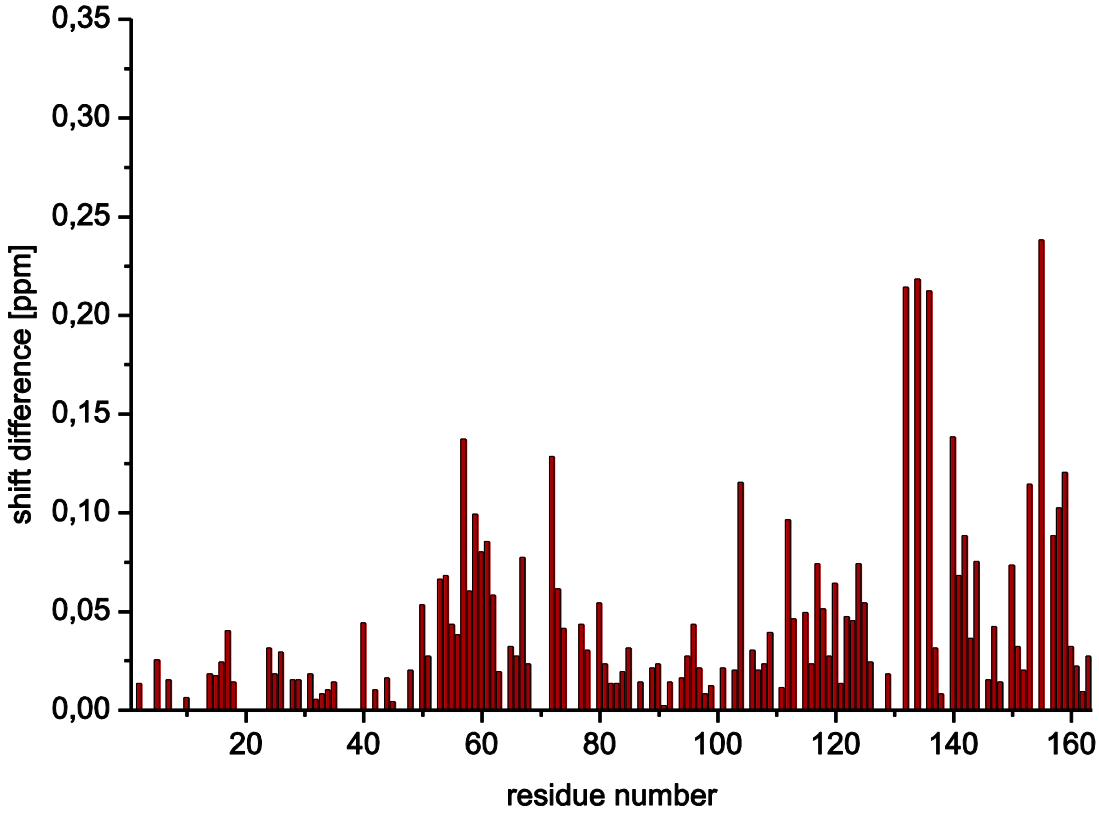

Figure 4.1.13 Chemical shift differences of amide resonances in the NMR spectrum of the Pin1 and Pin1 with an access of DP in the buffer containing phosphate and sulfate ions.

In the stack plot of the chemical shift differences of the amide resonances between the reference spectrum of Pin1 recorded in sulfate/ phosphate buffer and the spectrum upon addition of an access of DP there are numerous strong shifts localized mostly within the catalytic domain (residues 45-163)(Figure 4.1.13). Comparison of these perturbations with the chemical shift differences before and after titration with DP for the spectra recorded in the Tris buffer has shown the significantly larger DP-indued chemical shifts for Pin1 (Figure 4.1.14).

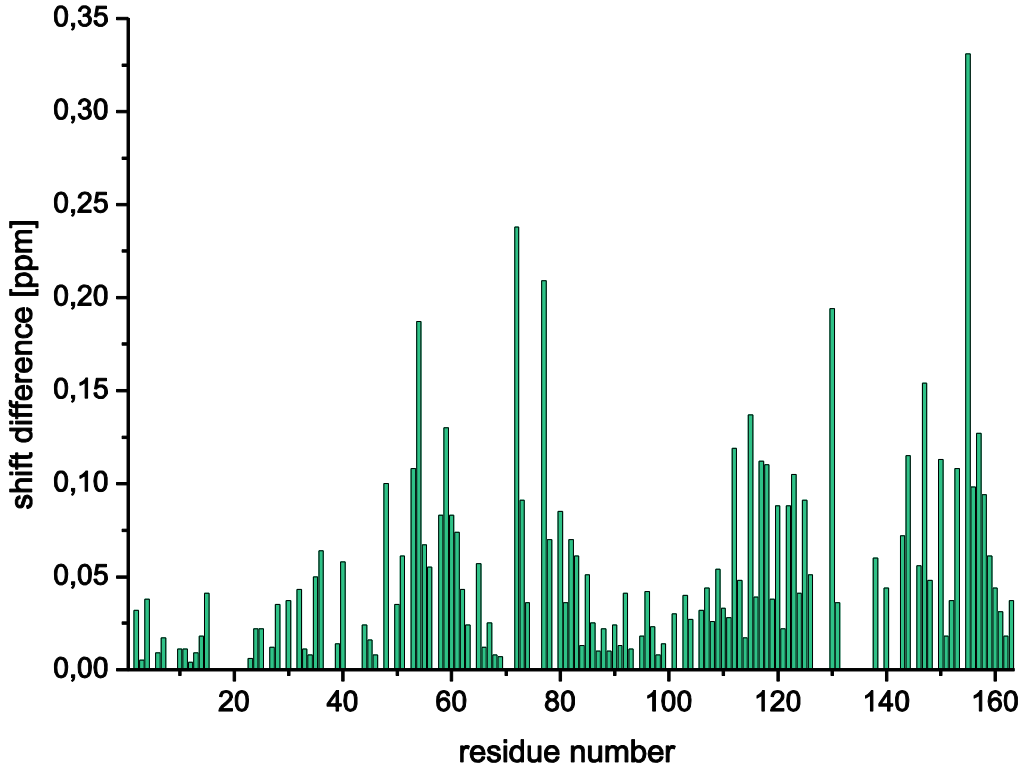

Figure 4.1.14 Chemical shift differences of amide resonances in the NMR spectrum of the Pin1 and Pin1 with an access of DP in the Tris buffer.

4.1.6 Structure of Pin1 with dexamethasone-21-phosphate

4.1.6.1 Crystallization of Pin1 with dexamethasone-21-phosphate

The Pin1-R14A mutant was used for crystallization purposes, because it has favorable crystallization properties while retaining the binding functionality of the wild-type enzyme (Lu et al. 1999; Zhang et al. 2007). The protein was obtained as described in Part 4.1.1. After gel filtration, in order to check whether the protein is pure and well-folded, the NMR spectrum of Pin1-R14A was recorded. NMR showed properly folded protein (Figure 4.1.15).

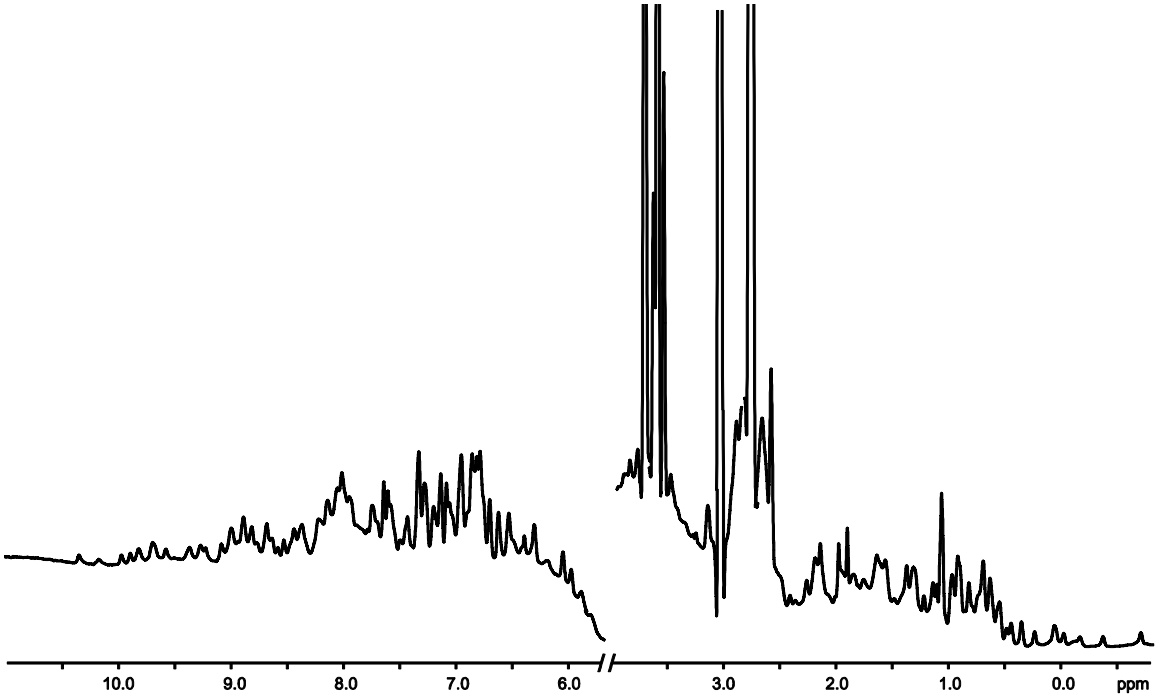

Figure 4.1.15 1D ^{1}H spectrum of Pin1-R14A used for crystallization.

The protein was then concentrated up to 18 mg/ml. Crystals of human Pin1-R14A (Zhang et al., 2007) were obtained using the sitting-drop vapor-diffusion method. The Pin1 was mixed 1:1 (v/v) with a mother liquor of 2.1-2.4 M $(NH_4)_2SO_4$, 0.1 M HEPES (pH 7.5), 1-5% PEG 400. Crystals appeared within two days at 4ºC and were up to 1 mm long (Figure 4.1.16).

Crystals of the ligand-bound complexes were prepared by adding 0.2 µl of the solution of 10 mM dexamethasone-21-phosphate (DP) in water to the crystals of apo-Pin1-R14A in mother liquor for a period of 24 h before harvesting. Prior to the data collection, all crystals were transferred to a cryosolvent containing 30% glycerol in the mother liquor. The crystals were frozen in liquid nitrogen.

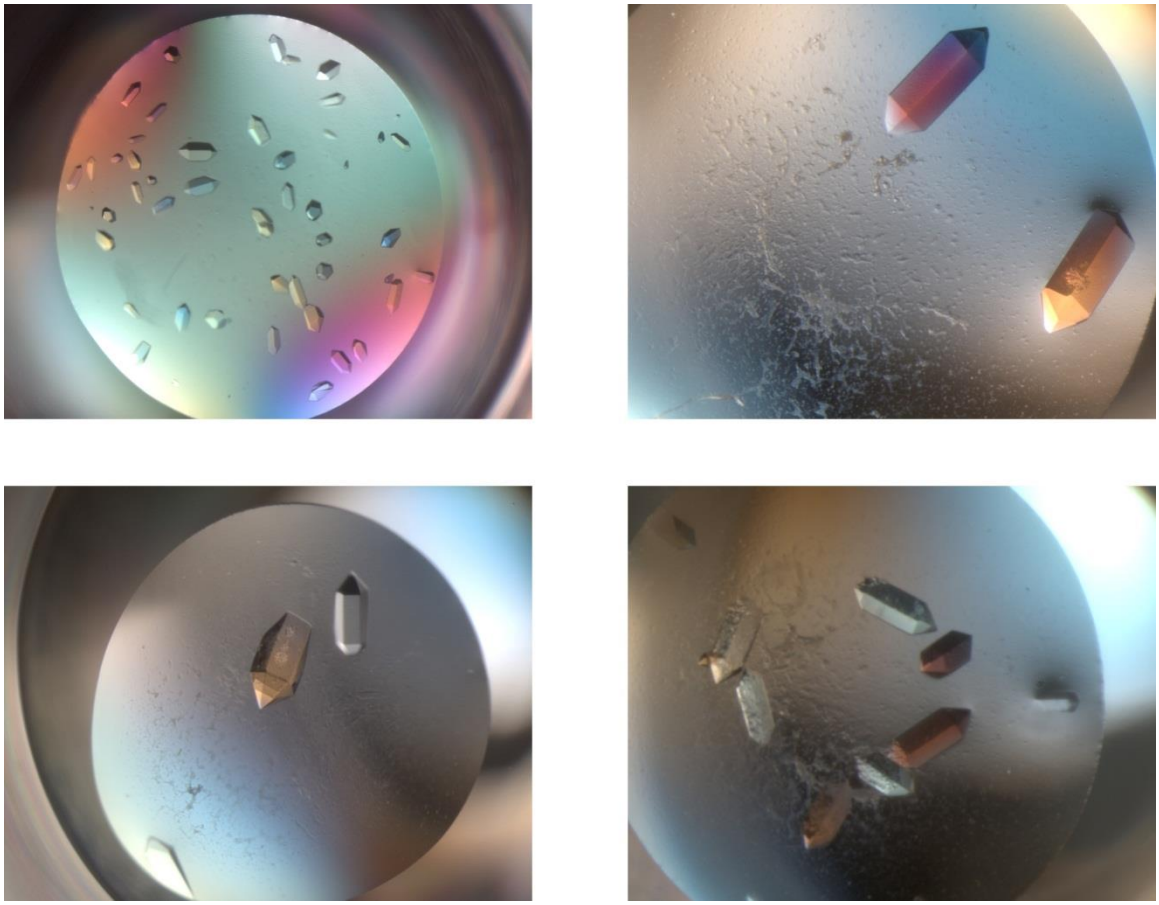

Figure 4.1.16 Crystals of Pin1-R14A (2.1-2.4 M $(NH_4)_2SO_4$, 0.1 M HEPES pH 7.0-8.0, 1-5% PEG 400).

4.1.6.2 Data collection

Data sets with resolutions of up to 1.4 Å were collected on the SLS beamline PXII at the Paul Scherrer Institute, Villigen, Switzerland. The collected data were integrated, scaled and merged by XDS and XSCALE (Kabsch, 1993). The structures were determined by molecular replacement using Molrep (Vagin and Teplyakov, 1997) from the CCP4 (Collaborative Computational Project, 1994). The structure of the human Pin1-R14A mutant (Zhang et al., 2007) (pdb entry: 2ZR6) was used as a probe. Models were refined by Refmac5 (Murshudov et al., 1997), and rebuilt by MiFit (McRee, 2004) and by a subsequent Refmac5 refinement. The refinement was carried out for the resolution range from 19.7-1.4 Å. Signals outside this range did not carry sufficient information to improve the model. Water molecules were added with the Arp/Warp program (Perrakis et al., 1997). The final models were evaluated using Procheck

(Morris et al., 1992). Residues 38-51 are missing in the structure of the complex due to insufficient electron density.

Table 4.1.1 Data collection and structure refinement

Data collection	
Space group	P 3_1 2 1
Cell constants (Å)	
	a = 68.36
	b = 68.36
	c = 79.37
Resolution range (Å)	59-1.4
Wavelength (Å)	1
Observed reflections	297502
Unique reflections	42028
Whole resolution range:	
Completeness (%)	98,3
*R*merge (%)	6,8
I/σ(I)	18,3
Last resolution shell	
Resolution range (Å)	1.7-1.4
Completeness (%)	96.9
*R*merge (%)	33.8
I/σ(I)	4.67
Refinement	
No. of reflections	32347
Resolution (Å)	19.7-1.4
R-factor (%)	17.5
Rfree (%)	21.1
Average B (Å2)	15,4
R.m.s bond ength (Å)	0.007
R.m.s. angles (Å)	1.146
Content of asymmetric unit	
RMSD of monomers (Å)	NA
No. of complexes	1
No. of protein residues/atoms	143/1135
No. of solvent atoms	266

4.1.6.3 Structure analysis

Crystallographic analysis of Pin1 bound to DP confirmed the localization of the ligand's phosphate group in the positive patch of the Pin1 substrate- binding domain formed by Lys63, Arg68, and Arg69 (Figures 4.1.17 and Figure 4.1.18A). This is consistent with the NMR experiments. The keto group in the ligand's side chain is located in a hydrophilic pocket between of Ser154, His59, and His157 (Figures 4.1.17 and Figure 4.1.18B). The methyl group attached to C-16, the spatial orientation of which solely accounts for the activity difference between DP and BP, is appropriately positioned for a hydrophobic interaction with Phe134 of Pin1. The more hydrophobic side of the inhibitor's tetracyclic ring system is accommodated by the hydrophobic pocket composed of Phe134, Leu122, and Met130, which forms the binding pocket for the proline ring in Pin1 substrates (Daum et al. 2006) and extends to Phe125.

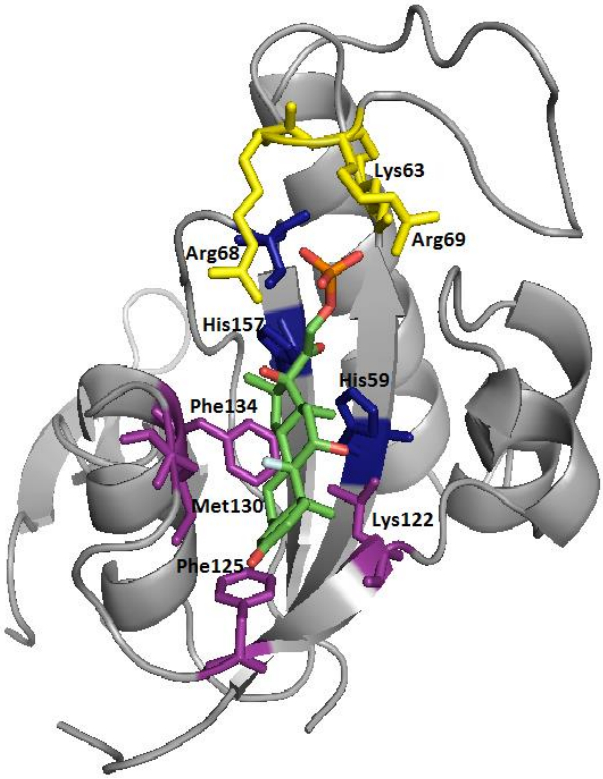

Figure 4.1.17 X-ray structure of the complex of Pin1-R14A mutant and dexamethasone-21-phosphate (PDB code 3TC5). Amino acids are color-coded based on their functional contribution to binding of DP. Yellow, phosphate binding; light blue, exocyclic carbonyl oxygen binding; magenta, hydrophobic core and C-16 methyl group binding.

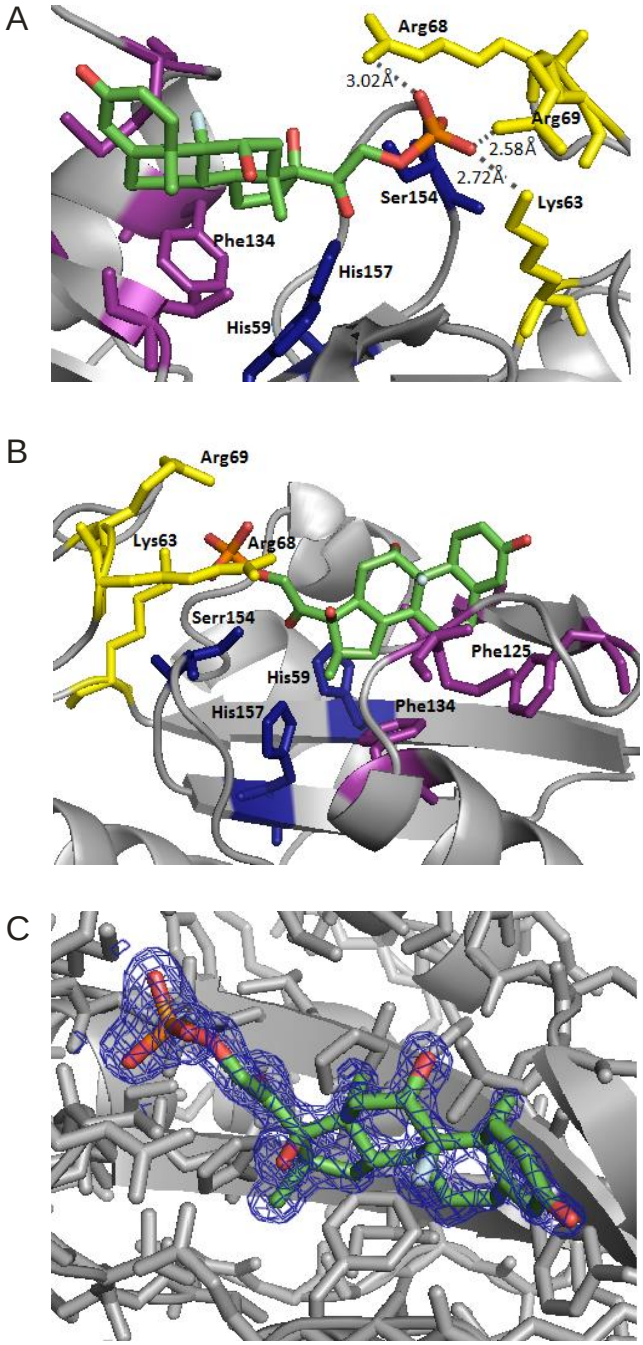

Figure 4.1.18 Alternative depictions of the X-ray structure of the complex of Pin1-R14A and dexamethasone-21-phosphate (PDB code 3TC5). Pin1 Lys63, Arg68, and Arg69 form hydrogen bonds with the phosphate group of DP (A). Close-up of the accommodation of the methyl group attached to C-16 and the exocyclic carbonyl group of DP by Pin1 (B). Electron density of DP is depicted as a SigmaA-weighed $2F_0 – F_c$ electron density map contoured at 1.5 σ (C).

4.1.7 Summary and perspectives

Along with aryl indanyl ketones (Daum et al. 2006), phenyl-imidazole-based compound (Potter et al. 2010) quinazoline derivatives, (Zhu et al. 2011) and (Guo et al. 2009; Xu and Etzkorn 2009; Dong et al. 2010; Potter et al. 2010) (Zhang et al. 2007; Duncan et al. 2011) tetraxobenzophenanthrolines (Uchida et al. 2003) dexamethasone-21-phosphate is among the few non-peptidic and non-reactive inhibitors of Pin1 with activities below 10 µM. Importantly, DP is the only member of this group whose specificity was tested against a panel of related phosphorylation-dependent protein binding domains and which thus can be regarded as Pin1-specific with regards to this class of protein domains. The Pin1 inhibitor Juglone is thought to interact covalently with the enzyme (Hennig et al. 1998) and has been reported to exert additional biological activities (Xu and Etzkorn 2009). While a number of non-reactive ligands for the substrate-binding domain/enzymatic domain of Pin1 with submicromolar or nanomolar affinities have been described, these agents comprise either peptides (Zhang et al. 2007; Duncan et al. 2011) or peptide mimetics (Guo et al. 2009; Xu and Etzkorn 2009; Dong et al. 2010; Potter et al. 2010).

Subsequent introduction of protecting groups that mask the phosphonate's negative charges and are prone to intracellular hydrolysis can generate cell-permeable compounds, as was impressively shown in a number of recent studies (Liu et al. 2004; Laketa et al. 2009; Mandal et al. 2011). Efforts to develop dexamethasone-21-phosphate into highly potent agent suitable for use in whole cells are currently ongoing. On a wider note, our data indicate that it would be advisable to analyze the activities of uncleaved phosphate prodrugs intended for clinical use with respect to phosphorylation-dependent protein binding domains.

4.2 SEI AIDA

The SEI-AIDA method was illustrated with lead compounds that block the MDM2−p53 interaction in humans and with inhibitors of human cyclin-dependent kinase 2 (CDK2) (Figure 4.2.1) (Shvarts et al. 1996; Knockaert et al. 2002; Marx 2007; Shangary and Wang 2008).

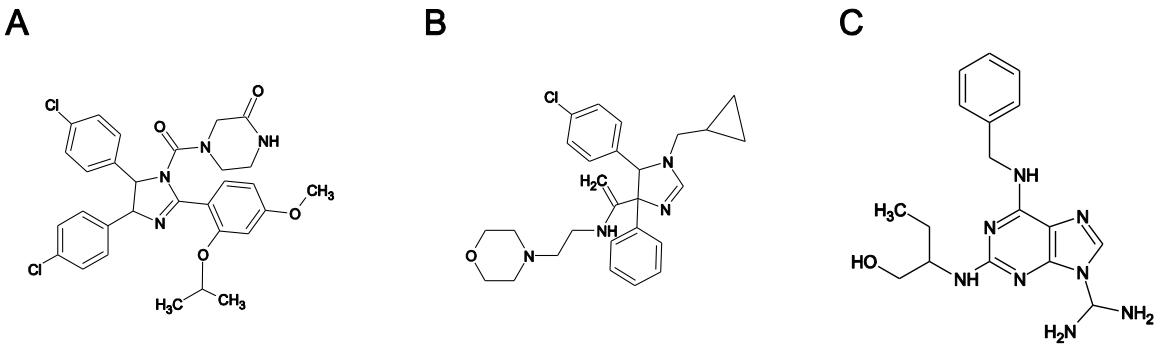

Figure 4.2.1 Structure of inhibitors of MDM2-p53: nutlin-3 (A); PB10 (B); inhibitor of CDK2: roscovitine (C).

All of the spectra were acquired using the SEI pulse sequence, the complex concentration (for MDM2 inhibitors) was 36 μM and acquisition was carried out within 2 minutes. Examples of the assay for two antagonists of the MDM2−p53 interaction: a strongly binding nutlin-3 and a weakly binding PB10, are shown in Figure 4.2.2 parts A and B, respectively. Since AIDA is a competition experiment, the K_D of protein−antagonist interaction can be determined in a single measurement as described in (Krajewski et al. 2007). For nutlin-3, our assay produces the K_D of the binding to MDM2 of 90 nM, in agreement with the literature data (Vassilev et al. 2004; Shangary and Wang 2008). The SEI AIDA indicates that compound PB10 binds weakly to MDM2 (Figure 4.2.2D), with an estimated K_D of 3 μM, in agreement with the binary titration on the MDM2 T101W mutant acquired also using the SEI pulse sequence (Figure 4.2.3). In the measurement with the T101W mutant the compound is in the fast exchange regime on the NMR timescale, thus the NH^{ε} peak of W101 MDM2 (indicated with an asterisk) moves continuously from its initial to final position.

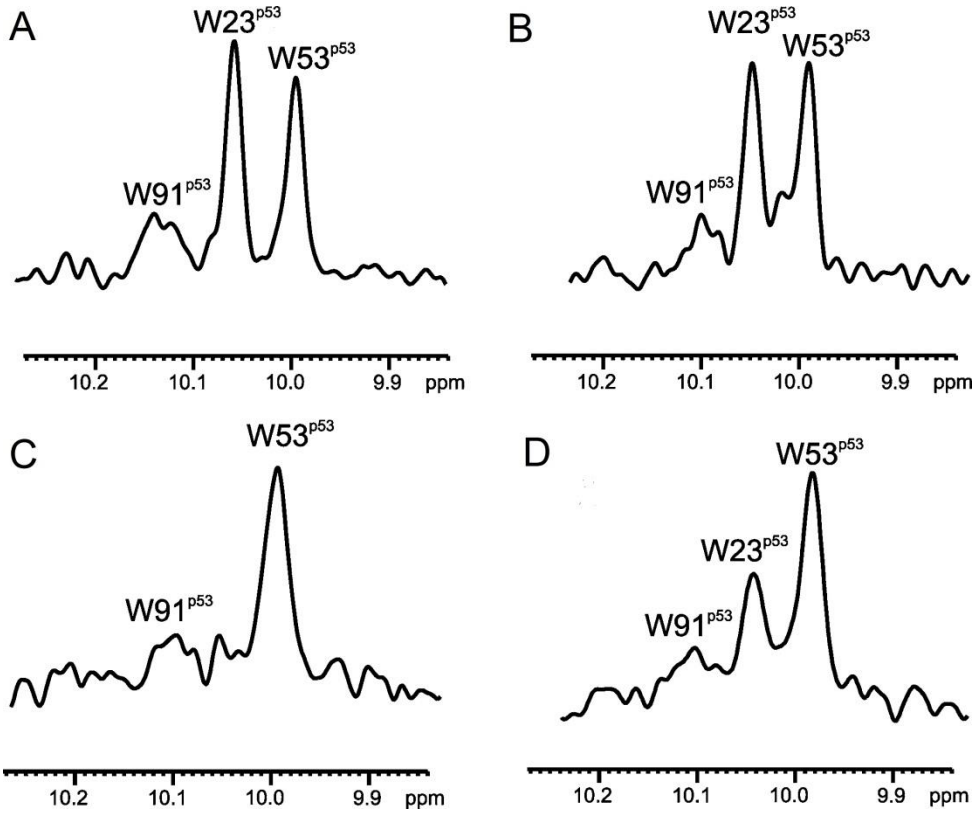

Figure 4.2.2 The NH^{ε} indole Trp region of 1D 1H NMR spectra of the MDM2−p53 complex. The signal of Trp23 of p53 is used for monitoring the ligand/MDM2−p53 interactions. Free p53 (A); the MDM2-p53 complex titrated with nutlin-3; the protein: inhibitor molar ratio 1:2 (B), the MDM2−p53 complex (C), the MDM2-p53 complex titrated with compound PB10; the protein: inhibitor molar ratio 1:2 (D).

CDK2, the second protein chosen as a model, together with its associated cyclin, controls the passage of the cell through different phases in cell division. Inhibiting CDKs in tumor cells should arrest or stop the progression of the uncontrolled tumor cell division (Knockaert et al. 2002; Rothweiler et al. 2008). Figure 4.2.3 E−G shows the application of the SEI-AIDA to roscovitine (Figure 4.2.1C), an extensively characterized small-molecule inhibitor of CDK2 with the nanomolar affinity (Knockaert et al. 2002; Rothweiler et al. 2008). The compound is in slow exchange with CDK2 and, thus, the NH^{ε} peak originating from the newly introduced W93 (indicated with a cross) is split into 2 peaks originating from the bound and free fractions of CDK2-A93W.

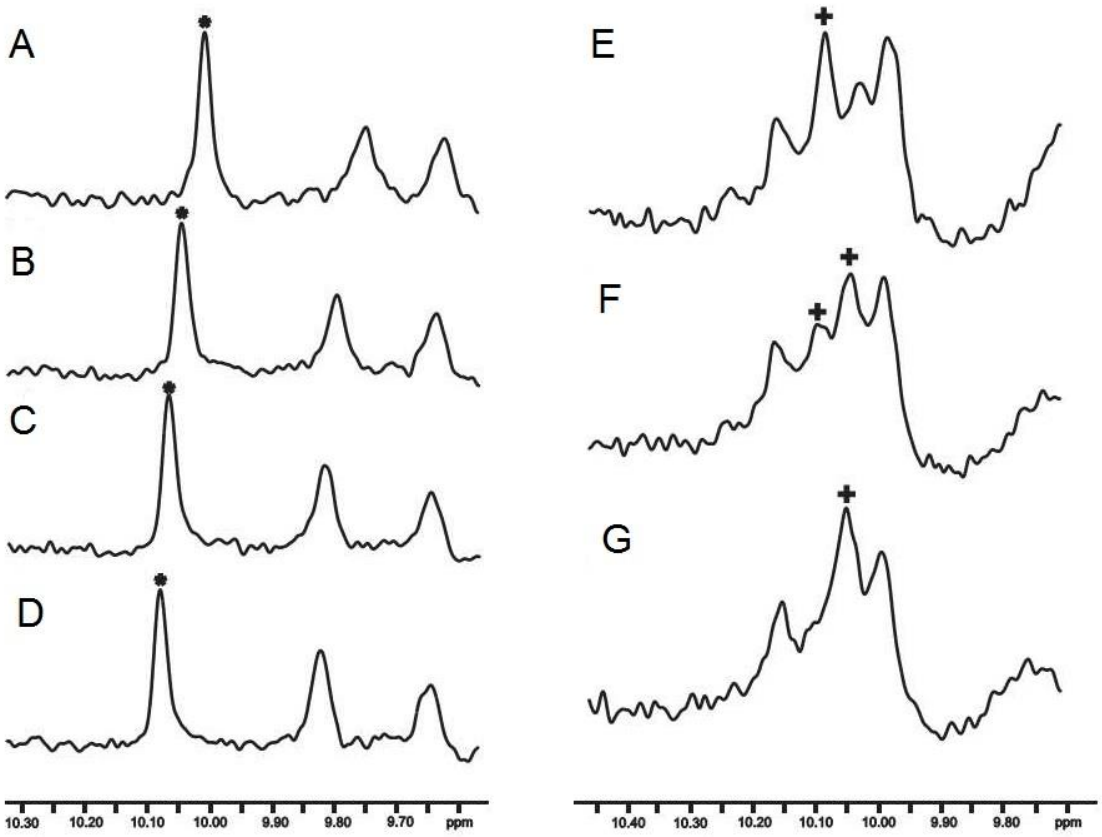

Figure 4.2.3 Binary NMR titrations of small molecule ligands with the 20 μM solutions of the MMD2-T101W and the CDK2-A93W mutants using the SEI pulse sequence. Titration of the 20 μM solution of the MDM2-101W mutant with increasing amounts of compound PB10; the compound: protein molar ratio: 0:1 (A), 1:1 (B), 2:1(C), 5:1(D), respectively; Titration of the 20 μM CDK2 A93W mutant with increasing amount of roscovitine; the compound: protein molar ratio: 0:1(E), 0.5:1(F); 1:1(G)

The experimental time for each step of the shown experiments was only 10 min. The SEI pulse sequence gives approximately ten-fold reduction in experimental time compared to the corresponding proton spectra acquired using 90^{o} hard pulses. The SEI experiment gives spectra with a reduced bandwidth and significantly increased signal-to-noise ratio, thus the concentration of the protein used can be significantly reduced: even tenfold reduction has still allowed to record a good-quality spectrum.

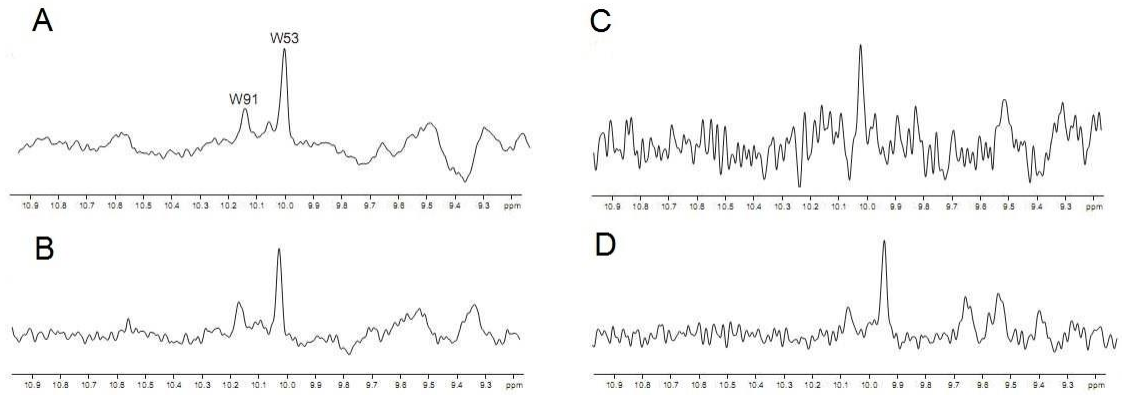

Figure 4.2.4 1D ^{1}H NMR spectra of the MDM2-p53 complex: Spectrum of the 35 μM solution of the Mdm2-p53 complex recorded using a 90^{o} hard pulse followed by a WATERGATE-W3 sequence (acquisition time: 0.5 h) (A); spectrum of the 35 μM solution of the Mdm2-p53 complex recorded using a 90 hard pulse followed by a WATERGATE-W3 sequence (acquisition time 2.5 min) (B); spectrum of the 35 μM solution of the p53-MDM2 complex recorded using the SEI pulse sequence (acquisition time 2.5 min) (C). Spectrum of the 3.5 μM solution of the MDM2-p53 complex recorded using the SEI pulse sequence (acquisition time 1 h) (D).

Since only well separated downfield or upfield shifted signals are recorded, the experiment is insensitive for common additives (buffering substances, detergents, etc.) and thus their predeuteration is not required. The water suppression scheme employed in the SEI sequence is insensitive for pulse miscalibration. The method may be therefore routinely applied without the need for precise pulse length calibration; i.e., it is possible to measure NMR samples with different solvent compositions without changing the experimental setup. Since only relatively short and low power pulses are employed, the method is safe for superconducting low-temperature NMR probes. The SEI pulse sequence can be in principle also used to improve the sensitivity of other separated proton signals (e.g., the aliphatic signals of proteins, if resolved).

In summary, we show that the combination of a simple SEI pulse sequence with 1D AIDA NMR screening is a straightforward, robust alternative to traditional NMR screening methods. Due to increased sensitivity, the SEI experiment is beneficial for the NMR of proteins difficult to obtain, whereas the reduction of experimental time can significantly increase the throughput of NMR screening. SEI AIDA-NMR can be used universally for monitoring ligand/protein−protein complexes because by introducing tryptophan residues through site-directed mutagenesis the method can also be applied to proteins that do not contain tryptophan in their natural amino acid sequence. Our

method is suitable also for chromophoric and fluorescent aromatic small molecule compounds and, thus, may complement assays based on the intrinsic fluorescence of tryptophan, which usually fail in these cases.

4.3 New inhibitors of MDM2/X

This part of the work was done as a joined project with the group of Professor Alexander Dömling form the University of Pittsburg in the USA. The aim of the study was to discover and develop dual inhibitors of the interaction between MDM2/X and p53. All compounds were designed based on the structural information of the interaction of the protein partners. At the initial stages of the project the core scaffolds were deigned. These were extended with the substituents in order to improve pharmacokinetic properties of the molecule and strengthen their affinity towards target protein. The compounds were qualitative and quantitative characterized for their ability to dissociate the MDM2-p53 and MDMX-p53 complexes by the means of the FP and NMR spectroscopy methods. Finally, the best compounds were crystallized.

4.3.1 Protein purification

MDM2

For the NMR and FP measurements the MDM2 construct comprising residues 25-111 (because of higher expression rates) and for crystallization the construct comprising residues 11-125 (based on better crystalizing properties) were purified as described in Chapter 2.2.6.1. For the NMR and FP measurements the last step of purification-gel filtration was performed in phosphate buffer and for crystallization in Tris buffer. In order to check quality and purity of our MDM2 protein, SDS-PAGE electrophoresis was run. An example of a chromatogram of purification by the means of gel filtration and a SDS-PAGE gel in shown in Figure 4.3.1

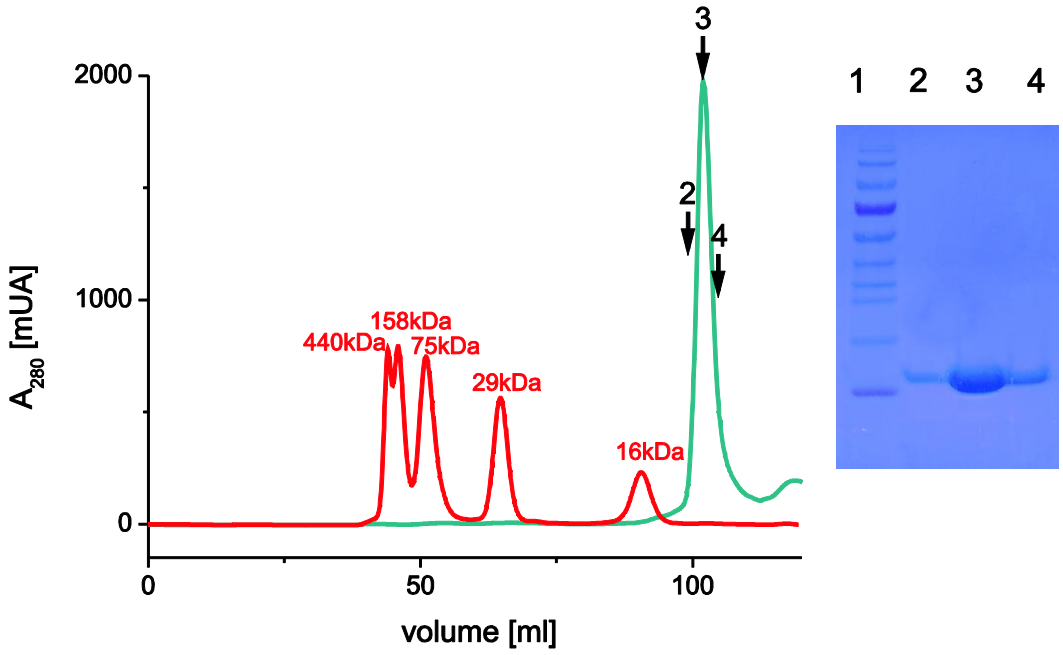

Figure 4.3.1. Chromatogram and the SDS-PAGE analysis of the MDM2 (11-125) after gel filtration; SDS-PAGE (lines 2-4 fractions marked with arrows in the chromatogram, respectively, marker: line 1).

MDMX

Purification process of MDMX was depending on further application of the protein. Since, IMAC chromatography is a fast and effective method of purifying proteins for the NMR and FP, MDMX for these purposes was purified from the native fraction as described in the Chapter 2.2.6.2. For these applications the presence of the affinity tag did not affected the results of the experiment. However, an uncleaved tag can impair protein crystallization. Therefore for crystallization purposes was used MDMX construct (23-111) mostly expressed in incusion bodies. Purification was performed as described in chapter 2.2.6.1. The protocol was amended with an additional step of ion- exchange chromatography. An example of a chromatogram of purification by the means of anion-exchange chromatography and SDS-PAGE gel in presented in Figure 4.3.2.

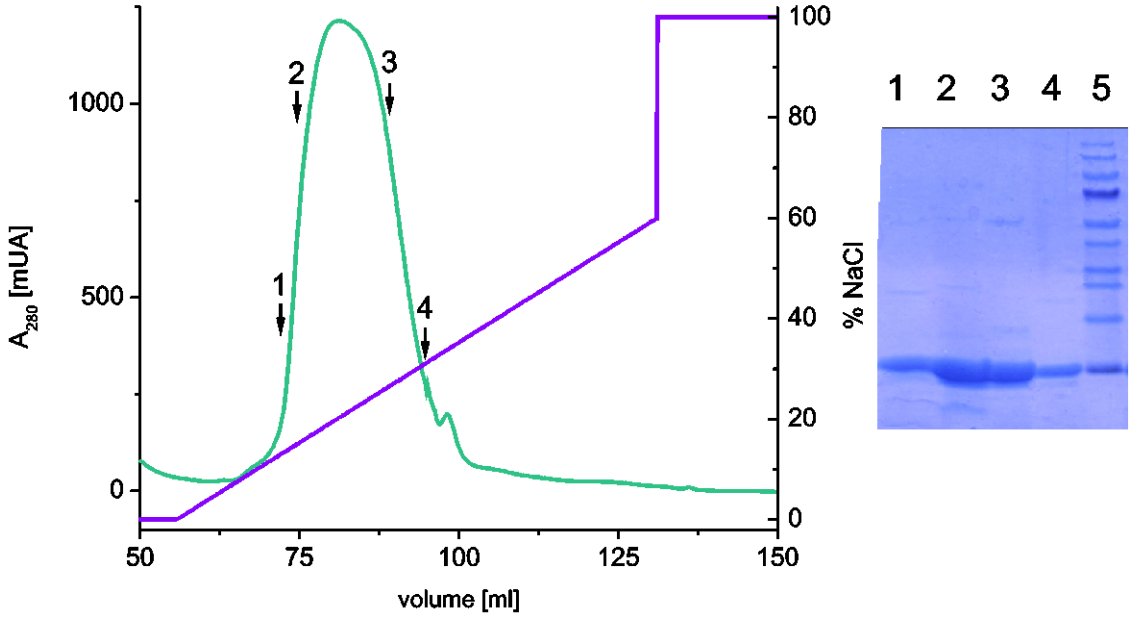

Figure 4.3.2 Chromatogram and the SDS-PAGE analysis of the MDMX (23-111) after ion exchange chromatography-SP Superdex; SDS-PAGE (lines 1-4 fractions marked on the chromatogram with arrows, respectively, marker: line 5).Purple line- rising gradient of concentration of NaCl.

Gel filtration was carried out in order to lower the concentration of NaCl used in elution step in the ion-exchange chromatography and to remove the aggregates (which could impair the crystallization). An example of a chromatogram of purification by the means of gel filtration and a SDS-PAGE gel afterwards is presented in Figure 4.3.3.

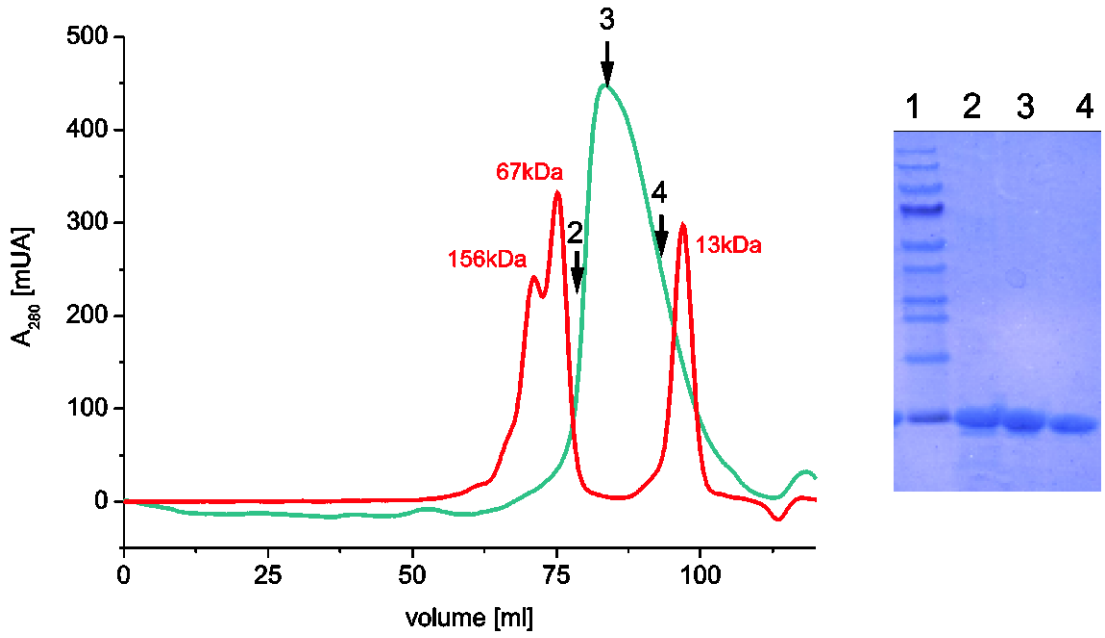

Figure 4.3.3. Chromatogram and the SDS-PAGE analysis of the MDMX after molecular filtration; SDS-PAGE gel (lines 2-4 fractions marked on the chromatogram with arrows, respectively, marker: line 1).

4.3.2 New inhibitors for MDMX

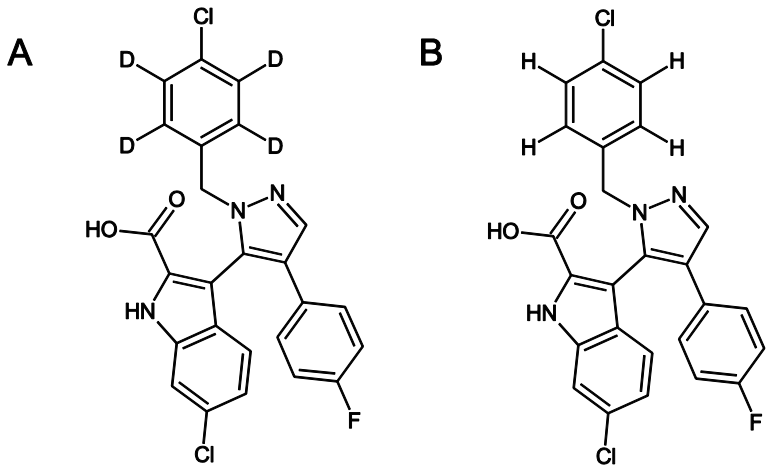

Figure 4.3.4 Structure of YH365 (A) and YH264 (B)

Figure 4.3.4 shows examples of the formulas of novel inhibitors of the MDM2/X-p53 interactions that we developed. The FP measurements showed the binding of the "best" of these compounds to be in the low micromolar range for MDMX (Figure 4.3.5), the estimated values of Ki were: 8.7 µM for YH365 and 9 µM for YH264.

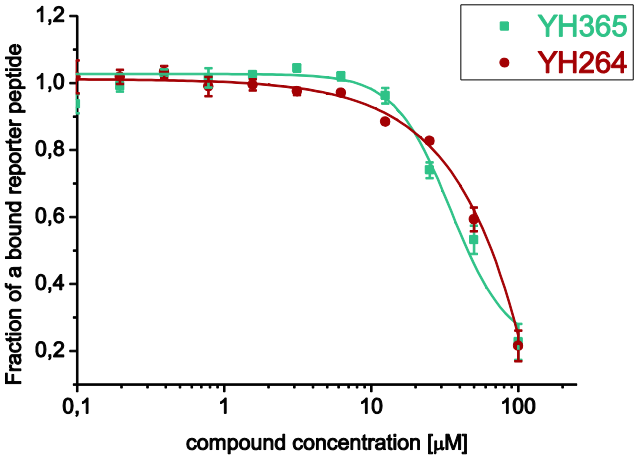

Figure 4.3.5 Activities of YH264 (green) and YH365 (red) in the fluorescence polarization assay with MDMX.

The FP assay is a high-throughput tool used as the initial step of the screening for the inhibitors, but, unfortunately it provides a lot of false positive results. The release of the target protein from the complex with fluorescently labeled peptide leads to reduction of the anisotropy of fluorescence polarization. The process can occur not only through binding of the inhibitor to the target protein, but also through protein precipitation. In order to exclude the compounds which are acting on the target protein through precipitation and based on this feature give positive results in the FP assay, the compounds giving positive results in the FP assay were additionally checked by the means of the NMR spectroscopy. The NMR titration was performed in two steps; in the first one the concentration ratio of protein to compound was 1:1 (Figures 4.3.6 and 4.3.7 blue spectra) and in the second step this ratio was 1:2 (Figures 4.3.6 and 4.3.7 green spectra).

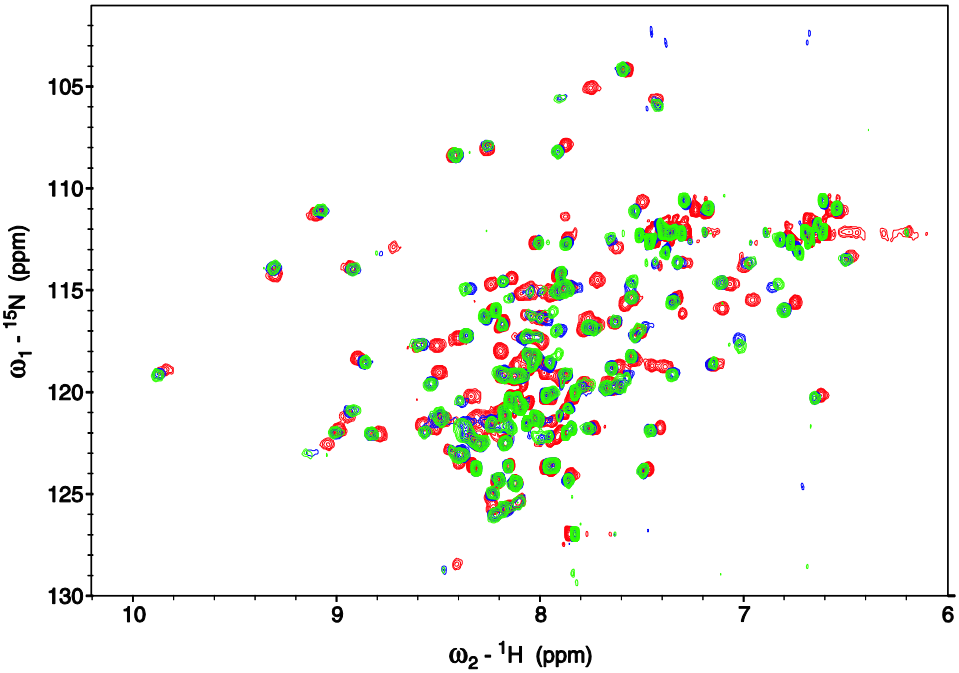

Figure 4.3.6 $^{1}H,^{15}N$ HSQC spectrum of MDMX (23-111) (red) with the molar concentration ratio YH365 to protein 1:1 (blue); with YH365 to protein 1:2 (green).

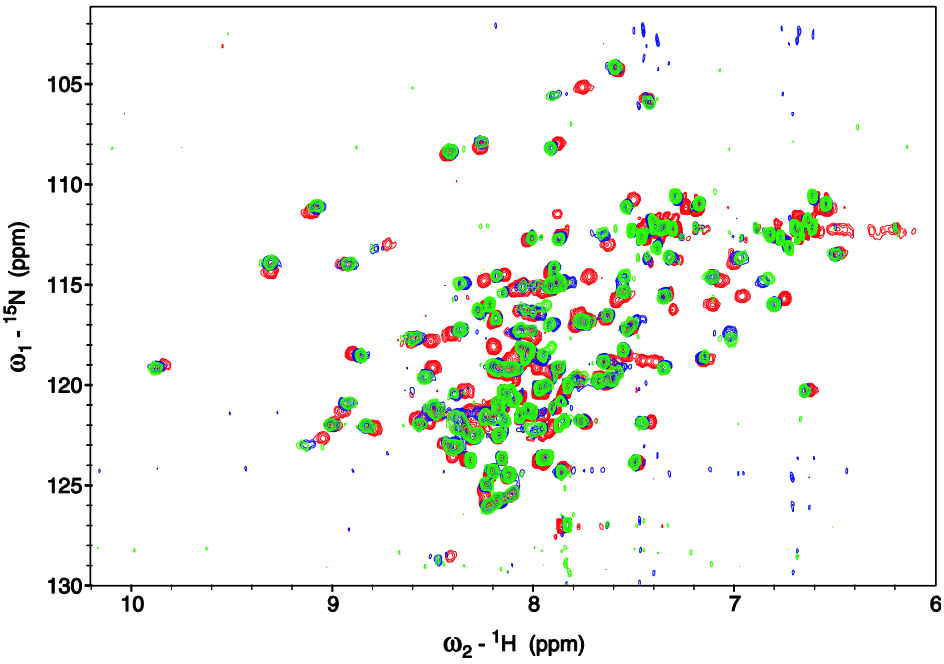

Figure 4.3.7 $^{1}H,^{15}N$ HSQC spectrum of MDMX (23-111) (red); with the molar concentration ratio of YH264 to protein 1:1 (blue); with YH264 to protein 1:2 (green).

Both spectra show several shifts indicating binding to MDMX. In order to estimate the K_D of the compounds by the means of NMR spectroscopy, the AIDA measurements have been performed (Figure 4.3.8). The estimated binding constants were 8 µM for YH365 and 9.5 µM for YH264.

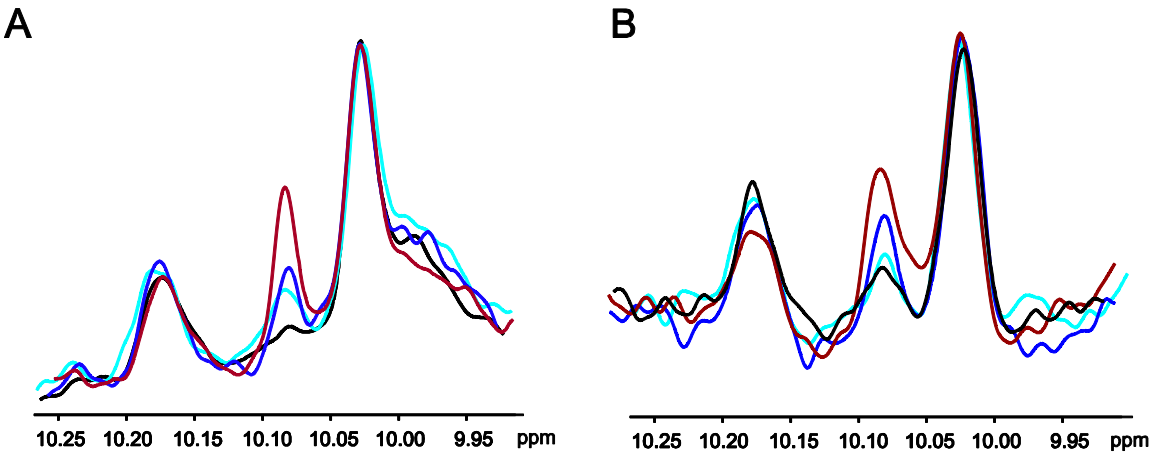

Figure 4.3.8 AIDA measurement of MDMX-p53 complex titrated with YH365 (A) and with YH264 (B); a reference spectrum of the MDMX-p53 complex , black; compound to complex ratio: 1:1 pale blue; 2:1 navy; 5:1 red.

4.3.3 New inhibitors for MDM2

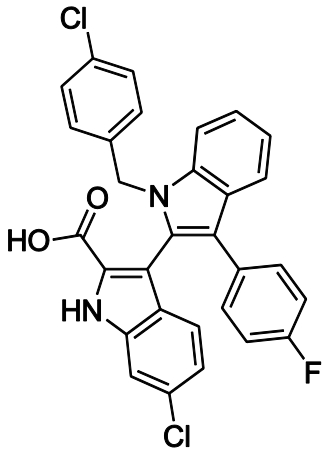

Figure 4.3.9 Structure of WK5-50-2

Compound WK 5-50-2 (Figure 4.3.9) was identified as a possible inhibitor of the MDM2-p53 interaction and showed strong binding in the FP assay with both MDM2 and

MDMX.The calculated K_i values were 0.7 and 1.5 µM, respectively. However, the analysis of the dissociation profile has indicated significant differences between the two proteins (Figure 4.3.10).

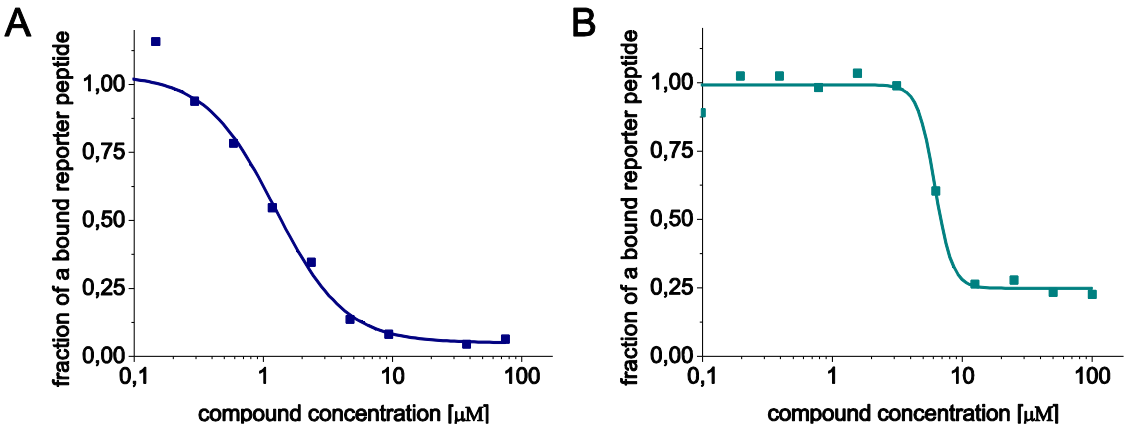

Figure 4.3.10 Activities of WK 5-50-2 in the fluorescence polarization assay with MDM2 (A) and MDMX (B).

In case of MDM2 addition of an inhibitor has caused a stepwise decrease of the intensity of the fluorescence polarization indicating dissociation of the complex of MDM2 with the fluorescence peptide. However, the complex with MDMX titrated in the same way seemed not to be affected at the initial stage and finally has turned to be completely dissociated. The fraction containing approximately 60% of the bound peptide is probably the mixture of the fractions of completely bound and fully released complex of MDMX with the fluorescent peptide. The potency of WK 5-50-2 as an inhibitor was additionally checked against both MDM2 and MDMX by the means of the NMR spectroscopy. The concentration of both proteins was approximately 0.3 mM. The ^{1}H, ^{15}N HSQC titration at the molar concentration 0.5 to 1 and 1 to 1 WK 5-50-2 to the protein is shown in Figure 4.3.11 and Figure 4.3.13.

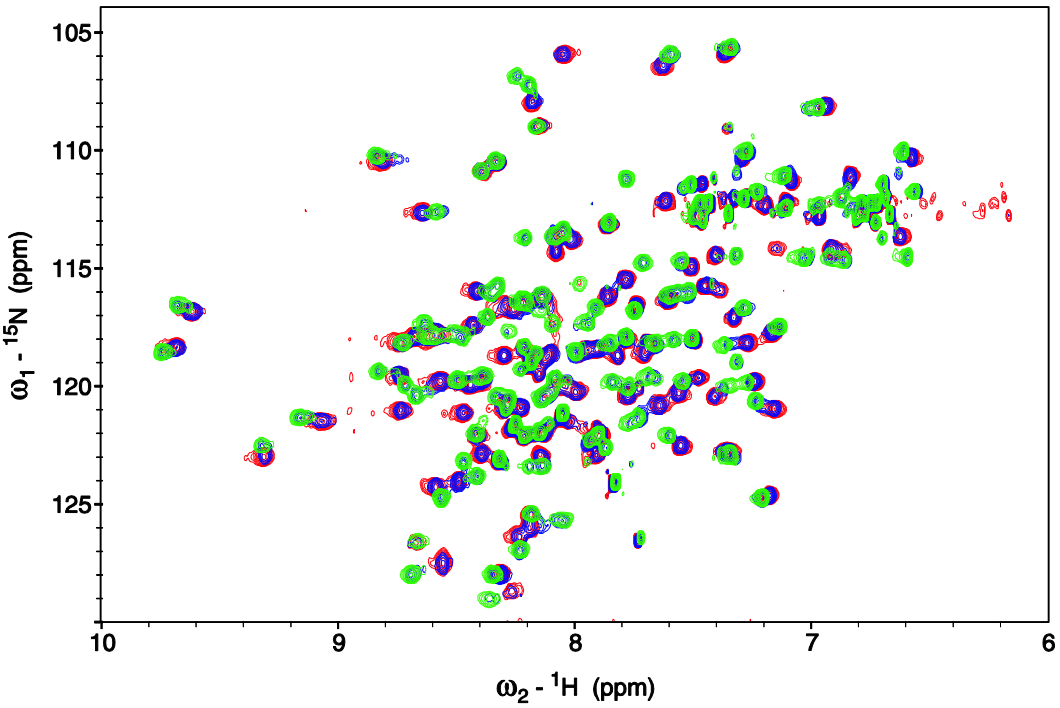

Figure 4.3.11 ^{1}H-^{15}N HSQC spectrum of MDM2 with addition of 1:0.5 of WK 5-50-2 (blue) with addition of 1:1 (green).

At 50% saturation of the protein numerous double peaks are visible, indicating that the compound affinity towards MDM2 is below 1 μM and the binding is in a slow exchange NMR regime. The magnification of the affected regions is shown in the Figure 4.3.12. The cross-peaks are those of the residues localized within the p53 binding pocket of MDM2; however the spectrum shows that upon binding of WK5-50-2 significant changes are present in the whole protein.

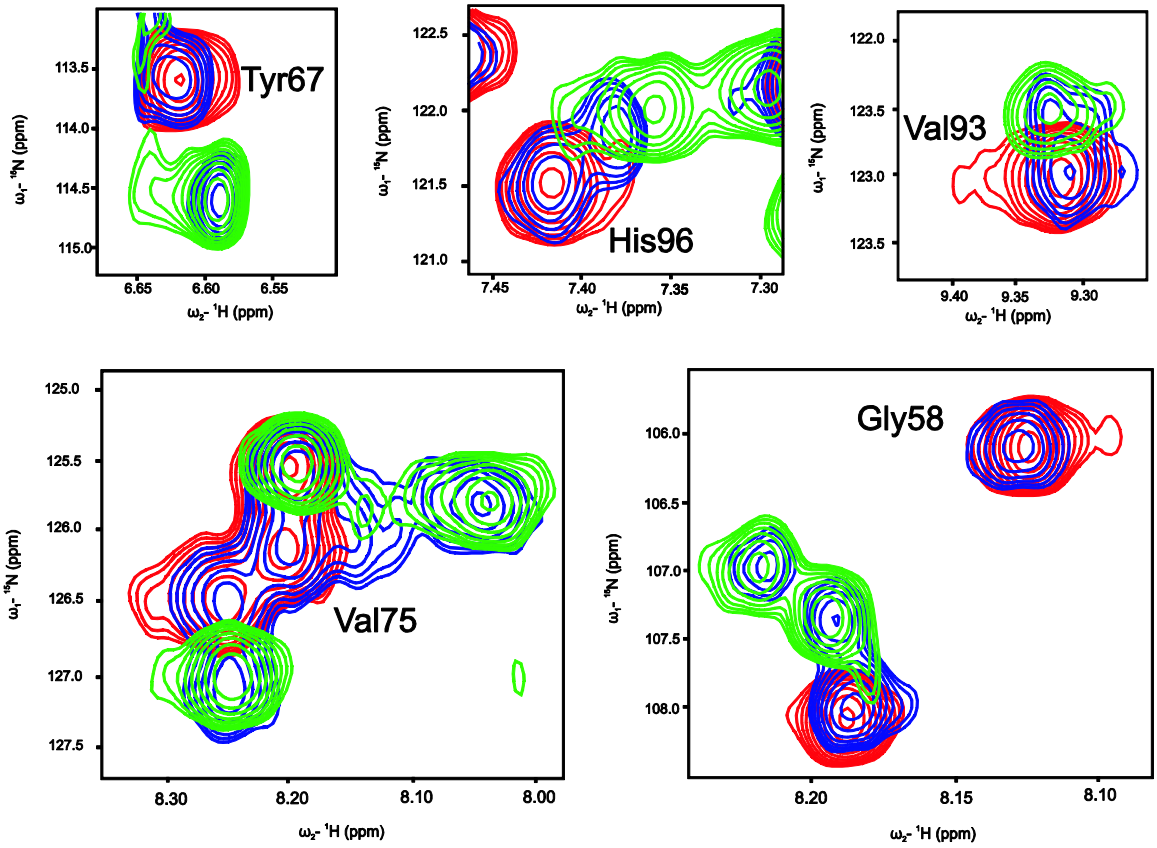

Figure 4.3.12. Magnification of ^{1}H,^{15}N-HSQC spectra showing example of the residues affected upon addition of WK5-50-2.

Titration of MDMX with WK 5-50-2 was also carried out in the same same compound to protein molar ratio as for MDM2. The experiment indicated protein precipitation upon addition of the compound (Figure 4.3.13). A stepwise disappearing of the numerous resonances is observed. The result is consistent with the FP data and proofs that WK5-50-2 recovers p53-peptide by precipitating the MDMX. Thus the application of WK5-50-2 as a dual inhibitor of MDM2 and MDMX is questionable.

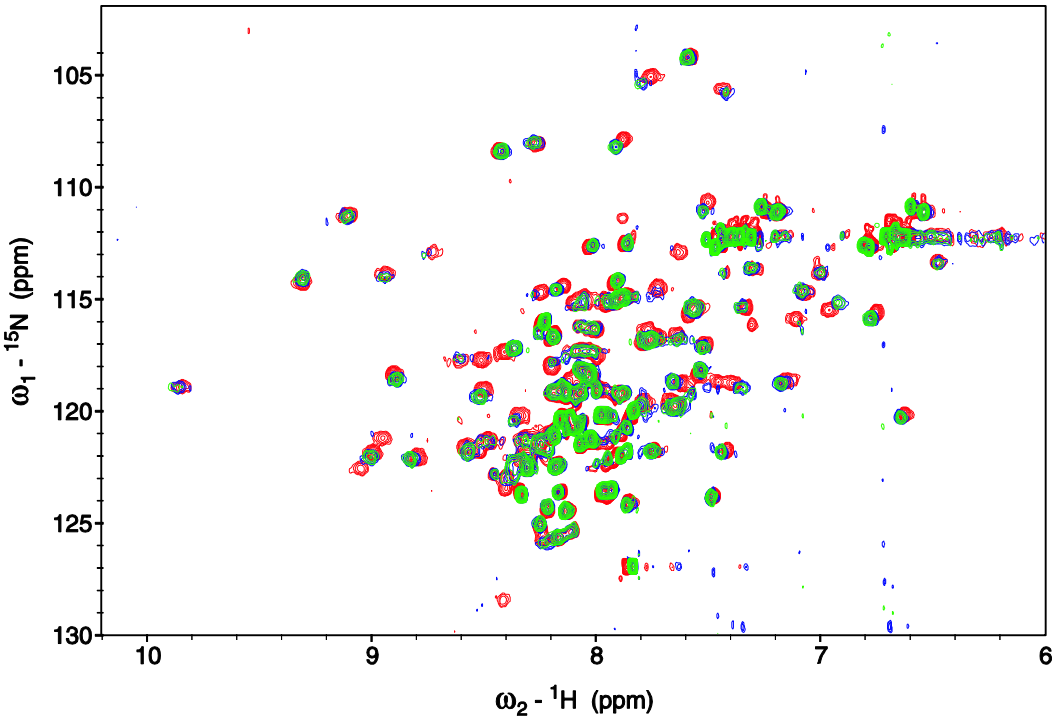

Figure 4.3.13 ^{1}H-^{15}N HSQC spectrum of MDMX with addition of WK 5-50-2 (1:0.5 of the protein to WK5-50-2)(blue) with addition of 1:1 (green).

4.3.4 Crystallization

The protein constructs used for crystallization were obtained as describecd in chapter 4.3.1. At the end of the purification procedure (to remove the aggregates and exchange the buffer for 5 mM Tris/HCl, 50 mM NaCl, pH 8.0; the one used for crystallization), gel filtration was carried out. In order to check whether the proteins are pure and properly folded, 1D proton spectra were recorded. The NMR proton spectra of both proteins for crystallization have shown a typical pattern indicating the structured state: numerous resonances in the aliphatic region and well-speeded resonances within the amide region, see spectra of MDM2 and MDMX (Figures 4.3.14 and Figure 4.3.15, respectively).

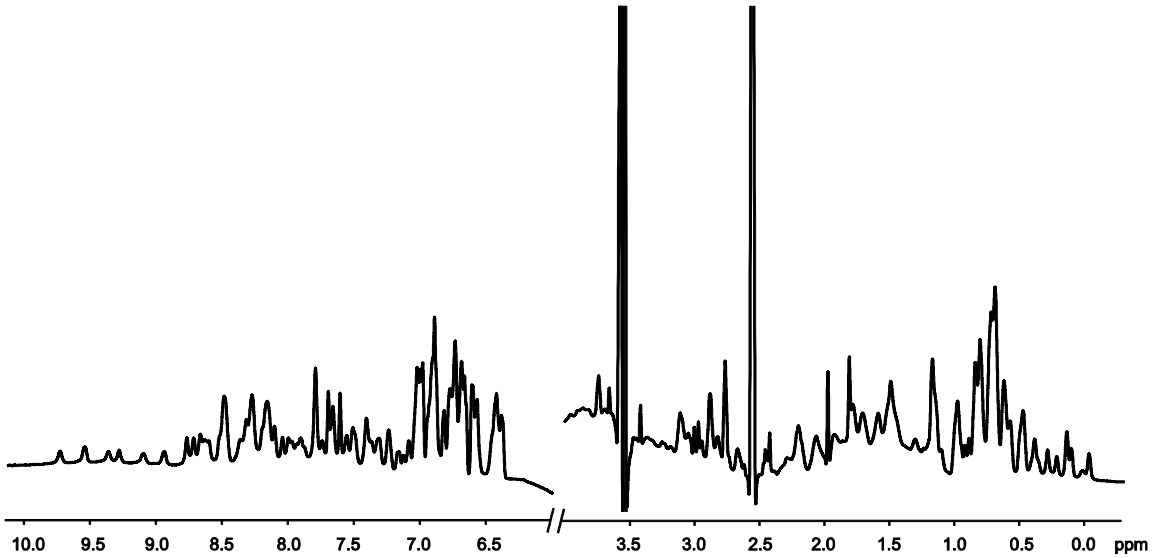

Figure 4.3.15 1D proton spectrum of MDM2 used for crystallization.

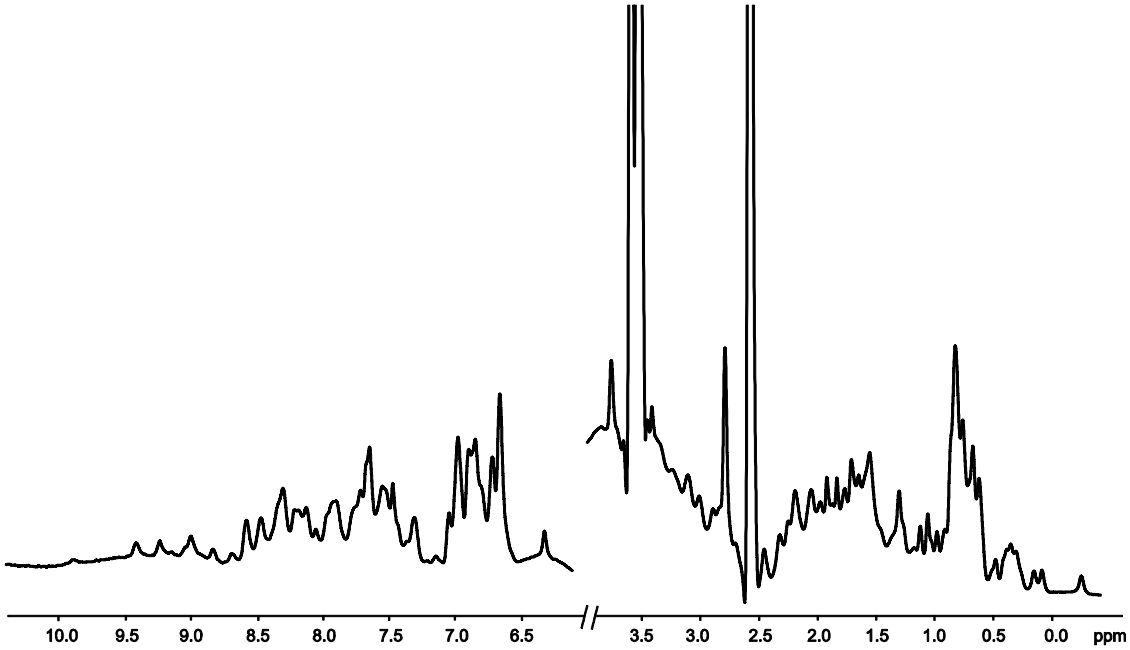

Figure 4.3.16 1D proton spectrum of MDMX used for crystallization.

The preparation of the protein-compound complexes of MDM2 with WK 5-50-2 and of MDMX with YH264 and YH365 was carried out in a similar way to that previously described for crystallization of MDM2/X with other small molecule inhibitors and/or different peptides (Czarna et al. 2009; Pazgier et al. 2009; Popowicz et al. 2010).

In order to select optimal crystallization conditions, more than 700 different conditions were tested in the small scale. Upon addition of an access of the inhibitor the protein was concentrated up to 10 mg/ml. Commercially available screens: Ammonium sulfate, Cation, Anion, PEGs, and Classics from Qiagen as well as Index from Hampton were used. All conditions were screened in two temperatures: at room temperature and in 4ºC. For the test purposes 100 nl drop of the protein-compound complex was mixed with 100 nl of the reservoir solution. Since it was not possible to reach higher concentration of MDM2-WK 5-50-2 complex than approximately 2-3 mg/ml, a higher amount of protein (like 300-400 nl of protein for 100 nl of the reservoir solution) was used. The experiments have been repeated several times with different batches of the protein, compounds originating from different synthesis runs and with slightly varying initial concentration of the protein used for the screen. Unfortunately, none of the conditions gave rise to the crystals of protein-compound complex.

4.3.5 Summary

In summary, we have identified an inhibitor with a new scaffold WK5-50-2 compound towards MDM2-p53 interaction and two new inhibitors for MDMX: YH365 and YH264. The affinities of the compounds were estimated with two independent methods (FP assay and NMR spectroscopy) and are in a good agreement with each other. The NMR measurements have shown that the compounds bind the proteins without impairing their secondary structure.

Since there are already known numerous structures of different compounds in complex with MDM2 (Vassilev 2004; Grasberger et al. 2005; Popowicz et al. 2010) the structure of WK5-50-2 could deliver an inside into MDM2 compound interactions and identify, the differences in the binding mode. WK 5-50-2 seems to be the next promising new scaffold for further optimization. Probably, changes within the side chains of the compound can improve its crystallization properties and allow estimating the structure of the complex.

The both identified inhibitors of MDMX show unambiguously binding to the target protein. The reason why the crystals of the complex were not obtained is not clear.

Several structures of the protein with different p53 peptides were reported. However, these peptides are binding MDMX much stronger than YH365/YH264. The only known small molecule compound co-crystallized with MDMX was binding the protein with K_i 11 µM (Popowicz et al. 2010) - thus weaker than our compounds. However, the binding of WK298 was apparently stabilizing the protein allowing for the crystallization of the small-molecule/MDMX complex. Therefore, in case of the MDMX inhibitors the efforts should be concentrated on increasing their affinity specifically toward the target protein. Until now, most of the inhibitors were optimized for binding to MDM2 and their affinity to MDMX was significantly weaker. Inhibitors optimized for binding with MDMX would probably also have relatively high affinities toward MDM2. Regarding the fact that at the later stages of the studies more than 90% of the inhibitors turn out to be cytotoxic or are not active in the cell-lines the bigger number of 'in vitro positive' inhibitors the higher probability of discovery of the clinically applicable antagonists.

4.4 High-sensitive NMR AIDA

Among different screening methods of small-molecule inhibitors the one providing fast and reliable information about the affinity of the compound is AIDA NMR. The method in its original 2D form (D'Silva et al. 2005; Krajewski et al. 2007; Rothweiler et al. 2008) can be simplified to a simple 1D proton spectrum providing, that the signals to monitor the antagonist binding are present and well-resolved. Those signals can originate either from the natural existing or genetically introduced residues (Rothweiler et al. 2008). Application of SEI-AIDA pulse sequence, despite other advantages, has allowed for significant reduction of acquisition time of the AIDA experiment and made the technique a useful tool for a high-throughput screening. Unfortunately, the experiment has some limitations like the affinity of the inhibitors which can be detected. The AIDA-NMR is a competition assay based on the interaction of two proteins (fulfilling the experimental criteria mentioned in Chapter 1.3.1) and the small-molecule inhibitor of one of the proteins (Krajewski et. al. 2005). The affinity of the two proteins is determined by naturally-existing surface interaction and is often relatively strong in low micromolar to nanomolar range. This feature in turn determines the weakest inhibitor

which can be detected in the AIDA-NMR experiment. In a competition assay the most reliable results are being obtained for the inhibitors of K_i similar to the K_D of the proteins building the complex. On the other hand too low affinity of interaction of the two proteins can lead to line broadening and impair the quantitative evaluation of the experiment. The aim of the study was to design such mutation which will allow for the estimation of K_D value, but are sensitive for weak binding inhibitors.

Since the main focus of the research in our group is the interaction between cancer–significant proteins and screening for the inhibitors for these proteins, as a model was chosen a complex of p53 and its major negative regulator MDM2 or its structural analog MDMX. The affinities of the proteins are 0.60 and 0.24 μM, respectively (Schon et. al 2002). 1D NMR-AIDA allows for detection of the compounds up to approximately 20 μM, for the weaker compounds, which still could be a good initial scaffolds for further optimization in the drug development process the method is not sensitive.

It has been reported that the three key residues of p53 responsible for interaction with MDM2/X are Phe19, Trp23, Leu26 additionally Leu22 was proved to have an important role in the protein-protein interaction (Schon et al. 2002). The NMR-AIDA assay for MDM2/X with p53 is based on the observation of recovery of Trp23 resonance upon addition of an inhibitor. Among the “key” amino acids the Trp23 residue is the most important, since the indole ring is protruding deeply into the binding pocket of MDM2/X and any mutations of this residue are completely impairing the binding. Similar, but not so strong effects have mutations within Phe19. That is why Leu22 and Leu26 residues were taken into account while designing the mutations to weaken the interaction of the binding partners.

Firstly, the smallest possible changes like shortening of the side chain or change of its isoform: L22I, L22V, L26I, L26V were introduced. By the means of isothermal titration calorimetry (ITC) for the designed mutants K_D values for both MDM2 and MDMX were measured. Next, the NMR spectra of the mentioned proteins were analyzed in terms of their further applications in AIDA-NMR assay. Based on the initial data, in order to additionally weaken the interaction, but still maintain the measurable conditions for the p53- MDM2/MDMX complex further mutations L22IL26V, L22VL26V and L22A were

designed. For the second “set” of mutations also the affinities and spectral properties were estimated. From the designed mutants L22IL26V and L22A were chosen for the test measurements with the inhibitors to evaluate their application in AIDA assay.

4.4.1 Protein purification

The purification of MDM2 and MDMX for the ITC and AIDA experiments was performed as described in Chapter 2.2.6.1 and in Chapter 2.2.6.2. Purification of mutants of p53 was performed in the same way as purification of p53-wt described in Chapter 2.2.6.2. A typical chromatogram and SDS-PAGE gel is shown in Figure 4.4.1.

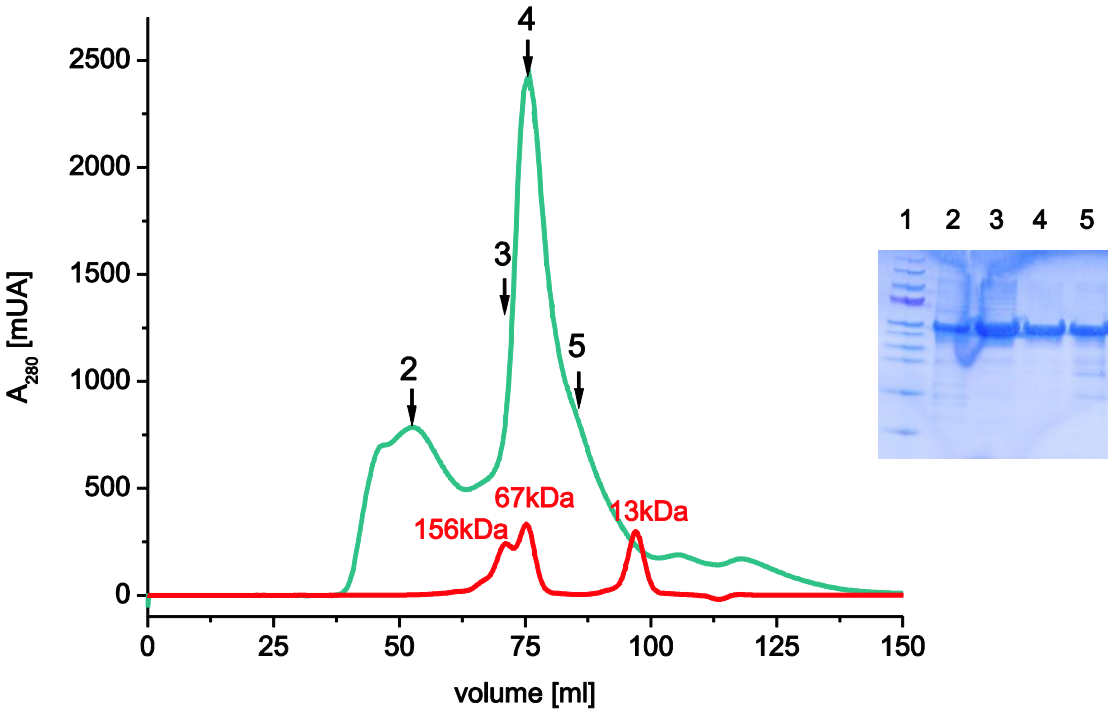

Figure 4.4.1 Chromatogram and the SDS-PAGE analysis of the p53-WT after molecular filtration; SDS-PAGE gel (lines 2-5 fractions marked on the chromatogram with arrows, respectively, marker: line 1).

4.4.2 ITC measurements

The ITC measurements were performed as described in Chapter 2.2.10. In order to verify the experimental settings there have been performed reference measurements

of p53-wt with MDM2 and MDMX (Figure 4.4.2). The estimated values of K_D: 0.60 and 0.24 µM, respectively; are consistent with the literature (Popowicz et al. 2007).

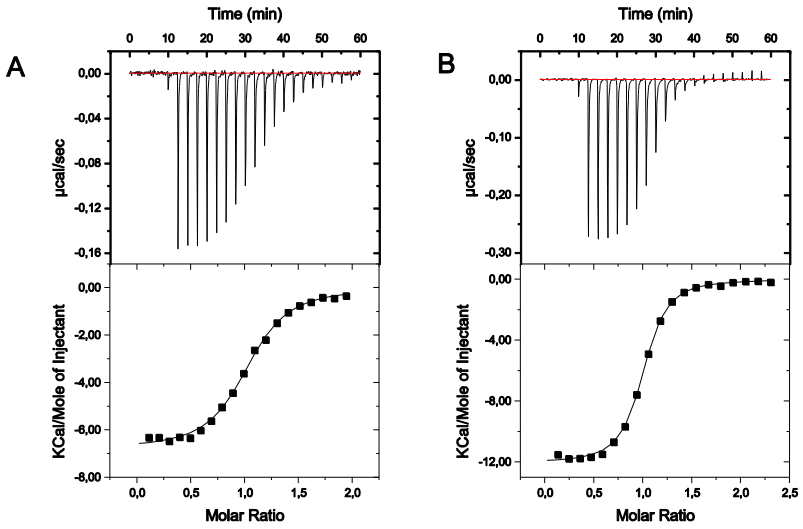

Figure 4.4.2 Results of isothermal titration calorimetry (ITC); binding to p53 (1-321)-wt of MDM2 (A) and MDMX(B).

Mutations of Leu22 have caused slight to significant changes in the binding with MDM2/X. Shortening or change of the isoform of the side chain of this amino acid has two-fold lowed the affinity compared with the p53-wt toward MDM2, what resulted in K_D of 1.34 µM for L22I and 1.37 µM for L22V (Figures 4.4.3.B and C). The affinity toward MDMX was 1.5 to approximately 3 fold reduced (Figure 4.4.4. B and C) with the K_D values: 0.39 µM and 0.86 µM, respectively. The almost complete elimination of the hydrophobic side-chain in case of L22A was leading in approximately 6-fold weakening of the interaction with both proteins: 3.75 µM for MDM2 and 1.54 µM for MDMX.

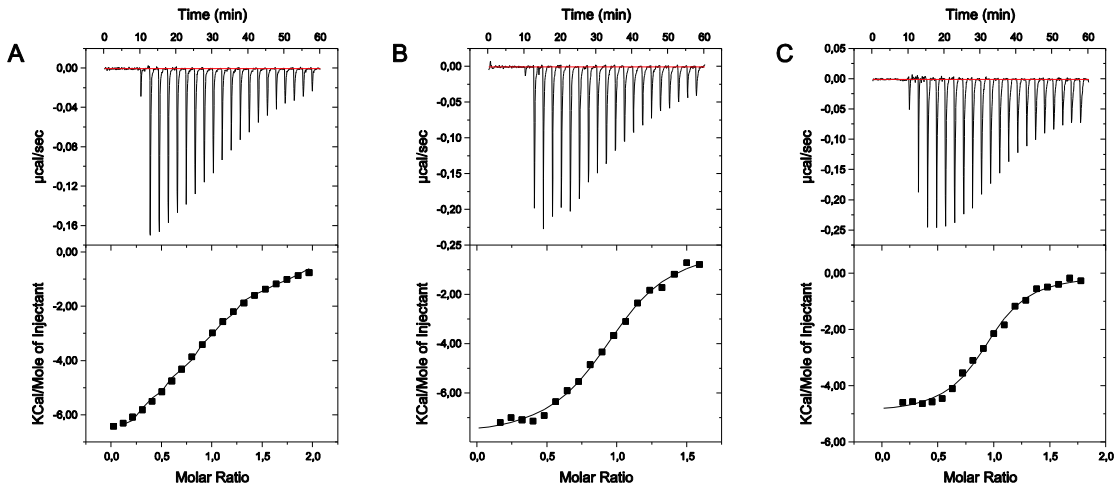

Figure 4.4.3 Results of isothermal titration calorimetry (ITC); binding of mutants of p53(1-321): L22A (A); L22I (B); L22V(C) with MDM2.

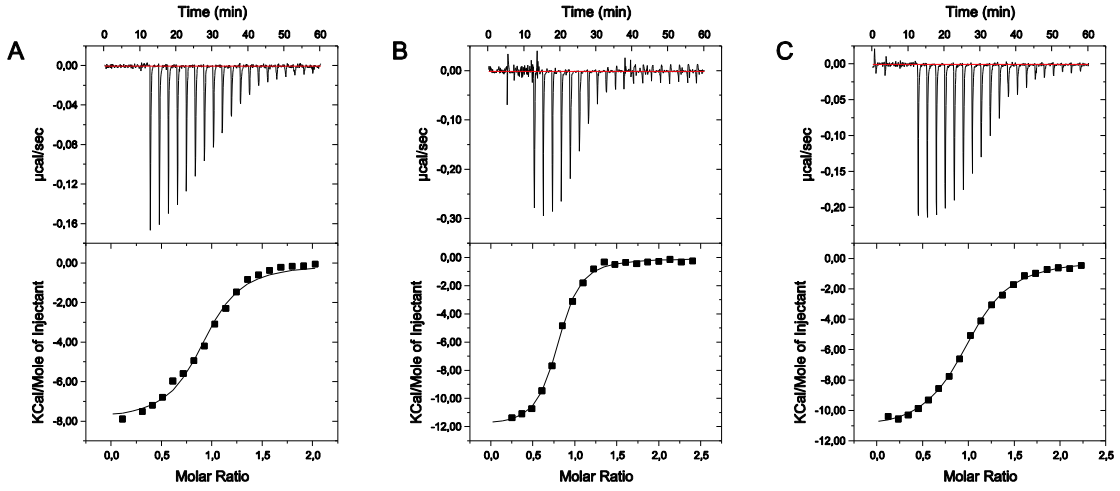

Figure 4.4.4 Results of isothermal titration calorimetry (ITC); binding of mutants of p53(1-321): L22A (A); L22I (B); L22V(C) with MDMX.

The analogous mutations, except from mutation to alanine, have been designed for Leu26. This leucin residue belongs to one of the three “key” amino acids of the interaction of p53 with MDM2/MDMX and any drastic change like complete elimination of the side chain reduces hydrophobic interactions significant for formation of the complex. That is why such modification weakens the interaction and makes the mutant not applicable in the AIDA measurements. For this mutation the estimated residual signal for a stoichiometric complex with MDM2/X would be more than 66% (Li et al. 2010). Mutation of Leu26 to isoleucine has led to increase of the affinity up to 0.32 µM in

case of MDM2 (Figure 4.4.5A), the same change to the isoform of leucin is only slightly weakening the interaction with MDMX up to 0.32 µM (Figure 4.4.6A).

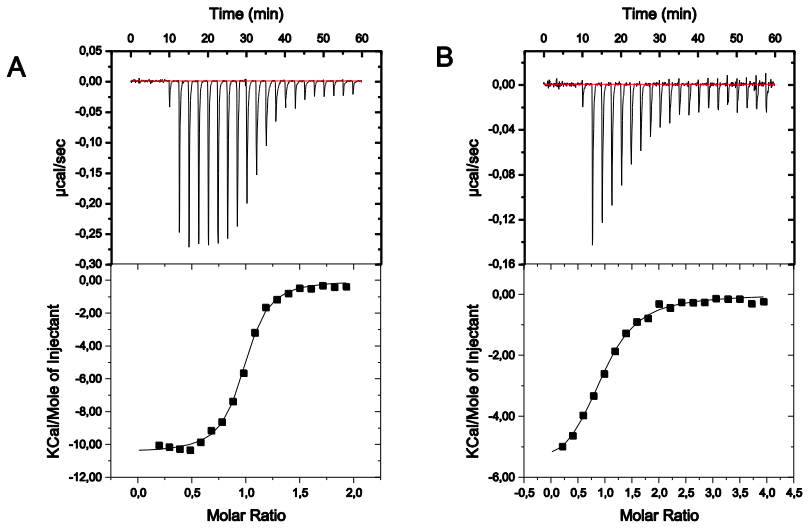

Figure 4.4.5 Results of isothermal titration calorimetry (ITC); binding of different mutants of p53(1-321): L26I (A); L26V (B) with MDM2.

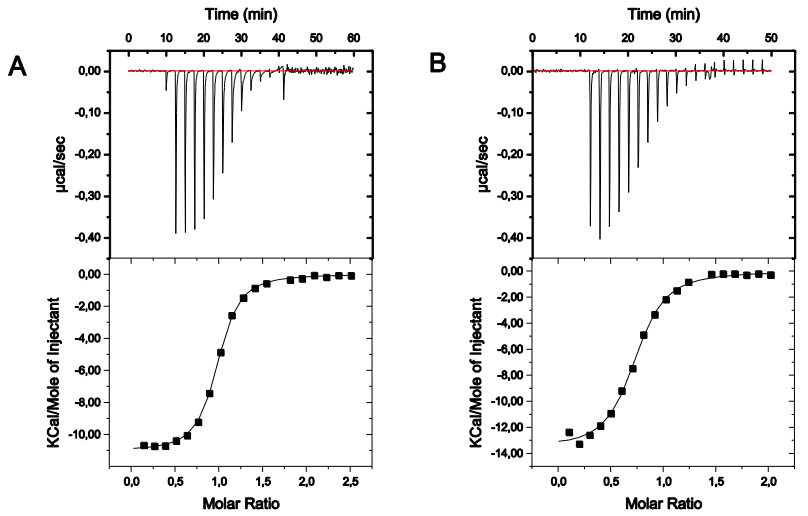

Figure 4.4.6 Results of isothermal titration calorimetry (ITC); binding of different mutants of p53(1-321): L26I (A); L26V (B) with MDMX.

Since, the L26I was not reducing, only enhancing strength of interaction between MDM2 and p53 and the affinity of this mutant to MDMX was only slightly lower

for further approaches were chosen L22I, L22V and L26V. Base on the present mutants, “double” mutants: L22IL26V and L22VL26V have been designed.

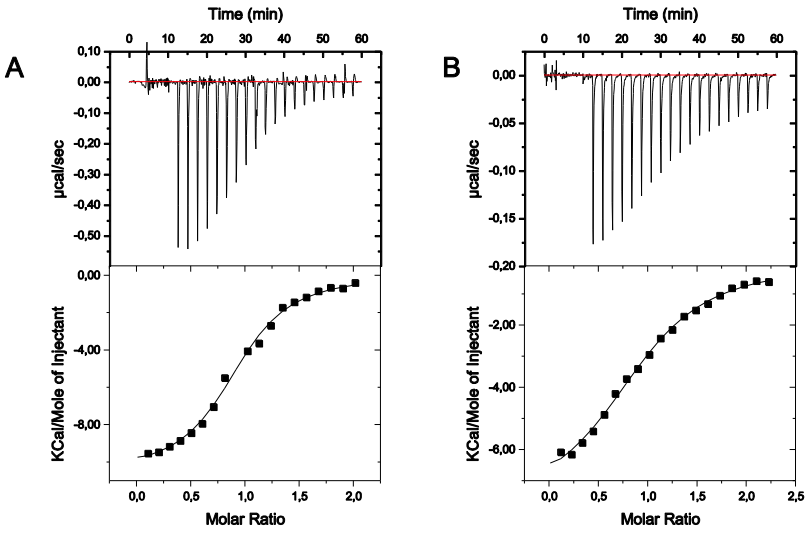

Figure 4.4.7 Results of isothermal titration calorimetry (ITC); binding of different mutants of p53(1-321):L22IL26I (A); L22IL26V (B) with MDM2.

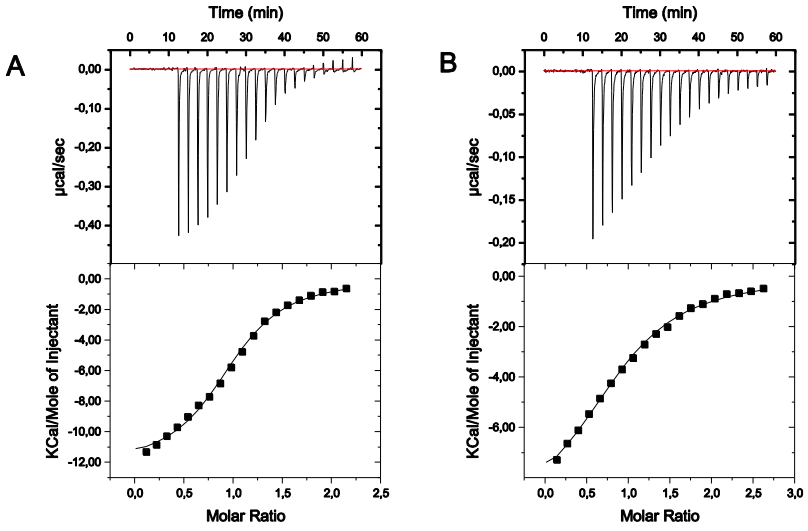

Figure 4.4.8 Results of the isothermal titration calorimetry (ITC); binding of different mutants of p53(1-321):L22IL26I (A); L22IL26V (B) with MDMX.

The isothermal titration calorimetry measurements have shown a synergistic effect of the double mutations on biding to MDM2 and MDMX. The exact comparison of L22IL26V and L22VL26V mutants shows that toward both proteins the affinity of

L22IL22V approximately 3 µM (Figures 4.4.8A and 4.4.7A) is higher than L22VL26V approximately 4 µM (Figures 4.4.8B and 4.4.7B). The result is consistent with the lower affinity of L22V mutant. However, surprising is the fact that L22VL26V is binding weaker to MDMX than to MDM2, when p53 and all of the p53 mutants were binding to MDMX much stronger than to MDM2. All of the calculated values of K_D for the designed mutants for MDM2 and MDMX are set together in the Table 4.4.1.

Table 4.4.1 Dissociation equilibrium constants of p53 and p53 mutants with MDM2 and MDMX

mutation of p53	MDM2 [µM]	MDMX [µM]
WT	0.60±0.02	0.24±0.02
L22A	3.75±0.05	1.54±0.03
L22I	1.34±0.01	0.39±0.03
L22V	1.37±0.07	0.86±0.02
L26I	0.31±0.02	0.32±0.02
L26V	1.78±0.12	0.60±0.04
L22IL26V	3.00±0.02	2.86±0.04
L22VL26V	3.95±0.10	4.64±0.26

4.4.3 NMR analysis

Similar to other transcription factors, p53 contains natively unstructured transactivation domains. Therefore the NMR spectrum shows the pattern typical for partially unfolded protein and only a few resonances indicating the folded state are observed (Figure 4.4.9).

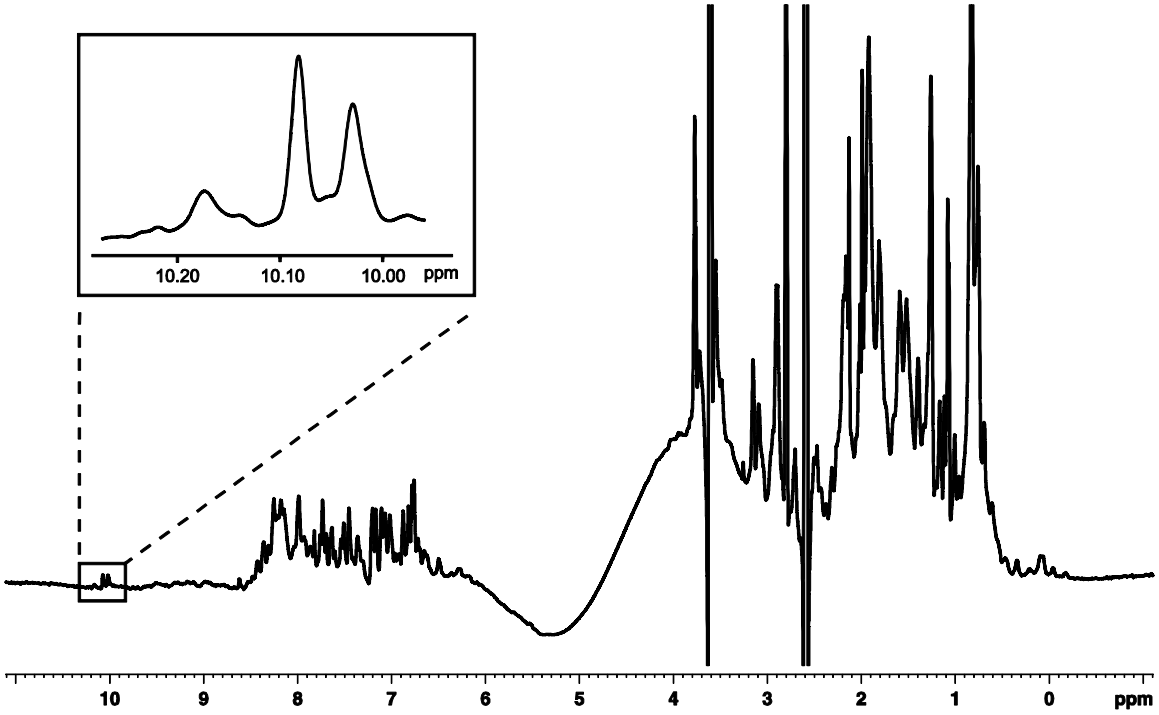

Figure 4.4.9 1D proton spectrum of p53-wt (1-321). Magnification of the aromatic aminoacides region showing three characteristic tryptophan residues: Trp23, Trp53, Trp91.

In order to examine the influence of mutations on protein structure for all p53 mutants were performed NMR comparability studies with the p53-wt. The introduced mutations were not significant for the protein structure and did not affect its overall fold. However, here can be observed small changes in the local magnetic environment of Trp23, the reporter residue in the NMR-AIDA assay, what results in a slight change of position of the resonance corresponding to the NH^{ε} proton of Trp23 (Figure 4.4.10) .

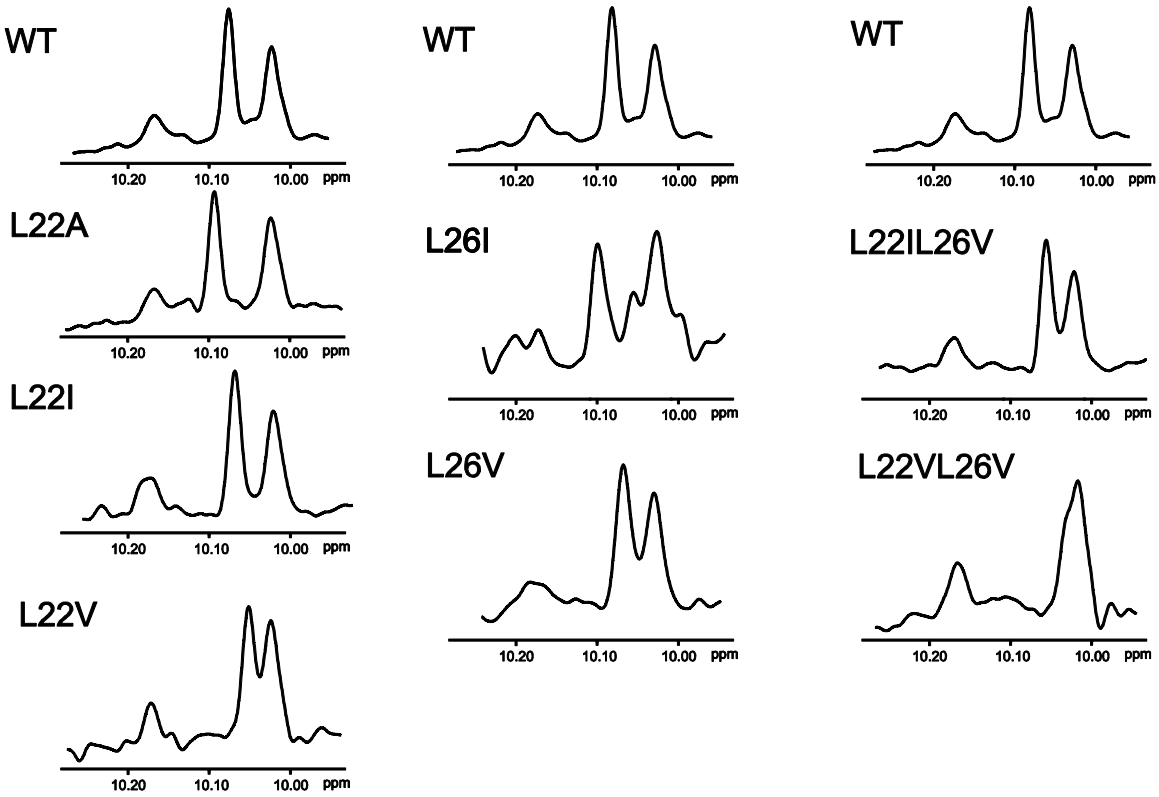

Figure 4.4.10 Magnification of the tryptophan region of 1D proton spectra of p53(1-321)-wt and p53 mutants; Left panel mutants of Leu22; mid panel mutants of Leu26; right panel double mutants of Leu22 and Leu26.

The change of leucine to isoleucine did not affect the resonance frequency of the Trp23. In case of L22V and L26V, the mutation has caused the downfield shift and led to a partial overlap of the Trp23 resonance with the Trp53. In L22A the resonance is shifted towards Trp91, what improves the separation from other resonances originating from the tryptophan residues. The analysis of the spectral properties and the binding affinity of the first "set" of mutations have delivered the significant information about the direction of further modifications.

For the quantitative evaluation of the NMR experiment, allowing for estimation of the K_D of the inhibitor, observation of well-dissolved resonances is necessary. Partial or complete overlap would cause difficulties or make the estimation even impossible. Based on the affinity estimate in ITC experiments and spectral properties of the second "set" of the mutants L22IL26V and L22A were chosen. They both indicated at least 5-fold reduction of affinity with maintaining relatively good spectral properties.

4.4.4 AIDA measurement

For the evaluation of the application of the chosen mutants L22IL26V and L22A in the NMR-AIDA have been performed measurements with different inhibitors which indicated binding in the FP assay. The titrations were performed as a two or three-step experiment with the compound to complex ratio 1: 1, 1:2 and 1:5, respectively. The complexes were prepared by stoichiometric mixing of MDM2/X with p53-wt, p53-L22A or p53-L22IL26V; the final concentrations of the complexes were between 0.015 and 0.030 µM.

For the trays with MDMX three inhibitors were chosen: described in Chapter 4.3.2 new inhibitor of MDMX: YH365 with the Ki 8 µM (Figure 4.4.11A), nutlin-3 binding MDMX with K_i approximately 20 µM (Figure 4.4.11B) and YH377 with the 27 µM affinity (Figure 4.4.11C)

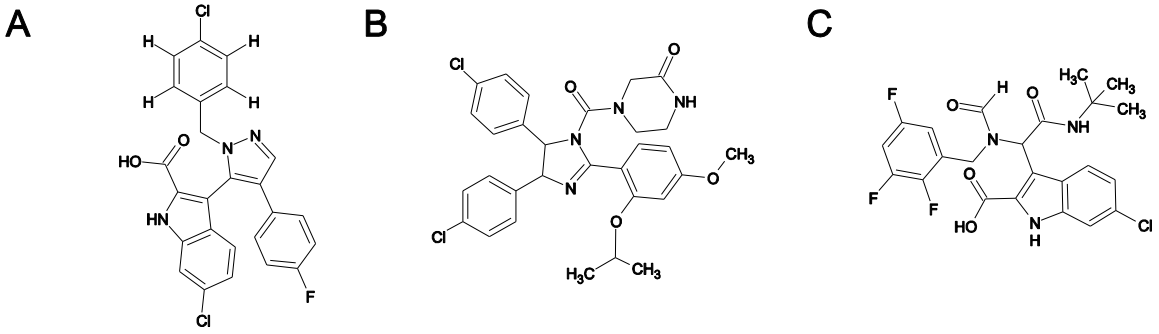

Figure 4.4.11 Structure of YH365 (A); nutlin-3 (B); YH377 (C).

Out of the chosen inhibitors only YH356 is detectable in the NMR-AIDA assay of the p53-wt complex with MDMX, for the further two compounds the experiment is not sensitive. In order to evaluate the model for p53, L22A and L22IL26V independently the Ki of the YH365 based on the results of the performed titrations (Figure 4.4.12) were estimated. NMR-AIDA with MDMX/p53L22A has delivered Ki of the compound 9 µM. For the complex L22IL26V with MDMX the first two steps of titration did not indicated any recovery and then finally approximately 70% recovery of the signal was observed, it can be supposed that the quantitative estimation for this mutation is not possible because the resonance upon binding of MDMX was additionally shifted toward Trp53.

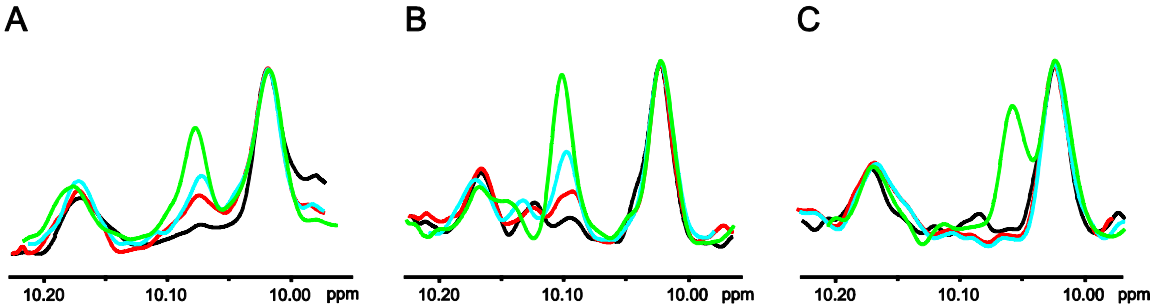

Figure 4.4.12 AIDA measurement of MDMX complex with -p53-wt (A), L22A (B) , L22IL26V (C) with YH365; reference spectrum of the complex –black; compound to complex ratio: 1:1 - red; 2:1 - blue; 5:1 - green.

The similar measurements were performed for nutlin-3 and YH377. For both compounds even with the 5-fold access of the compound to MDMX/p53-wt the interaction could not be detected even qualitatively. For the complex of MDMX/L22A the recovery of the signal was observed already in the first titration step. The estimated K_i values of the compounds were: 21 µM for Nutlin-3 (Figure 4.4.13 B) and 18 µM for YH377 (Figure 4.4.14 B). The same titration has also been performed for the complex MDMX/p53-L22IL26, here the recovery was not observed until the 5-fold access of the inhibitor was added (Figure 4.4.3). For the titration with the nutlin-3 the recovery was even smaller than for the MDMX/p53-L22A complex in the same conditions and titration of the MDMX/p53-L22IL26V with YH377 did not indicate a significant recovery. (Figure 4.4.14C).

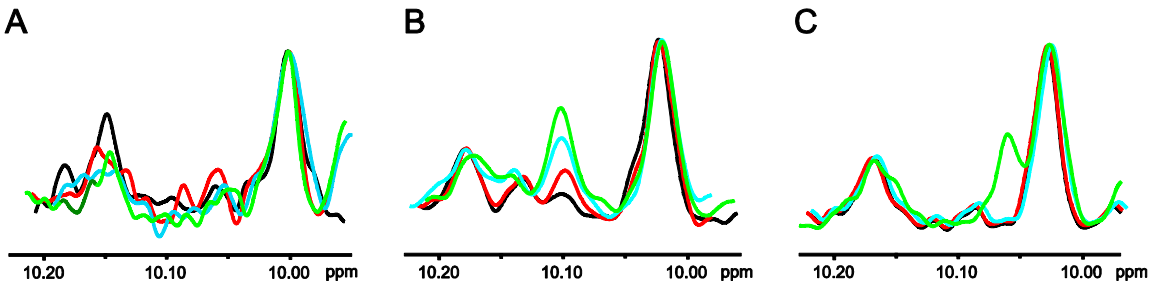

Figure 4.4.13 AIDA measurement of MDMX complex with -p53-wt (A), L22A (B) , L22IL26V (C) with nutlin-3; reference spectrum of the complex –black; compound to complex ratio: 1:1- red;2:1 blue; 5:1 green.

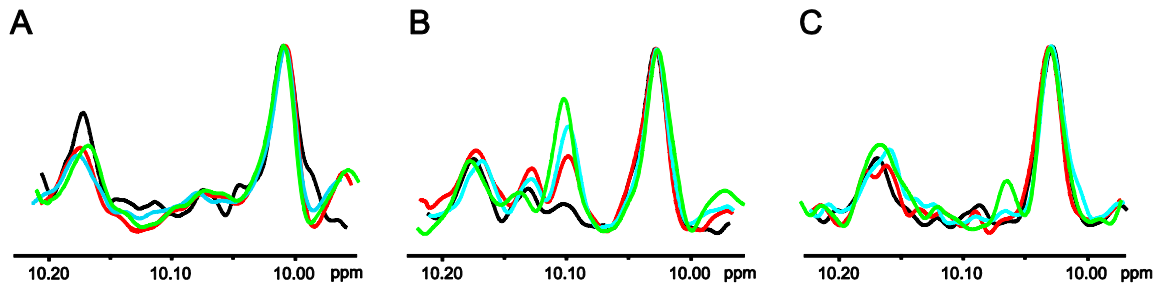

Figure 4.4.14 AIDA measurement of MDMX complex with -p53-wt (A), L22A (B) , L22IL26V (C) with YH377; reference spectrum of the complex –black; compound to complex ratio: 1:1-red;2:1- blue; 5:1- green.

For the measurements with MDM2 two inhibitors in the mikromolar range were chosen: YH334 with the Ki 6 µM (Figure 4.4.15A) and YH308 with the Ki 10 µM (Figure 4.4.15B).

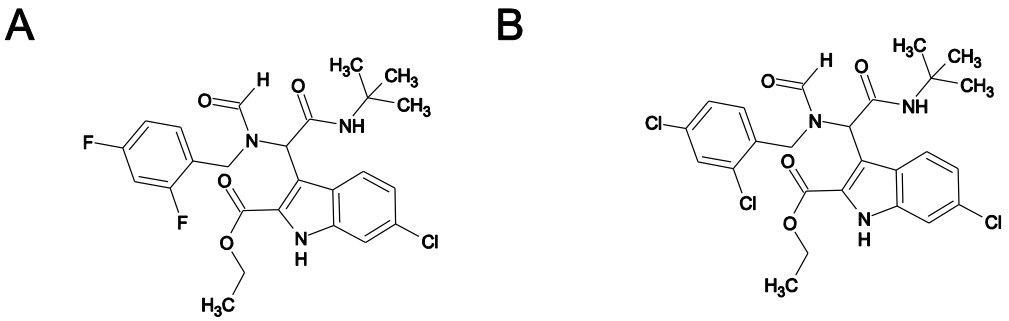

Figure 4.4.15 Structure of YH334 (A); YH308 (B).

Both compounds have the affinity high enough to be detected by the MDM2/p53-wt complex. The aim of the study was to examine the possibility of the complexes with the mutants to improve the sensitivity of detection for the inhibitors from the mid-micromolar range. The titrations were performed as a two-step experiment with the compound to complex ratio 1: 1 and 2:1.

For the compound YH334, which is binding MDM2 with the affinity approximately 6 µM all mutants were “active”. However, a significant difference in the sensitivity of the measurement can be observed. For the MDM2/p53-wt the recovery in the first step of titration is visible and in the second reaches approximately 50% (Figure 4.4.16A), but for the MDM2/p53-L22A the same molar ratio of the added inhibitor leads to complete recovery in the second step of titration (Figure 4.4.16B). The MDM2/p53-L22IL26V has

the affinity toward both proteins of approximately 4 µM, so it can be expected that the sensitivity of this approach would be higher than with the MDMX/p53-wt. However, the titration has indicated comparable or even lower sensitivity compared to MDM2/p53-wt, for and titration with the YH308- 10 µM and additionally not well-dissolved peaks make the MDM2/p53-L22IL26V (Figure 4.4.16C and 4.4.17C) less attractive approach than L22A.

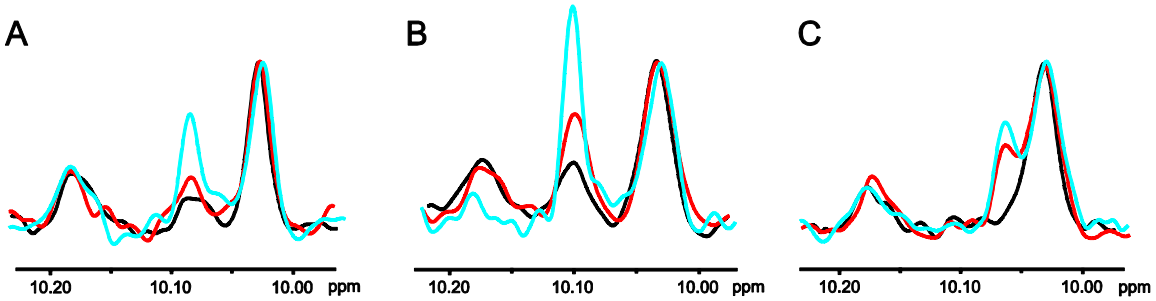

Figure 4.4.16 AIDA measurement of MDM2 complex with -p53-wt (A), L22A (B) , L22IL26V (C) with YH334; reference spectrum of the complex –black; compound to complex ratio: 1:1- red; 2:1 blue.

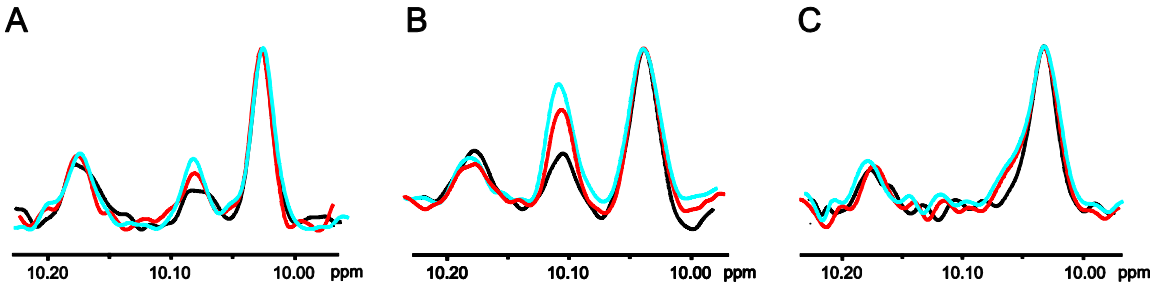

Figure 4.4.17 AIDA measurement of MDM2 complex with -p53-wt (A), L22A (B) , L22IL26V (C) with YH308; reference spectrum of the complex –black; compound to complex ratio: 1:1- red; 2:1 blue.

4.4.5 Summary and conclusions

Since we have developed the AIDA-NMR assay it has become in our group a method of choice for screening for the new inhibitors. Application of a 1D version of this approach has additionally simplified the experiment and eliminated the expensive labeling. A further innovation, exchange of the hard pulse sequence with the pulse sequence, has shortened the acquisition time and reduced the required amount of the protein. However, the detection limit of the method, which depends on the affinities of partners building the complex, was not modified. This limit for MDM2/X inhibitors is at

approximately 20µM and the weaker binding compounds could not be detected. Thus mutations of p53 weakening the complex affinity have been introduced.

Among designed mutants based on the estimated affinity toward MDM2/X and signal separation in the spectrum for the test NMR measurements were chosen two: L22A and L22IL26V. Out of the two “test” mutants, L22IL26V does not seem to work properly. Despite the lower affinity of L22IL26V than L22A toward both MDM2 and MDMX the effects on the respective complex reaction upon addition of the inhibitors were comparable or weaker than for p53-wt. In case of a partial overlap of the signal it is difficult to originate the reason for the missing recovery. It can be either line-broadening or an additional shift of the Trp23 resonance toward Trp53 upon addition of MDM2/X. Anyhow the mutant cannot by applied neither for qualitative nor for quantitative measurements.

The second mutation, L22A, which has been tested, shows a good resolution of the observed Trp23 resonance and a good separation from other tryptophan residues. Additionally, lowering the affinity in case of this mutant has met the criteria and the affinity seems to be still in the slow exchange. This allows for a quantitative evaluation of the experiment, what has been shown on several examples of MDM2/MDMX complexes with p53-L22A. Such complex with p53-L22A can be commonly used in a high-throughput NMR screening. To sum up, application of approaches like introduction of the mutations for the complexes used for AIDA-NMR should be considered for each system individually in order to avoid the effects which would make the later evaluation of the assay impossible.

5 Summary

The thesis comprises application of the structural biology methods for identification of the new small-molecule inhibitors for Pin1 and MDM2/MDMX, the proteins significant in development of cancer. The study can be divided into three parts: development of the inhibitor for Pin1, screening and optimization of the MDM2/MDMX dual inhibitor and development of a new NMR approach for identification of the weak-binding ligands.

Pin1, is an isomerase that specifically recognizes phosphorylated Ser/Thr-Pro and catalyzes the *cis/trans* isomer interconversion. Additionally, Pin1 activates or inactivates numerous oncogenes or tumor suppressors, which make it a particularly attractive candidate for cancer diagnosis and treatment. The overexpression of Pin1 has been observed in 60% human cancers and it is usually correlated with a poor clinical outcome. Until now no clinically useful small-molecule inhibitors of Pin1 has been developed. Herein we present the discovery of a natural product derivative dexamethasone 21-phosphate (DP), a new selective inhibitor of peptidyl-prolyl isomerase (Pin1). The compound inhibits isomerase activity of Pin1 *in vitro* and its affinity toward target protein estimated by the means of two independent methods (isothermal titration calorimetry (ITC) and fluorescence polarization (FP)) is in a low micromolar range. We have mapped the binding site of the DP on the protein and determined its co-crystal structure. The results have confirmed that DP is binding to Pin1 within the substrate binding domain and a phosphate group is localized in the positive patch, similarly as it was observed for Pin1's natural substrate. The subsequent introduction of protecting groups that mask the phosphate's negative charges and are prone to intracellular hydrolysis can generate a cell-permeable compound and develop DP into highly potent agent.

The second part of the study focused on screening and development of the dual inhibitor of the interaction of p53 with MDM2/MDMX. In approximately 50% of all human tumors the function of p53 is inactivated directly by mutations. In a significant percentage of the tumors having wild-type p53, its function is blocked by the major negative regulator MDM2/X. In this case the anti-cancer therapy would be focused on

dissociating the p53-MDM2/X complex in order to recover p53 function. The work based on application of the different screening methods and further optimization of the identified “hits”, has resulted in development of the two new inhibitors with the low micromolar affinity: WK5-50-2 and YH365 for MDM2 and MDMX, respectively.

Among different screening methods of the small-molecule inhibitors the one providing fast and reliable information about the affinity of the compound is AIDA NMR. Unfortunately, the assay has some limitations. In order to make it more sensitive to the weak-binding inhibitors of MDM2/X the mutations within the p53 affecting its affinity toward MDM2/X were introduced. The modifications were supposed to weaken the complex affinity while maintaining a good resolution of the reporter signals in the NMR spectrum. One of the designed mutations, p53-L22A, meets these criteria. It was shown that the MDMX/p53-L22A complex allowed for identification of the compounds, which were not detected using the standard approach. For the stronger compounds application of p53-L22A in complex with MDM2 or MDMX leads to improved sensitivity of the measurement. The approach, not only is more sensitive, than the standard NMR- AIDA, but also has allowed for the quantitative evaluation of the experiment and may be routinely used as a sensitive NMR-screening method.

6 Zusammenfassung

Diese Arbeit befasst sich mit der Anwendung strukturbiologischer Methoden für die Identifikation von neuen Niedermolekularen Inhibitoren, der in der Krebsentwicklung signifikanten Proteine: Pin1, MDM2, MDMX. Die Dissertation kann in drei Teile eingeteilt werden: der Entwicklung des Pin1-Inhibitors, dem Screening und der Optimierung von dualen MDM2/MDMX Inhibitoren und der Entwicklung einer neuen NMR Verfahren für die Identifikation von schwach bindenden Liganden.

Die Isomerase Pin1 (Peptidyl Prolyl Isomerase) erkennt spezifisch phosphoryliertes Ser/Thr und katalysiert die *cis/trans* Isomer-Umwandlung. Zusätzlich aktiviert bzw. inaktiviert Pin1 zalreiche Onco- oder Tumorsuperessogene, welche Pin1 zu einem besonders Ansprechenden Kandidaten für die Krebsdiagnose und Behandlung macht. Die Überexpression von Pin1 wurde in 60% aller humanen Krebsarten beobachtet und korreliert im Allgemeinen mit einer geringen Klinischen Wirkung . Bisher wurden noch keine klinisch Brauchbare Niedermolekularen Inhibitoren von Pin1 entwickelt. In dieser Arbeit wird die Entdeckung des natürlichen Produkt Derivants, Dexamethasone 21-phosphat (DP), ein neuer selektiver Pin1 Inhibitor präsentiert. Die Affinität chemischen Verbindung, die die Isomeraseaktivitat von Pin1 *in vitro* inhibiert wurde mittels zwei unabhängigen Methoden hinsichtlich dem Zielprotein gemessen, und liegt im mikromolaren Bereich. Die Bindungsstelle des DP wurde bestimmt und die Cokristallstruktur gelöst. Die Ergebnisse zeigen, dass DP an Pin1 innerhalb der Substratbindungsstelle bindet, und dass sich eine Phosphatgruppe innerhalb des positiv geledenen Bereichs, ähnlich wie im natürlich vorkommenden Pin1 Substrat, befindet. Die anschließende Einführung von schützenden Gruppen, die die negative Ladung des Phosphats maskieren kann zum Entwicklng des klinischen Inhibitors fuhren.

Die zweite Teil der Dissertation fokussiert sich auf das Screening und der Entwicklung dualer p53-MDM2 und p53-MDMX Inhibitoren. In ca. 50% aller menschlichen Tumore ist die Funktion von p53 durch Mutationen inaktiviert. In der restlichen 50% Tumoren, die das Wildtyp p53 enthalten ist die Funktion durch den Hauptsächlichen negativen Regulator MDM2/X inaktiviert. In diesem Fall fokussiert sich

die Antikrebstherapie auf die Dissoziation des p53-MDM2/X –Komplexes, um die Funktion wiederherzustellen. Diese Arbeit befasst sich mit der Anwendung verschiedener Screeningmethoden und der anschließenden Optimierung der Identifiezierten „hits“ und führte zu Entwicklung zweier Inhibitoren WK5-50-2 beziehungsweise YH365 für MDM2 und MDMX, mit Affinitäten in den mikromolaren Bereich.

Unter den verschiedenen Screeningmethoden für Niedermolekulare Inhibitoren befindet sich die AIDA-NMR Methode, welche schnelle und zuverlässiege Informationen über die Affinität der chemischen Verbindung gibt. Allerdings besitzt diese Methode einiege Einschränkungen. Um diese Methode sensitiver für die schwachbindende MDM2/X Inhibitoren zu machen, wurden Mutationenin p53 engeführt, die die Affinität zu MDM2/X beeinflusst. Die Modifikationen schwächen die Affinitat des Komplexes, wahrend die gute Auflösung der Reportersignale im NMR-Spektrum beibehalten werden soll. Dieses Kriterium wurde für die Mutation p53-L22A eingefüllt. Es wird beweisen, dass der MDMX/p53-L22A Komplex die Identifizierung von chemischen Verbindungen ermöglicht, die durch die Standardprozedur zuvor nicht detektiert wurden. Für die höher affinen Verbindungen zeigte sich, dass die Verwendung des p53-L22A in Komplex mit MDM2 oder MDMX zu einer hocherer Sensitivität der Messung führt. Diese Methode ist nicht nur sensitiver gegenüber der standard NMR-AIDA Methode, sondern erlaubt auch eine quantitative Bewertung des Experiments und könnte routinemaßig als sensitive NMR-Screeningmethode benutzt werden.

7 Appendix

7.1 Abbreviations and symbols

- 1D one-dimensional
- 2D two-dimensional
- Å Ångstrøm (10^{-10} m)
- aa amino acid
- AD Alzheimer's disease
- AIDA Antagonist Induced Dissociation Assay
- APP amyloid precursor protein
- APS ammonium peroxodisulfate
- bp base pair
- BP betadexamethasone 21-phosphate
- Da Dalton (g mol^{-1})
- DAK1 death associate kinase-1
- DMSO dimethylsulfoxide
- DP dexamethasone 21-phosphate
- DNA deoxyribonucleic acid
- EDTA ethylenediamine tetraacetic acid
- Emi1 early mitotic inhibitor 1
- g gravity (9.81 m s^{-2})
- HSQC heteronuclear single quantum coherence
- IMAC immobilized metal affinity chromatography
- IPTG isopropyl-β-thiogalactopyranoside
- K_D dissotation constant
- K_i inhibition constant
- LB Luria-Broth medium
- MDM2 murine double mute
- MM minimal medium
- NES nuclear export sequence

- NIMA never in mitosis gene a
- NFT neurofiblirally tanges
- Ni-NTA nickel-nitrilotriacetic acid
- NoLS nuclear localization signal
- NMR nuclear magnetic resonance
- NOE nuclear Overhauser effect
- OD optical density
- PAGE polyacrylamide gel electrophoresis
- PBS phosphate-buffered saline
- ppm parts per million
- PRR proline reach region
- RING really interesting new gen
- RMSD root mean square deviation
- SEI selective excitation inversion
- SDS sodium dodecyl sulfate
- TAD transcriptional activation domain
- TB terrific broth
- TEMED N,N,N’,N’-tetramethylethylendiamine
- TET tetramerization domain

7.2 Protein sequences

7.2.1 Human Pin1

Uniprot accession number: Q13526

```
        10         20         30         40         50         60
MADEEKLPPG WEKRMSRSSG RVYYFNHITN ASQWERPSGN SSSGGKNGQG EPARVRCSHL

        70         80         90        100        110        120
LVKHSQSRRP SSWRQEKITR TKEEALELIN GYIQKIKSGE EDFESLASQF SDCSSAKARG

       130        140        150        160
DLGAFSRGQM QKPFEDASFA LRTGEMSGPV FTDSGIHIIL RTE
```

7.2.2 Human p53

Uniprot accession number: P04637

```
       10         20         30         40         50         60
MEEPQSDPSV EPPLSQETFS DLWKLLPENN VLSPLPSQAM DDLMLSPDDI EQWFTEDPGP

        70         80         90        100        110        120
DEAPRMPEAA PPVAPAPAAP TPAAPAPAPS WPLSSSVPSQ KTYQGSYGFR LGFLHSGTAK

       130        140        150        160        170        180
SVTCTYSPAL NKMFCQLAKT CPVQLWVDST PPPGTRVRAM AIYKQSQHMT EVVRRCPHHE

       190        200        210        220        230        240
RCSDSDGLAP PQHLIRVEGN LRVEYLDDRN TFRHSVVVPY EPPEVGSDCT TIHYNYMCNS

       250        260        270        280        290        300
SCMGGMNRRP ILTIITLEDS SGNLLGRNSF EVRVCACPGR DRRTEEENLR KKGEPHHELP

       310        320        330        340        350        360
PGSTKRALPN NTSSSPQPKK KPLDGEYFTL QIRGRERFEM FRELNEALEL KDAQAGKEPG

       370        380        390
GSRAHSSHLK SKKGQSTSRH KKLMFKTEGP DSD
```

7.2.3 Human MDM2

Uniprot accession number: Q00987

```
        10         20         30         40         50         60
MCNTNMSVPT DGAVTTSQIP ASEQETLVRP KPLLLKLLKS VGAQKDTYTM KEVLFYLGQY

        70         80         90        100        110        120
IMTKRLYDEK QQHIVYCSND LLGDLFGVPS FSVKEHRKIY TMIYRNLVVV NQQESSDSGT

       130        140        150        160        170        180
```

```
SVSENRCHLE GGSDQKDLVQ ELQEEKPSSS HLVSRPSTSS RRRAISETEE NSDELSGERQ

       190        200        210        220        230        240
RKRHKSDSIS LSFDESLALC VIREICCERS SSSESTGTPS NPDLDAGVSE HSGDWLDQDS

       250        260        270        280        290        300
VSDQFSVEFE VESLDSEDYS LSEEGQELSD EDDEVYQVTV YQAGESDTDS FEEDPEISLA

       310        320        330        340        350        360
DYWKCTSCNE MNPPLPSHCN RCWALRENWL PEDKGKDKGE ISEKAKLENS TQAEEGFDVP

       370        380        390        400        410        420
DCKKTIVNDS RESCVEENDD KITQASQSQE SEDYSQPSTS SSIIYSSQED VKEFEREETQ

       430        440        450        460        470        480
DKEESVESSL PLNAIEPCVI CQGRPKNGCI VHGKTGHLMA CFTCAKKLKK RNKPCPVCRQ

       490
PIQMIVLTYF P
```

7.2.4 Human MDMX

Uniprot accession number: O15151

```
        10         20         30         40         50         60
MTSFSTSAQC STSDSACRIS PGQINQVRPK LPLLKILHAA GAQGEMFTVK EVMHYLGQYI

        70         80         90        100        110        120
MVKQLYDQQE QHMVYCGGDL LGELLGRQSF SVKDPSPLYD MLRKNLVTLA TATTDAAQTL

       130        140        150        160        170        180
ALAQDHSMDI PSQDQLKQSA EESSTSRKRT TEDDIPTLPT SEHKCIHSRE DEDLIENLAQ

       190        200        210        220        230        240
DETSRLDLGF EEWDVAGLPW WFLGNLRSNY TPRSNGSTDL QTNQDVGTAI VSDTTDDLWF

       250        260        270        280        290        300
LNESVSEQLG VGIKVEAADT EQTSEEVGKV SDKKVIEVGK NDDLEDSKSL SDDTDVEVTS

       310        320        330        340        350        360
EDEWQCTECK KFNSPSKRYC FRCWALRKDW YSDCSKLTHS LSTSDITAIP EKENEGNDVP

       370        380        390        400        410        420
DCRRTISAPV VRPKDAYIKK ENSKLFDPCN SVEFLDLAHS SESQETISSM GEQLDNLSEQ

       430        440        450        460        470        480
RTDTENMEDC QNLLKPCSLC EKRPRDGNII HGRTGHLVTC FHCARRLKKA GASCPICKKE

       490
IQLVIKVFIA
```

8 References

(1994). "The CCP4 suite: programs for protein crystallography." Acta Crystallogr D Biol Crystallogr **50**(Pt 5): 760-763.

Allen, J. G., et al. (2009). "Discovery and optimization of chromenotriazolopyrimidines as potent inhibitors of the mouse double minute 2-tumor protein 53 protein-protein interaction." J Med Chem **52**(22): 7044-7053.

Andorfer, C., et al. (2003). "Hyperphosphorylation and aggregation of tau in mice expressing normal human tau isoforms." J Neurochem **86**(3): 582-590.

Atchison, F. W., et al. (2003). "Pin1 regulates the timing of mammalian primordial germ cell proliferation." Development **130**(15): 3579-3586.

Ayala, G., et al. (2003). "The prolyl isomerase Pin1 is a novel prognostic marker in human prostate cancer." Cancer Res **63**(19): 6244-6251.

Balastik, M., et al. (2007). "Pin1 in Alzheimer's disease: multiple substrates, one regulatory mechanism?" Biochim Biophys Acta **1772**(4): 422-429.

Bao, L., et al. (2004). "Prevalent overexpression of prolyl isomerase Pin1 in human cancers." Am J Pathol **164**(5): 1727-1737.

Bayer, E., et al. (2003). "Structural analysis of the mitotic regulator hPin1 in solution: insights into domain architecture and substrate binding." J Biol Chem **278**(28): 26183-26193.

Behrsin, C. D., et al. (2007). "Functionally important residues in the peptidyl-prolyl isomerase Pin1 revealed by unigenic evolution." J Mol Biol **365**(4): 1143-1162.

Bernis, C., et al. (2007). "Pin1 stabilizes Emi1 during G2 phase by preventing its association with SCF(betatrcp)." EMBO Rep **8**(1): 91-98.

Boeckler, F. M., et al. (2008). "Targeted rescue of a destabilized mutant of p53 by an in silico screened drug." Proc Natl Acad Sci U S A **105**(30): 10360-10365.

Brooks, C. L. and W. Gu (2006). "p53 ubiquitination: Mdm2 and beyond." Mol Cell **21**(3): 307-315.

Brown, C. J., et al. (2009). "Awakening guardian angels: drugging the p53 pathway." Nat Rev Cancer **9**(12): 862-873.

Bullock, A. N. and A. R. Fersht (2001). "Rescuing the function of mutant p53." Nat Rev Cancer **1**(1): 68-76.

Butterfield, D. A., et al. (2006). "Pin1 in Alzheimer's disease." J Neurochem **98**(6): 1697-1706.

Butterfield, D. A., et al. (2006). "Redox proteomics identification of oxidatively modified brain proteins in inherited Alzheimer's disease: an initial assessment." J Alzheimers Dis **10**(4): 391-397.

Chao, S. H., et al. (2001). "Juglone, an inhibitor of the peptidyl-prolyl isomerase Pin1, also directly blocks transcription." Nucleic Acids Res **29**(3): 767-773.

Chung, C. T., et al. (1989). "One-step preparation of competent Escherichia coli: transformation and storage of bacterial cells in the same solution." Proc Natl Acad Sci U S A **86**(7): 2172-2175.

Clackson, T. and J. A. Wells (1995). "A hot spot of binding energy in a hormone-receptor interface." Science **267**(5196): 383-386.

Czarna, A., et al. (2009). "High affinity interaction of the p53 peptide-analogue with human Mdm2 and Mdmx." Cell Cycle **8**(8): 1176-1184.
D'Silva, L., et al. (2005). "Monitoring the effects of antagonists on protein-protein interactions with NMR spectroscopy." J Am Chem Soc **127**(38): 13220-13226.
Daum, S., et al. (2006). "Aryl indanyl ketones: efficient inhibitors of the human peptidyl prolyl cis/trans isomerase Pin1." Angew Chem Int Ed Engl **45**(44): 7454-7458.
de Graaf, P., et al. (2003). "Hdmx protein stability is regulated by the ubiquitin ligase activity of Mdm2." J Biol Chem **278**(40): 38315-38324.
Ding, K., et al. (2006). "Structure-based design of spiro-oxindoles as potent, specific small-molecule inhibitors of the MDM2-p53 interaction." J Med Chem **49**(12): 3432-3435.
Dong, L., et al. (2010). "Structure-based design of novel human Pin1 inhibitors (II)." Bioorg Med Chem Lett **20**(7): 2210-2214.
Duncan, K. E., et al. (2011). "Discovery and characterization of a nonphosphorylated cyclic peptide inhibitor of the peptidylprolyl isomerase, Pin1." J Med Chem **54**(11): 3854-3865.
Eckerdt, F., et al. (2005). "Polo-like kinases and oncogenesis." Oncogene **24**(2): 267-276.
Ernst, R. R. (1987). "Methodology of magnetic resonance imaging." Q Rev Biophys **19**(3-4): 183-220.
Finch, R. A., et al. (2002). "mdmx is a negative regulator of p53 activity in vivo." Cancer Res **62**(11): 3221-3225.
Foster, B. A., et al. (1999). "Pharmacological rescue of mutant p53 conformation and function." Science **286**(5449): 2507-2510.
Friedler, A., et al. (2002). "A peptide that binds and stabilizes p53 core domain: chaperone strategy for rescue of oncogenic mutants." Proc Natl Acad Sci U S A **99**(2): 937-942.
Fukuchi, M., et al. (2006). "Prolyl isomerase Pin1 expression predicts prognosis in patients with esophageal squamous cell carcinoma and correlates with cyclinD1 expression." Int J Oncol **29**(2): 329-334.
Galat, A. (2003). "Peptidylprolyl cis/trans isomerases (immunophilins): biological diversity--targets--functions." Curr Top Med Chem **3**(12): 1315-1347.
Geyer, R. K., et al. (2000). "The MDM2 RING-finger domain is required to promote p53 nuclear export." Nat Cell Biol **2**(9): 569-573.
Gill, S. C. and P. H. von Hippel (1989). "Calculation of protein extinction coefficients from amino acid sequence data." Anal Biochem **182**(2): 319-326.
Gomez-Monterrey, I., et al. (2010). "Identification of the Spiro(oxindole-3,3'-thiazolidine)-Based Derivatives as Potential p53 Activity Modulators." J Med Chem.
Grasberger, B. L., et al. (2005). "Discovery and cocrystal structure of benzodiazepinedione HDM2 antagonists that activate p53 in cells." J Med Chem **48**(4): 909-912.
Guo, C., et al. (2009). "Structure-based design of novel human Pin1 inhibitors (I)." Bioorg Med Chem Lett **19**(19): 5613-5616.
Hamdane, M., et al. (2006). "Pin1 allows for differential Tau dephosphorylation in neuronal cells." Mol Cell Neurosci **32**(1-2): 155-160.

Han, C. H., et al. (2010). "The functional promoter polymorphism (-842G>C) in the PIN1 gene is associated with decreased risk of breast cancer in non-Hispanic white women 55 years and younger." Breast Cancer Res Treat **122**(1): 243-249.
Hanes, S. D., et al. (1989). "Sequence and mutational analysis of ESS1, a gene essential for growth in Saccharomyces cerevisiae." Yeast **5**(1): 55-72.
Haupt, Y., et al. (1997). "Mdm2 promotes the rapid degradation of p53." Nature **387**(6630): 296-299.
Hennig, L., et al. (1998). "Selective inactivation of parvulin-like peptidyl-prolyl cis/trans isomerases by juglone." Biochemistry **37**(17): 5953-5960.
Hollstein, M., et al. (1994). "Database of p53 gene somatic mutations in human tumors and cell lines." Nucleic Acids Res **22**(17): 3551-3555.
Iqbal, K., et al. (2009). "Mechanisms of tau-induced neurodegeneration." Acta Neuropathol **118**(1): 53-69.
Jeffrey, P. D., et al. (1995). "Crystal structure of the tetramerization domain of the p53 tumor suppressor at 1.7 angstroms." Science **267**(5203): 1498-1502.
Joerger, A. C. and A. R. Fersht (2008). "Structural biology of the tumor suppressor p53." Annu Rev Biochem **77**: 557-582.
Kabsch, W. (2010). "Xds." Acta Crystallogr D Biol Crystallogr **66**(Pt 2): 125-132.
Kawai, H., et al. (2003). "DNA damage-induced MDMX degradation is mediated by MDM2." J Biol Chem **278**(46): 45946-45953.
Knockaert, M., et al. (2002). "Pharmacological inhibitors of cyclin-dependent kinases." Trends Pharmacol Sci **23**(9): 417-425.
Kostic, M., et al. (2006). "Solution structure of the Hdm2 C2H2C4 RING, a domain critical for ubiquitination of p53." J Mol Biol **363**(2): 433-450.
Kozany, C., et al. (2009). "Fluorescent probes to characterise FK506-binding proteins." Chembiochem **10**(8): 1402-1410.
Krajewski, M., et al. (2007). "An NMR-based antagonist induced dissociation assay for targeting the ligand-protein and protein-protein interactions in competition binding experiments." J Med Chem **50**(18): 4382-4387.
Kubbutat, M. H., et al. (1997). "Regulation of p53 stability by Mdm2." Nature **387**(6630): 299-303.
Kupce, E., et al. (1995). "Short selective pulses for biochemical applications." J Magn Reson B **106**(3): 300-303.
Kuramochi, J., et al. (2006). "High Pin1 expression is associated with tumor progression in colorectal cancer." J Surg Oncol **94**(2): 155-160.
Kussie, P. H., et al. (1996). "Structure of the MDM2 oncoprotein bound to the p53 tumor suppressor transactivation domain." Science **274**(5289): 948-953.
Laketa, V., et al. (2009). "Membrane-permeant phosphoinositide derivatives as modulators of growth factor signaling and neurite outgrowth." Chem Biol **16**(11): 1190-1196.
Lam, P. B., et al. (2008). "Prolyl isomerase Pin1 is highly expressed in Her2-positive breast cancer and regulates erbB2 protein stability." Mol Cancer **7**: 91.
Lane, D. P. and L. V. Crawford (1979). "T antigen is bound to a host protein in SV40-transformed cells." Nature **278**(5701): 261-263.
Lee, T. H., et al. (2011). "Peptidyl-prolyl cis-trans isomerase Pin1 in ageing, cancer and Alzheimer disease." Expert Rev Mol Med **13**: e21.

Lee, T. H., et al. (2009). "Essential role of Pin1 in the regulation of TRF1 stability and telomere maintenance." Nat Cell Biol **11**(1): 97-105.
Lee, W., et al. (1994). "Solution structure of the tetrameric minimum transforming domain of p53." Nat Struct Biol **1**(12): 877-890.
Lepre, C. A., et al. (2004). "Theory and applications of NMR-based screening in pharmaceutical research." Chem Rev **104**(8): 3641-3676.
Leung, K. W., et al. (2009). "Pin1 overexpression is associated with poor differentiation and survival in oral squamous cell carcinoma." Oncol Rep **21**(4): 1097-1104.
Li, C., et al. (2010). "Systematic mutational analysis of peptide inhibition of the p53-MDM2/MDMX interactions." J Mol Biol **398**(2): 200-213.
Li, Q. M., et al. (2007). "Opposite regulation of oligodendrocyte apoptosis by JNK3 and Pin1 after spinal cord injury." J Neurosci **27**(31): 8395-8404.
Liao, Y., et al. (2009). "Peptidyl-prolyl cis/trans isomerase Pin1 is critical for the regulation of PKB/Akt stability and activation phosphorylation." Oncogene **28**(26): 2436-2445.
Liou, Y. C., et al. (2002). "Loss of Pin1 function in the mouse causes phenotypes resembling cyclin D1-null phenotypes." Proc Natl Acad Sci U S A **99**(3): 1335-1340.
Liou, Y. C., et al. (2003). "Role of the prolyl isomerase Pin1 in protecting against age-dependent neurodegeneration." Nature **424**(6948): 556-561.
Liou, Y. C., et al. (2011). "Prolyl isomerase Pin1 as a molecular switch to determine the fate of phosphoproteins." Trends Biochem Sci **36**(10): 501-514.
Liu, M., et al. (2010). "D-peptide inhibitors of the p53-MDM2 interaction for targeted molecular therapy of malignant neoplasms." Proc Natl Acad Sci U S A **107**(32): 14321-14326.
Liu, T., et al. (2010). "Membrane permeable cyclic peptidyl inhibitors against human Peptidylprolyl Isomerase Pin1." J Med Chem **53**(6): 2494-2501.
Liu, W. Q., et al. (2004). "Structure-activity relationships of small phosphopeptides, inhibitors of Grb2 SH2 domain, and their prodrugs." J Med Chem **47**(5): 1223-1233.
Lotharius, J. and P. Brundin (2002). "Pathogenesis of Parkinson's disease: dopamine, vesicles and alpha-synuclein." Nat Rev Neurosci **3**(12): 932-942.
Lu, J., et al. (2009). "A novel functional variant (-842G>C) in the PIN1 promoter contributes to decreased risk of squamous cell carcinoma of the head and neck by diminishing the promoter activity." Carcinogenesis **30**(10): 1717-1721.
Lu, K. P. (2004). "Pinning down cell signaling, cancer and Alzheimer's disease." Trends Biochem Sci **29**(4): 200-209.
Lu, K. P., et al. (2007). "Prolyl cis-trans isomerization as a molecular timer." Nat Chem Biol **3**(10): 619-629.
Lu, K. P., et al. (1996). "A human peptidyl-prolyl isomerase essential for regulation of mitosis." Nature **380**(6574): 544-547.
Lu, K. P., et al. (2006). "Targeting carcinogenesis: a role for the prolyl isomerase Pin1?" Mol Carcinog **45**(6): 397-402.
Lu, K. P. and X. Z. Zhou (2007). "The prolyl isomerase PIN1: a pivotal new twist in phosphorylation signalling and disease." Nat Rev Mol Cell Biol **8**(11): 904-916.

Lu, P. J., et al. (1999). "The prolyl isomerase Pin1 restores the function of Alzheimer-associated phosphorylated tau protein." Nature **399**(6738): 784-788.
Lu, P. J., et al. (2002). "Critical role of WW domain phosphorylation in regulating phosphoserine binding activity and Pin1 function." J Biol Chem **277**(4): 2381-2384.
Lu, P. J., et al. (1999). "Function of WW domains as phosphoserine- or phosphothreonine-binding modules." Science **283**(5406): 1325-1328.
Ludwig, C. and U. L. Guenther (2009). "Ligand based NMR methods for drug discovery." Front Biosci **14**: 4565-4574.
MacLachlan, T. K., et al. (2000). "BRCA1 effects on the cell cycle and the DNA damage response are linked to altered gene expression." J Biol Chem **275**(4): 2777-2785.
Magnusdottir, A., et al. (2006). "The crystal structure of a human PP2A phosphatase activator reveals a novel fold and highly conserved cleft implicated in protein-protein interactions." J Biol Chem **281**(32): 22434-22438.
Mandal, P. K., et al. (2011). "Potent and selective phosphopeptide mimetic prodrugs targeted to the Src homology 2 (SH2) domain of signal transducer and activator of transcription 3." J Med Chem **54**(10): 3549-3563.
Mantovani, F., et al. (2004). "Pin1 links the activities of c-Abl and p300 in regulating p73 function." Mol Cell **14**(5): 625-636.
Marine, J. C. and A. G. Jochemsen (2005). "Mdmx as an essential regulator of p53 activity." Biochem Biophys Res Commun **331**(3): 750-760.
Marx, J. (2007). "Oncology. Recruiting the cell's own guardian for cancer therapy." Science **315**(5816): 1211-1213.
Mattson, M. P. (1997). "Cellular actions of beta-amyloid precursor protein and its soluble and fibrillogenic derivatives." Physiol Rev **77**(4): 1081-1132.
Mayer, T. U., et al. (1999). "Small molecule inhibitor of mitotic spindle bipolarity identified in a phenotype-based screen." Science **286**(5441): 971-974.
McRee, D. E. (2004). "Differential evolution for protein crystallographic optimizations." Acta Crystallogr D Biol Crystallogr **60**(Pt 12 Pt 1): 2276-2279.
Mercier, K. A., et al. (2006). "FAST-NMR: functional annotation screening technology using NMR spectroscopy." J Am Chem Soc **128**(47): 15292-15299.
Migliorini, D., et al. (2002). "Hdmx recruitment into the nucleus by Hdm2 is essential for its ability to regulate p53 stability and transactivation." J Biol Chem **277**(9): 7318-7323.
Miyashita, H., et al. (2003). "Expression status of Pin1 and cyclins in oral squamous cell carcinoma: Pin1 correlates with Cyclin D1 mRNA expression and clinical significance of cyclins." Oncol Rep **10**(4): 1045-1048.
Moellering, R. E., et al. (2009). "Direct inhibition of the NOTCH transcription factor complex." Nature **462**(7270): 182-188.
Mohan, A., et al. (2006). "Analysis of molecular recognition features (MoRFs)." J Mol Biol **362**(5): 1043-1059.
Momand, J., et al. (1998). "The MDM2 gene amplification database." Nucleic Acids Res **26**(15): 3453-3459.
Momand, J., et al. (1992). "The mdm-2 oncogene product forms a complex with the p53 protein and inhibits p53-mediated transactivation." Cell **69**(7): 1237-1245.

Monje, P., et al. (2005). "Regulation of the transcriptional activity of c-Fos by ERK. A novel role for the prolyl isomerase PIN1." J Biol Chem **280**(42): 35081-35084.
Mori, S., et al. (1995). "Improved sensitivity of HSQC spectra of exchanging protons at short interscan delays using a new fast HSQC (FHSQC) detection scheme that avoids water saturation." J Magn Reson B **108**(1): 94-98.
Morris, A. L., et al. (1992). "Stereochemical quality of protein structure coordinates." Proteins **12**(4): 345-364.
Muhandiram, D. R., et al. (1997). "Specific (15)N, NH correlations for residues in(15) N, (13)C and fractionally deuterated proteins that immediately follow methyl-containing amino acids." J Biomol NMR **10**(3): 283-288.
Murshudov, G. N., et al. (2011). "REFMAC5 for the refinement of macromolecular crystal structures." Acta Crystallogr D Biol Crystallogr **67**(Pt 4): 355-367.
Nikolovska-Coleska, Z., et al. (2004). "Development and optimization of a binding assay for the XIAP BIR3 domain using fluorescence polarization." Anal Biochem **332**(2): 261-273.
Nunan, J. and D. H. Small (2002). "Proteolytic processing of the amyloid-beta protein precursor of Alzheimer's disease." Essays Biochem **38**: 37-49.
Nurse, P. (2002). "Cyclin dependent kinases and cell cycle control (nobel lecture)." Chembiochem **3**(7): 596-603.
Okamoto, K. and N. Sagata (2007). "Mechanism for inactivation of the mitotic inhibitory kinase Wee1 at M phase." Proc Natl Acad Sci U S A **104**(10): 3753-3758.
Olivier, M., et al. (2002). "The IARC TP53 database: new online mutation analysis and recommendations to users." Hum Mutat **19**(6): 607-614.
Pahlke, D., et al. (2005). "Statistically significant dependence of the Xaa-Pro peptide bond conformation on secondary structure and amino acid sequence." BMC Struct Biol **5**: 8.
Pahlke, D., et al. (2005). "COPS--cis/trans peptide bond conformation prediction of amino acids on the basis of secondary structure information." Bioinformatics **21**(5): 685-686.
Pal, D. and P. Chakrabarti (1999). "Cis peptide bonds in proteins: residues involved, their conformations, interactions and locations." J Mol Biol **294**(1): 271-288.
Pan, Y. and J. Chen (2003). "MDM2 promotes ubiquitination and degradation of MDMX." Mol Cell Biol **23**(15): 5113-5121.
Pang, R., et al. (2004). "PIN1 overexpression and beta-catenin gene mutations are distinct oncogenic events in human hepatocellular carcinoma." Oncogene **23**(23): 4182-4186.
Pastorino, L., et al. (2006). "The prolyl isomerase Pin1 regulates amyloid precursor protein processing and amyloid-beta production." Nature **440**(7083): 528-534.
Pazgier, M., et al. (2009). "Structural basis for high-affinity peptide inhibition of p53 interactions with MDM2 and MDMX." Proc Natl Acad Sci U S A **106**(12): 4665-4670.
Pellecchia, M., et al. (2008). "Perspectives on NMR in drug discovery: a technique comes of age." Nat Rev Drug Discov **7**(9): 738-745.
Pellecchia, M., et al. (2002). "NMR in drug discovery." Nat Rev Drug Discov **1**(3): 211-219.

Perrakis, A., et al. (1997). "wARP: improvement and extension of crystallographic phases by weighted averaging of multiple-refined dummy atomic models." Acta Crystallogr D Biol Crystallogr **53**(Pt 4): 448-455.
Pervushin, K., et al. (2002). "Longitudinal (1)H relaxation optimization in TROSY NMR spectroscopy." J Am Chem Soc **124**(43): 12898-12902.
Picksley, S. M., et al. (1994). "Immunochemical analysis of the interaction of p53 with MDM2;--fine mapping of the MDM2 binding site on p53 using synthetic peptides." Oncogene **9**(9): 2523-2529.
Popowicz, G. M., et al. (2008). "Structure of the human Mdmx protein bound to the p53 tumor suppressor transactivation domain." Cell Cycle **7**(15): 2441-2443.
Popowicz, G. M., et al. (2007). "Molecular basis for the inhibition of p53 by Mdmx." Cell Cycle **6**(19): 2386-2392.
Popowicz, G. M., et al. (2010). "Structures of low molecular weight inhibitors bound to MDMX and MDM2 reveal new approaches for p53-MDMX/MDM2 antagonist drug discovery." Cell Cycle **9**(6): 1104-1111.
Popowicz, G. M., et al. (2011). "The structure-based design of Mdm2/Mdmx-p53 inhibitors gets serious." Angew Chem Int Ed Engl **50**(12): 2680-2688.
Potter, A., et al. (2010). "Discovery of cell-active phenyl-imidazole Pin1 inhibitors by structure-guided fragment evolution." Bioorg Med Chem Lett **20**(22): 6483-6488.
Ranganathan, R., et al. (1997). "Structural and functional analysis of the mitotic rotamase Pin1 suggests substrate recognition is phosphorylation dependent." Cell **89**(6): 875-886.
Robertson, K. D. and P. A. Jones (1998). "The human ARF cell cycle regulatory gene promoter is a CpG island which can be silenced by DNA methylation and down-regulated by wild-type p53." Mol Cell Biol **18**(11): 6457-6473.
Rothweiler, U., et al. (2008). "NMR screening for lead compounds using tryptophan-mutated proteins." J Med Chem **51**(16): 5035-5042.
Rustighi, A., et al. (2009). "The prolyl-isomerase Pin1 is a Notch1 target that enhances Notch1 activation in cancer." Nat Cell Biol **11**(2): 133-142.
Ryo, A., et al. (2003). "Prolyl isomerase Pin1: a catalyst for oncogenesis and a potential therapeutic target in cancer." J Cell Sci **116**(Pt 5): 773-783.
Ryo, A., et al. (2002). "PIN1 is an E2F target gene essential for Neu/Ras-induced transformation of mammary epithelial cells." Mol Cell Biol **22**(15): 5281-5295.
Ryo, A., et al. (2001). "Pin1 regulates turnover and subcellular localization of beta-catenin by inhibiting its interaction with APC." Nat Cell Biol **3**(9): 793-801.
Ryo, A., et al. (2006). "Prolyl-isomerase Pin1 accumulates in lewy bodies of parkinson disease and facilitates formation of alpha-synuclein inclusions." J Biol Chem **281**(7): 4117-4125.
Schagger, H. and G. von Jagow (1987). "Tricine-sodium dodecyl sulfate-polyacrylamide gel electrophoresis for the separation of proteins in the range from 1 to 100 kDa." Anal Biochem **166**(2): 368-379.
Schanda, P. and B. Brutscher (2005). "Very fast two-dimensional NMR spectroscopy for real-time investigation of dynamic events in proteins on the time scale of seconds." J Am Chem Soc **127**(22): 8014-8015.
Schanda, P. and B. Brutscher (2006). "Hadamard frequency-encoded SOFAST-HMQC for ultrafast two-dimensional protein NMR." J Magn Reson **178**(2): 334-339.

Schanda, P., et al. (2005). "SOFAST-HMQC experiments for recording two-dimensional heteronuclear correlation spectra of proteins within a few seconds." J Biomol NMR **33**(4): 199-211.
Schon, O., et al. (2002). "Molecular mechanism of the interaction between MDM2 and p53." J Mol Biol **323**(3): 491-501.
Shangary, S. and S. Wang (2008). "Targeting the MDM2-p53 interaction for cancer therapy." Clin Cancer Res **14**(17): 5318-5324.
Shen, M., et al. (1998). "The essential mitotic peptidyl-prolyl isomerase Pin1 binds and regulates mitosis-specific phosphoproteins." Genes Dev **12**(5): 706-720.
Shvarts, A., et al. (1996). "MDMX: a novel p53-binding protein with some functional properties of MDM2." EMBO J **15**(19): 5349-5357.
Stark, J. L. and R. Powers (2012). "Application of NMR and molecular docking in structure-based drug discovery." Top Curr Chem **326**: 1-34.
Stewart, D. E., et al. (1990). "Occurrence and role of cis peptide bonds in protein structures." J Mol Biol **214**(1): 253-260.
Stommel, J. M. and G. M. Wahl (2004). "Accelerated MDM2 auto-degradation induced by DNA-damage kinases is required for p53 activation." EMBO J **23**(7): 1547-1556.
Stukenberg, P. T. and M. W. Kirschner (2001). "Pin1 acts catalytically to promote a conformational change in Cdc25." Mol Cell **7**(5): 1071-1083.
Suizu, F., et al. (2006). "Pin1 regulates centrosome duplication, and its overexpression induces centrosome amplification, chromosome instability, and oncogenesis." Mol Cell Biol **26**(4): 1463-1479.
Sultana, R., et al. (2006). "Oxidative modification and down-regulation of Pin1 in Alzheimer's disease hippocampus: A redox proteomics analysis." Neurobiol Aging **27**(7): 918-925.
Tan, X., et al. (2010). "Pin1 expression contributes to lung cancer: Prognosis and carcinogenesis." Cancer Biol Ther **9**(2): 111-119.
Thinakaran, G. and E. H. Koo (2008). "Amyloid precursor protein trafficking, processing, and function." J Biol Chem **283**(44): 29615-29619.
Uchida, T., et al. (2003). "Pin1 and Par14 peptidyl prolyl isomerase inhibitors block cell proliferation." Chem Biol **10**(1): 15-24.
Vagin, A. and A. Teplyakov (2010). "Molecular replacement with MOLREP." Acta Crystallogr D Biol Crystallogr **66**(Pt 1): 22-25.
van Drogen, F. and M. Peter (2004). "Revealing protein dynamics by photobleaching techniques." Methods Mol Biol **284**: 287-306.
Vassilev, L. T. (2004). "Small-molecule antagonists of p53-MDM2 binding: research tools and potential therapeutics." Cell Cycle **3**(4): 419-421.
Vassilev, L. T., et al. (2004). "In vivo activation of the p53 pathway by small-molecule antagonists of MDM2." Science **303**(5659): 844-848.
Werner-Allen, J. W., et al. (2011). "cis-Proline-mediated Ser(P)5 dephosphorylation by the RNA polymerase II C-terminal domain phosphatase Ssu72." J Biol Chem **286**(7): 5717-5726.
Wiegand, S., et al. (2009). "The rotamase Pin1 is up-regulated, hypophosphorylated and required for cell cycle progression in head and neck squamous cell carcinomas." Oral Oncol **45**(10): e140-149.

Wildemann, D., et al. (2006). "Nanomolar inhibitors of the peptidyl prolyl cis/trans isomerase Pin1 from combinatorial peptide libraries." J Med Chem **49**(7): 2147-2150.
Wu, X., et al. (1993). "The p53-mdm-2 autoregulatory feedback loop." Genes Dev **7**(7A): 1126-1132.
Wulf, G. M., et al. (2002). "Role of Pin1 in the regulation of p53 stability and p21 transactivation, and cell cycle checkpoints in response to DNA damage." J Biol Chem **277**(50): 47976-47979.
Wulf, G. M., et al. (2001). "Pin1 is overexpressed in breast cancer and cooperates with Ras signaling in increasing the transcriptional activity of c-Jun towards cyclin D1." EMBO J **20**(13): 3459-3472.
Xu, G. G. and F. A. Etzkorn (2009). "Pin1 as an anticancer drug target." Drug News Perspect **22**(7): 399-407.
Xu, Y. X. and J. L. Manley (2007). "The prolyl isomerase Pin1 functions in mitotic chromosome condensation." Mol Cell **26**(2): 287-300.
Yaffe, M. B., et al. (1997). "Sequence-specific and phosphorylation-dependent proline isomerization: a potential mitotic regulatory mechanism." Science **278**(5345): 1957-1960.
Yeh, E., et al. (2004). "A signalling pathway controlling c-Myc degradation that impacts oncogenic transformation of human cells." Nat Cell Biol **6**(4): 308-318.
You, H., et al. (2002). "IGF-1 induces Pin1 expression in promoting cell cycle S-phase entry." J Cell Biochem **84**(2): 211-216.
Zacchi, P., et al. (2002). "The prolyl isomerase Pin1 reveals a mechanism to control p53 functions after genotoxic insults." Nature **419**(6909): 853-857.
Zarrinpar, A. and W. A. Lim (2000). "Converging on proline: the mechanism of WW domain peptide recognition." Nat Struct Biol **7**(8): 611-613.
Zhang, Y., et al. (2007). "Structural basis for high-affinity peptide inhibition of human Pin1." ACS Chem Biol **2**(5): 320-328.
Zhang, Y. and Y. Xiong (2001). "Control of p53 ubiquitination and nuclear export by MDM2 and ARF." Cell Growth Differ **12**(4): 175-186.
Zhao, R., et al. (2000). "Analysis of p53-regulated gene expression patterns using oligonucleotide arrays." Genes Dev **14**(8): 981-993.
Zhao, S. and F. A. Etzkorn (2007). "A phosphorylated prodrug for the inhibition of Pin1." Bioorg Med Chem Lett **17**(23): 6615-6618.
Zheng, H., et al. (2002). "The prolyl isomerase Pin1 is a regulator of p53 in genotoxic response." Nature **419**(6909): 849-853.
Zhou, X. Z., et al. (2000). "Pin1-dependent prolyl isomerization regulates dephosphorylation of Cdc25C and tau proteins." Mol Cell **6**(4): 873-883.
Zhu, L., et al. (2011). "Synthesis and biological evaluation of novel quinazoline-derived human Pin1 inhibitors." Bioorg Med Chem **19**(9): 2797-2807.
Zita, M. M., et al. (2007). "Post-phosphorylation prolyl isomerisation of gephyrin represents a mechanism to modulate glycine receptors function." EMBO J **26**(7): 1761-1771.